

AD-A168 578

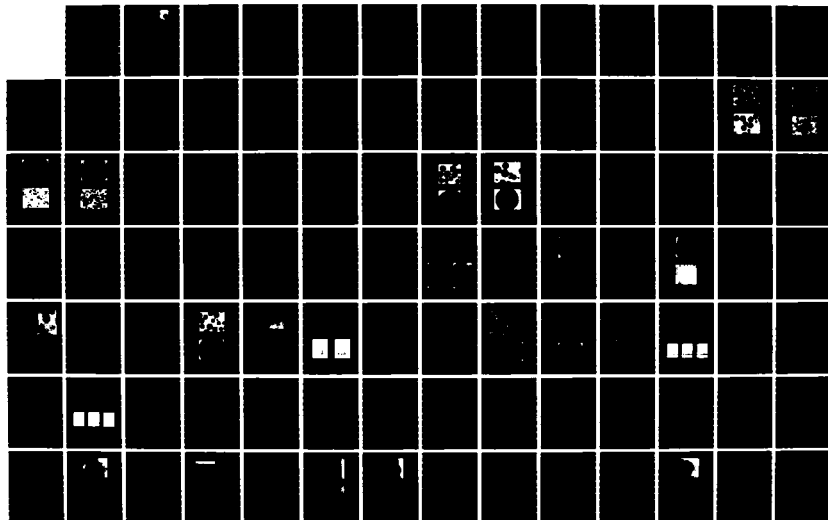
DEVELOPMENT OF IRON ALUMINIDES(U) TRW MATERIALS AND  
MANUFACTURING CENTER EUCLID OH 8 C CULBERTSON ET AL.  
MAR 86 ER-8215-6 AFMIL-TR-85-4155 F33615-81-C-5155

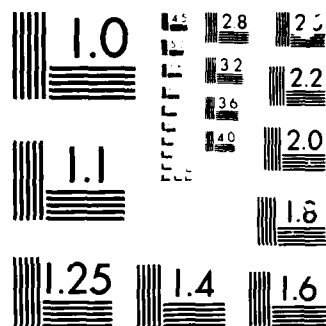
1/2

UNCLASSIFIED

F/B 11/6

NL





MICROCOPY

CHART

AD-A168 578

AFWAL-TR-85-4155

DEVELOPMENT OF IRON ALUMINIDES

G. Culbertson  
C. S. Kortovich

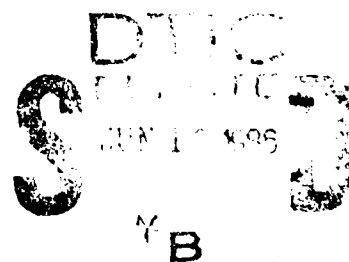
TRW Inc.  
Materials & Manufacturing Center  
23555 Euclid Avenue  
Euclid, Ohio 44117

March 1986

Final Report for Period September 1981 - November 1985

Approved for public release; distribution is unlimited.

DTIC FILE COPY



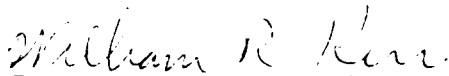
MATERIALS LABORATORY  
AIR FORCE WRIGHT AERONAUTICAL LABORATORIES  
AIR FORCE SYSTEMS COMMAND  
WRIGHT-PATTERSON AIR FORCE BASE, OHIO 45433-6533

NOTICE

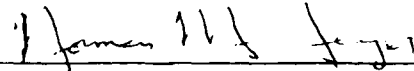
When Government drawings, specifications, or other data are used for any purpose other than in connection with a definitely related Government procurement operation, the United States Government thereby incurs no responsibility nor any obligation whatsoever; and the fact that the government may have formulated, furnished, or in any way supplied the said drawings, specifications, or other data, is not to be regarded by implication or otherwise as in any manner licensing the holder or any other person or corporation, or conveying any rights or permission to manufacture use, or sell any patented invention that may in any way be related thereto.

This report has been reviewed by the Office of Public Affairs (ASD/PA) and is releasable to the National Technical Information Service (NTIS). At NTIS, it will be available to the general public, including foreign nations.

This technical report has been reviewed and is approved for publication.

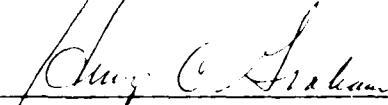


William R. Kerr  
Project Engineer



Norman M. Geyer, Technical Area Manager  
Processing & High Temperature  
Materials Branch  
Metals & Ceramics Division

FOR THE COMMANDER



Henry C. Graham, Chief  
Processing & High Temperature  
Materials Branch  
Metals & Ceramics Division

If your address has changed, if you wish to be removed from our mailing list, or if the addressee is no longer employed by your organization please notify AFWAL/MLLM, W-PAFB, OH 45433 to help us maintain a current mailing list.

Copies of this report should not be returned unless return is required by security considerations, contractual obligations, or notice on a specific document.

Unclassified

ADA 168375

SECURITY CLASSIFICATION OF THIS PAGE

## REPORT DOCUMENTATION PAGE

1a. REPORT SECURITY CLASSIFICATION Unclassified			1b. RESTRICTIVE MARKINGS	
2a. SECURITY CLASSIFICATION AUTHORITY			3. DISTRIBUTION/AVAILABILITY OF REPORT	
2b. DECLASSIFICATION/DOWNGRADING SCHEDULE			Approved for public release; distribution is unlimited.	
4. PERFORMING ORGANIZATION REPORT NUMBER(S) EP-8215-6			5. MONITORING ORGANIZATION REPORT NUMBER(S) AFWAL-TR-85-4155	
6a. NAME OF PERFORMING ORGANIZATION TRW Inc. Materials & Manufacturing Technology Center		6b. OFFICE SYMBOL (If applicable)	7a. NAME OF MONITORING ORGANIZATION Air Force Materials Laboratory MLLM	
6c. ADDRESS (City, State and ZIP Code) 23555 Euclid Avenue Euclid, Ohio 44117		7b. ADDRESS (City, State and ZIP Code) Air Force Wright Aeronautical Laboratories Wright-Patterson AFB, Ohio 45433-6533		
8a. NAME OF FUNDING/SPONSORING ORGANIZATION Air Force Materials Laboratory		8b. OFFICE SYMBOL (If applicable) MLLM	9. PROCUREMENT INSTRUMENT IDENTIFICATION NUMBER F33615-81-C-5155	
8c. ADDRESS (City, State and ZIP Code) Air Force Wright Aeronautical Laboratories Wright-Patterson AFB, Ohio 45433-6533		10. SOURCE OF FUNDING NOS.		
11. TITLE (Include Security Classification) Development of Iron Aluminides		PROGRAM ELEMENT NO 62102F	PROJECT NO 2420	TASK NO. 02
				WORK UNIT NO 11
12. PERSONAL AUTHOR(S) G. Culbertson, C.S. Kortovich				
13a. TYPE OF REPORT Final Technical Report		13b. TIME COVERED FROM Sept. 1981 to May 1985	14. DATE OF REPORT (Yr., Mo., Day) 1986 March	15. PAGE COUNT 187
16. SUPPLEMENTARY NOTATION				
17. COSATI CODES			18. SUBJECT TERMS (Continue on reverse if necessary and identify by block number)	
FIELD	GROUP	SUB GR	Iron Aluminides Hot Extrusion	
11	06		Powder Metallurgy Alloy Development	
			Isothermal Forging	
19. ABSTRACT (Continue on reverse if necessary and identify by block number)				
<p>A program was conducted to develop improved iron-aluminide alloys with higher elevated temperature strength and room temperature ductility compared to the baseline Fe<sub>3</sub>Al alloy. The technical approach involved the screening evaluation of two experimental series of alloys which then formed the basis for the selection of a single alloy composition for more complete properties testing. The screening studies involved the evaluation of precipitation strengthening as well as solid solution strengthening alloy additions to the Fe<sub>3</sub>Al system. The most optimum of the precipitation strengthened alloys contained 2 at/o Nb and in the fully solution heat treated and aged condition exhibited 4 times the 600°C (1112°F) yield strength of Fe<sub>3</sub>Al, with about 60% the room temperature elongation. A negative feature of the two-phase alloys, however, was the occurrence of quench cracking, discovered during heat treatment of isothermally forged material. The most optimum of the solid solution strengthened alloys contained 3.5 Cr + 0.5 Mo (atomic percent) and exhibited 1.3 times the 600°C (1112°F) yield strength of Fe<sub>3</sub>Al, with equivalent room temperature ductility (4.8 percent elongation).</p>				
20. DISTRIBUTION AVAILABILITY OF ABSTRACT UNCLASSIFIED UNLIMITED <input checked="" type="checkbox"/> SAME AS RPT <input type="checkbox"/> DTIC USERS <input type="checkbox"/>			21. ABSTRACT SECURITY CLASSIFICATION Unclassified	
22a. NAME OF RESPONSIBLE INDIVIDUAL W. R. Kerr			22b. TELEPHONE NUMBER (Include Area Code) 613-255-4763	22c. OFFICE SYMBOL MLLM

DD FORM 1473, 83 APR

EDITION OF 1 JAN 73 IS OBSOLETE

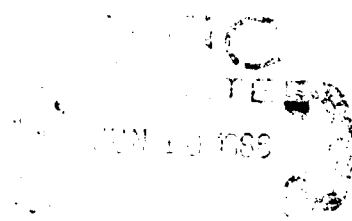
Unclassified

SECURITY CLASSIFICATION OF THIS PAGE

Additional positive features of all the alloys were the attractive oxidation resistance compared to the  $\text{Fe}_3\text{Al}$  baseline and the high degree of workability demonstrated during upset isothermal forging studies. Final alloy evaluation was conducted on Fe-35Al-4Cr-2Mo. (in atomic percent), selected to take advantage of the solid solution strengthening demonstrated by Cr and Mo additions and to enhance specific strength by utilizing a base alloy exhibiting a lower density than the  $\text{Fe}_3\text{Al}$  baseline. This alloy exhibited 1.6 times the yield strength of  $\text{Fe}_3\text{Al}$  at  $600^\circ\text{C}$  ( $1112^\circ\text{F}$ ) but with only approximately 50% of the room temperature ductility (percent elongation). Creep rupture properties including rupture time (300 hours versus 20 hours) and time to 0.1% creep (34 hours versus less than one hour) at  $570^\circ\text{C}$  ( $1058^\circ\text{F}$ )/207 Mpa (30 Ksi) were superior to commercial 410 martensitic stainless steel heat treated to the same 345 Mpa (50 Ksi) yield strength at  $600^\circ\text{C}$  ( $1112^\circ\text{F}$ ). The room temperature high cycle fatigue endurance limit lies between 345 Mpa (50 Ksi) and 410 Mpa (59.5 Ksi). The  $600^\circ\text{C}$  ( $1112^\circ\text{F}$ ) low cycle fatigue properties were poor because of the presence of pre-existing cracks in the portion of the hot extruded vacuum induction melted ingot used to characterize low cycle fatigue resistance. Oxidation testing at  $816^\circ\text{C}$  ( $1500^\circ\text{F}$ ) for 240 hours indicated no specific weight change.

## FOREWORD

The work described in this final report was performed by the Materials and Manufacturing Technology Center of TRW Inc. and Systems Research Laboratories (SRL) under United States Air Force Contract F33615-81-C-5155. The work was performed under the direction of Mr. G. I. Friedman, the Program Manager, with Mr. G. C. Culbertson as the Principal Investigator. Dr. C. S. Kortovich provided technical assistance. Dr. M. G. Mendiratta was the Principal Investigator for SRL. Mr. W. R. Kerr, AFWAL/MLLM, of the Processing & High Temperature Materials Branch, Metals & Ceramics Division, was the Air Force Program Manager.



✓  
PER CALL JC

A-1

## TABLE OF CONTENTS

	<u>PAGE</u>
1.0 INTRODUCTION	1
2.0 PROGRAM OUTLINE	3
2.1 Task I - Powder for Alloy Development	3
2.2 Task II - Alloy Development Studies	3
2.2.1 Series I Alloys	5
2.2.2 Series II Alloys	5
2.2.3 Alloy Characterization	5
3.0 TASK I - POWDER FOR ALLOY DEVELOPMENT	7
3.1 Procurement of FeAl and Fe <sub>3</sub> Al	7
3.2 Procurement of Fe-Al-X Powders	13
4.0 TASK II - ALLOY DEVELOPMENT STUDIES	20
4.1 Series I Alloys	20
4.1.1 Alloy Selection	20
4.1.2 Material Procurement/Processing	22
4.1.3 Screening Evaluations	61
4.1.4 Series I Summary	94
4.2 Series II Alloys	95
4.2.1 Alloy Selection	95
4.2.2 Material Procurement/Processing	97
4.2.3 Screening Evaluations	117
4.2.4 Series II Summary	124
4.3 Alloy Characterization	125
4.3.1 Alloy Selection	125
4.3.2 Material Procurement/Processing	125
4.3.3 Properties Characterization	132
4.3.4 Alloy Characterization Summary	142
5.0 SUMMARY AND CONCLUSIONS	146
 APPENDIX I	 A1



## LIST OF ILLUSTRATIONS

<u>FIGURE</u>		<u>PAGE</u>
1	Program work breakdown structure.	4
2	SEM (a) and light (b) photos of -60+140 mesh size FeAl powder. 100X Magnification.	9
3	SEM (a) and light (b) photos of -140+200 mesh size FeAl powder. 100X Magnification.	10
4	SEM (a) and light (b) photos of -200 mesh size FeAl powder. 100X Magnification.	11
5	SEM (a) and light (b) photos of -140+200 mesh size Fe <sub>3</sub> Al powder. 100X Magnification.	12
6	Light photos of PREP Fe <sub>65</sub> V <sub>10</sub> Al <sub>25</sub> powder showing large central voids and dispersed microporosity.	18
7	Light photos of PREP Fe <sub>70</sub> Nb <sub>5</sub> Al <sub>25</sub> powder showing presence of second phase precipitates.	19
8	Schematic illustration of extrusion can configuration used for consolidation of Task II/Series I alloy powders.	24
9	Light photos of as-extruded Fe <sub>3</sub> Al baseline alloy (transverse section) showing presence of non-metallic inclusions.	29
10	Light photos of as-extruded Ti-5 a/o (Alloy I-2) powder blend (transverse section) showing presence of non-metallic inclusions.	30

# LIST OF ILLUSTRATIONS (Continued)

<u>FIGURE</u>		<u>PAGE</u>
11	Light photos of as-extruded V-5 a/o (Alloy I-3) powder blend (transverse section) showing presence of non-metallic inclusions and non-homogeneous structure.	31
12	Light (100X Magnification) and SEM (200X, 500X Magnification) photos of as-extruded V-10 a/o (Alloy I-4) prealloyed powder (transverse section) showing predominantly intergranular cracking.	32
13a,b	Light photos of as-extruded Cr-1 a/o (Alloy I-5) powder blend (transverse section) showing presence of non-metallic inclusions and non-homogeneous etching structure.	33
13c	SEM photo of as-extruded Cr-1 a/o (Alloy I-5) powder blend (transverse section) showing overlapping of continuous grain boundaries by non-homogeneous etching structure.	34
14a,b	Light photos of as-extruded Cr-5 a/o (Alloy I-6) prealloyed powder (transverse section) showing presence of non-metallic inclusions and non-homogeneous etching structure.	35
14c,d	SEM and EDAX photos of as-extruded Cr-5 a/o (Alloy I-6) powder (transverse section) showing areas of chromium depletion.	36
15	Light photos of as-extruded Mn-6 a/o (Alloy I-7) prealloyed powder (transverse section) showing non-metallic inclusions decorating prior particle boundaries.	38
16	SEM, EDAX and light photos of as-extruded Ni-3 a/o (Alloy I-9) powder blend (transverse section) showing presence of non-homogeneous structure.	39

# LIST OF ILLUSTRATIONS (Continued)

<u>FIGURE</u>		<u>PAGE</u>
17	Light photos of as-extruded Ni-10 a/o (Alloy I-10) prealloyed powder (transverse section) showing non-metallic inclusions decorating prior particle boundaries.	40
18	Light photos of as-extruded Nb-2 a/o (Alloy I-11) prealloyed powder (transverse section) showing presence of second phase precipitate particles.	41
19	Light photos of PREP Nb-2 a/o (Alloy I-11) powder	42
20	SEM photos of PREP Nb-2 a/o (Alloy I-11) powder showing presence of second phase precipitate particles in grain boundary and interdendritic regions.	43
21	SEM and EDAX photos of as-extruded Nb-5 a/o (Alloy I-12) prealloyed powder (transverse section).	44
22	SEM photos of PREP Nb-5 a/o (Alloy I-12) powder showing presence of second phase precipitate particles and continuous films.	45
23	Light (100X Magnification) and SEM (200X Magnification) photos of as-extruded Mo-3 a/o (Alloy I-13) prealloyed powder showing presence of non-homogeneous etching structure.	47
24	Light (100X, 500X Magnification) and SEM (200X Magnification) photos of as-extruded Mo-6 a/o (Alloy I-14) prealloyed powder (transverse section).	48

# LIST OF ILLUSTRATIONS (Continued)

<u>FIGURE</u>		<u>PAGE</u>
25	Light (100X, 500X Magnification) and SEM (200X Magnification) photos of as-extruded Ta-1 a/o (Alloy I-15) prealloyed powder (transverse section) showing presence of non-metallic inclusions decorating prior particle boundaries.	49
26	SEM and EDAX photos of as-extruded Ta-5 a/o (Alloy I-16) prealloyed powder (transverse section).	50
27	SEM photos of PREP Ta-5 a/o (Alloy I-16) prealloyed powder showing presence of duplex second phase particle distribution.	51
28	Light photos of as-extruded Cu-10 a/o (Alloy I-18) prealloyed powder (transverse section).	53
29	SEM and EDAX photos of as-extruded Cu-10 a/o (Alloy I-18) prealloyed powder (transverse section).	54
30	Light photos of as-extruded Si-3 a/o (Alloy I-19) powder blend (transverse section) showing presence of non-metallic inclusions.	55
31	Light photo of Cr-5 a/o (Alloy I-6) prealloyed powder homogenized 168 hours at 1100°C (2012°F). 100X Magnification.	58
32	Light photos of Cr-1 a/o (Alloy I-5) powder blend homogenized 168 hours at 1000°C (1832°F).	60
33	Schematic illustration of tensile test specimen configuration.	62
34	Summary of Task II/Series I tensile data.	65

# LIST OF ILLUSTRATIONS (Continued)

<u>FIGURE</u>		<u>PAGE</u>
35	Light photos of Fe <sub>3</sub> Al failed room temperature tensile test specimen showing structure near the fracture surface.	66
36	Light photos of Fe <sub>3</sub> Al failed 600°C (1112°F) tensile test specimen showing structure near the fracture surface and the grip area. 100X Magnification.	68
37	Light photos of Mo-3 a/o (Alloy I-13) failed room temperature tensile test specimen showing localized abnormal grain growth.	70
38	Light photos of Ni-10 a/o (Alloy I-10) failed room temperature tensile test specimen showing structure near the fracture surface.	72
39	Light photos of Ni-10 a/o (Alloy I-10) failed 600°C (1112°F) tensile test specimen showing structures near the fracture surface and grip area. 100X Magnification.	73
40	Light photos of Nb-2 a/o (Alloy I-11) and Nb-5 a/o (Alloy I-12) failed 600°C (1112°F) tensile test specimens showing structure near the fracture area. 500X Magnification.	75
41	Light photos of Cu-10 a/o (Alloy I-18) failed 600°C (1112°F) tensile test specimen showing structures near the fracture surface and grip areas. 100X Magnification.	78
42	Photograph of prealloyed Task I/Series I Alloys after exposure to 816°C (1500°F) air for 96 hours.	83
43	Photograph of selected Task I/Series I Alloys showing effect of alloying additions on oxidation resistance after exposure to 816°C (1500°F) air. 2X Magnification.	84

# LIST OF ILLUSTRATIONS (Continued)

<u>FIGURE</u>		<u>PAGE</u>
44	SEM and EDAX photos of Ti-5 a/o (Alloy I-2) after 240 hour exposure to 816 <sup>0</sup> C (1500 <sup>0</sup> F) air. 16X magnification.	85
45	Photograph of Fe <sub>3</sub> Al forging preform and as-forged specimen.	87
46	Load versus height curve for Nb-2 a/o (Alloy I-11) for deformation at 954 <sup>0</sup> C (1750 <sup>0</sup> F) and 8/second strain rate.	88
47	Light photo of Ta-5 a/o (Alloy I-16) hot deformation specimen (longitudinal section) showing cracking near precipitate/matrix interface.	92
48	Light photos of Ta-1 a/o (Alloy I-15) hot deformation specimen (a-transverse section, b-longitudinal section) showing cracking associated with non-metallic inclusion stringers.	93
49	Photograph of ceramic mold (left) used to cast ingot (center) which was machined into a forging preform (right) for the Task II/Series I alloy studies.	100
50	Light photos of as-cast Cr-1 a/o, Mo-1 a/o (Alloy II-1) ingot showing coarse grain size.	103
51	Light photos of as-forged Cr-1 a/o, Mo-1 a/o (Alloy II-1) sub-size specimen isothermally forged at 954 <sup>0</sup> C (1750 <sup>0</sup> F) and 6:1 height reduction (longitudinal section) showing structure after normal etch (a) and heavy etch (b).	104
52	Light photos of as-cast Ta-0.75 a/o, Mo-1 a/o (Alloy II-5) ingot showing coarse grain size.	106

# LIST OF ILLUSTRATIONS (Continued)

<u>FIGURE</u>		<u>PAGE</u>
53	Light photos of as-forged Ta-0.75 a/o, Mo-1 a/o (Alloy II-5) sub-size specimen isothermally forged at 954°C (1750°F) and 6:1 height reduction (longitudinal section).	107
54	Light photos of as-cast Ta-2 a/o (Alloy II-8) ingot showing coarse grain size.	108
55	Light photos of as-forged Ta-2 a/o (Alloy II-8) sub-size specimen isothermally forged at 954°C (1750°F) and 6:1 height reduction (longitudinal section).	109
56	Light photos of as-cast Nb-1 a/o, Cr-2 a/o (Alloy II-9) ingot showing coarse grain size.	111
57	Light photos of as-forged Nb-1 a/o, Cr-2 a/o (Alloy II-9) sub-size specimen isothermally forged at 954°C (1750°F) and 6:1 height reduction (longitudinal section).	112
58	Light photos of as-cast Nb-2 a/o, V-1 a/o (Alloy II-15) ingot showing coarse grain size.	113
59	Light photos of as-forged Nb-2 a/o, V-1 a/o (Alloy II-15) sub-size specimen isothermally forged at 954°C (1750°F) and 6:1 height reduction (longitudinal section).	114
60a&b	Light photos of Cr-4 a/o, Mo-2 a/o (Alloy II-4) sub-size specimen isothermally forged at 730°C (1350°F) and 6:1 height reduction. 100X Magnification.	116

# LIST OF ILLUSTRATIONS (Continued)

<u>FIGURE</u>		<u>PAGE</u>
61	Light photos of as-forged Nb-2 a/o, V-1 a/o (Alloy II-15) sub-size specimen isothermally forged at 730°C (1350°F) and 6:1 height reduction.	118
62	Photograph of typical Series II full-size preform and pancake isothermally forged at 730°C (1350°F) and 6:1 height reduction.	121
63a&b	Light photos of as-extruded Fe-35Al-4Cr-2Mo vacuum induction melted ingot extruded at 843°C (1550°F) and a 3.5:1 reduction ratio.	128
64a&b	Light photos of as-extruded Fe-35Al-4Cr-2Mo vacuum induction melted ingot extruded at (a) 899°C (1650°F) and a 9:1 reduction ratio and (b) 927°C (1700°F) and a 36:1 reduction ratio. 100X Magnification.	130
65	Light photos of as-extruded Fe-35Al-4Cr-2Mo vacuum induction melted ingot extruded at 954°C (1750°F) and a 16:1 reduction ratio.	131
66	Light photos of Fe-35Al-4Cr-2Mo failed (a) room temperature and (b) 600°C (1112°F) tensile test specimens showing structures at the fracture surfaces. 100X Magnification.	133
67	Light photos of Fe-35Al-4Cr-2Mo failed (a) 570°C (1058°F)/ 207 Mpa (30 Ksi) and (b) 649°C (1200°F)/241 Mpa (35 Ksi) creep rupture test specimens showing structures at the fracture surfaces. 100X Magnification.	136
68	Light photos of Fe-35Al-4Cr-2Mo room temperature high cycle fatigue test specimen loaded at 345 Mpa (50 Ksi) showing crack initiation sites.	139



LIST OF ILLUSTRATIONS (Continued)

<u>FIGURE</u>		<u>PAGE</u>
69	Light photos of Fe-35Al-4Cr-2Mo failed 600°C (1112°F) low cycle fatigue test specimen No.2 showing structure (a) at the fracture surface and (b) in the grip area. 100X Magnification.	141
70	Photograph of Fe-35Al-4Cr-2Mo oxidation test coupon after exposure to 816°C (1500°F) laboratory air for 240 hours.	143

# LIST OF TABLES

<u>TABLE NO.</u>	<u>NAME OF TABLE</u>	<u>PAGE NO.</u>
I	COMPOSITION OF TASK I - INERT GAS ATOMIZED FE-AL POWDERS	8
II	TASK I - FE-AL-X ALLOYS	14
III	CHEMICAL COMPOSITION OF TASK I - FE-AL-X ALLOY CASTINGS	15
IV	PRODUCTS OF PREP POWDER MAKING OF TASK I - FE-AL-X ALLOYS	16
V	TASK II/SERIES I ALLOYS	21
VI	CHEMICAL COMPOSITION OF TASK II/SERIES I ALLOY EXTRUSIONS	26
VII	INTERSTITIAL CONTENT OF TASK II/SERIES I ALLOY EXTRUSIONS	27
VIII	ROOM TEMPERATURE TENSILE DATA FOR TASK II/SERIES I ALLOYS	63
IX	600°C (1112°F) TENSILE DATA FOR TASK II/SERIES I ALLOYS	64
X	OXIDATION RESULTS FOR TASK II/SERIES I ALLOYS	82
XI	WORKABILITY RESULTS FOR TASK II/SERIES I ALLOYS ISOTHERMALLY FORGED AT 954°C. (1750°F.) AND 8/SECOND	90
XII	TASK II/SERIES II ALLOYS	96
XIII	CHARGE WEIGHTS FOR TASK II/SERIES II ALLOYS (GRAMS)	99
XIV	CHEMICAL COMPOSITION OF TASK II/SERIES II ALLOYS SELECTED FOR SCREENING EVALUATIONS	119
XV	YIELD STRENGTH RESULTS FOR TASK II/SERIES II ALLOYS	123
XVI	EXTRUSION RESULTS FOR Fe-35Al-4Cr-2Mo ALLOY	127
XVII	TENSILE AND CREEP-RUPTURE DATA FOR Fe-35Al-4Cr-2Mo ALLOY	137
XVIII	FATIGUE DATA FOR Fe-35Al-4Cr-2Mo ALLOY	140

## 1.0 INTRODUCTION

The development of advanced materials and methods to process these materials have traditionally played a key role in the evolution of technology for the aerospace industry. This is particularly true for the gas turbine engine industry, where the requirements for enhanced temperature capability with lower specific fuel consumption have continually been upgraded. The additional realization that raw materials and energy sources are finite has placed a new perspective on technology developments for this industry. This new perspective relates particularly to the vulnerability of the U.S. gas turbine industry in terms of its heavy reliance upon non-domestic sources for much of its strategic metals requirements. These considerations are especially important in a number of Air Force systems because of the austenitic stainless steels and nickel-base superalloys used in gas turbine engines. The questionable future availability of chromium, for example, poses a potential serious threat to these applications. The replacement of stainless steels and certain of the nickel-base superalloys with a material of similar properties, but which does not contain strategic elements would be of long term benefit with respect to cost and dependence on imported chromium.

The iron-aluminum based alloys have generated considerable interest for possible Air Force system applications. The advantage of this class of alloys includes the potential for non or low strategic element compositions with outstanding oxidation resistance and reduced densities compared to conventional high temperature materials. Previously, these alloys were investigated extensively in the mid-1950's through the early 1960's, but no significant commercialization occurred because of difficulties with room temperature ductility, processing and control of microstructure. Recent developments in the metallurgy of these materials have demonstrated potential for overcoming these problems. These developments include an improved understanding of iron-aluminum alloy ordering reactions, rapid solidification powder metallurgy technology, an improved understanding and control of compaction processes, and improved deformation processing techniques such as isothermal forging. A need, thus, exists to apply these developments for prospective Air Force applications.

The present investigation was conducted, then, to apply these concepts for improved iron-aluminum alloys for potential Air Force applications. More specifically, efforts were focused on the  $\text{Fe}_3\text{Al}$  system which exhibits the  $\text{DO}_3$  ordered crystal lattice with particular effort being addressed towards improving the high temperature strength and room temperature ductility of this system. The experimental approach involved the screening evaluation of two experimental series of alloys which then formed the basis for the selection of a single alloy composition for more complete properties testing. The alloy design philosophy was based on the concept of improving strength and ductility through an investigation of the effects of ternary and quaternary element additions on the resultant microstructures and changes in the  $\text{DO}_3 \rightleftharpoons \text{B2}$  transformation temperatures. Powder metallurgy as well as isothermal forging processing routes were explored for these experimental alloys.

The results of this study are summarized in this final report. It includes a review of the program outline to develop iron aluminides, a discussion of the materials procurement and processing, a summary of the experimental results, and a discussion of these results and recommendations.

## 2.0 PROGRAM OUTLINE

The basic goal of the program was the development of iron aluminides with improved high temperature strength and room temperature ductility compared to the baseline  $\text{Fe}_3\text{Al}$  alloy composition. To accomplish this goal, ternary and quaternary element additions were made to the baseline to establish the effects on microstructure, ordering temperature, oxidation resistance, workability, and mechanical properties performance. The study consisted of two technical tasks and followed the outline presented in the Work Breakdown Structure of Figure 1. Task I of the investigation involved the preparation of iron aluminide powders for subsequent study at AFWAL. Task II consisted of the screening evaluation of two series of experimental iron aluminide alloys as well as a more complete evaluation of a single alloy designed on the basis of the screening study. For the Task II portion of this program, TRW was teamed with Systems Research Laboratories, Inc. (SRL), with SRL responsible for in-depth microstructural characterization of the alloys under investigation.

### 2.1 Task I - Powder for Alloy Development

The objective of this task was to supply iron aluminide powder to AFWAL. The alloy powders included  $\text{FeAl}$ ,  $\text{Fe}_3\text{Al}$ , and twelve ternary alloys based on  $\text{Fe}_3\text{Al}$ . The  $\text{FeAl}$  and  $\text{Fe}_3\text{Al}$  powders were produced by conventional inert gas atomization and sieved into various size fractions possessing different cooling rates, with the smaller particles having faster cooling rates. The ternary alloy powders were produced by the Plasma Rotating Electrode Process (PREP).

### 2.2 Task II - Alloy Development Studies

The objective of this task was to study the effect of ternary additions on  $\text{Fe}_3\text{Al}$ . This was accomplished by an evaluation of two series of experimental alloys based upon  $\text{Fe}_3\text{Al}$  which was followed by a more complete characterization of an alloy defined on the basis of the results of the first two series of alloys.

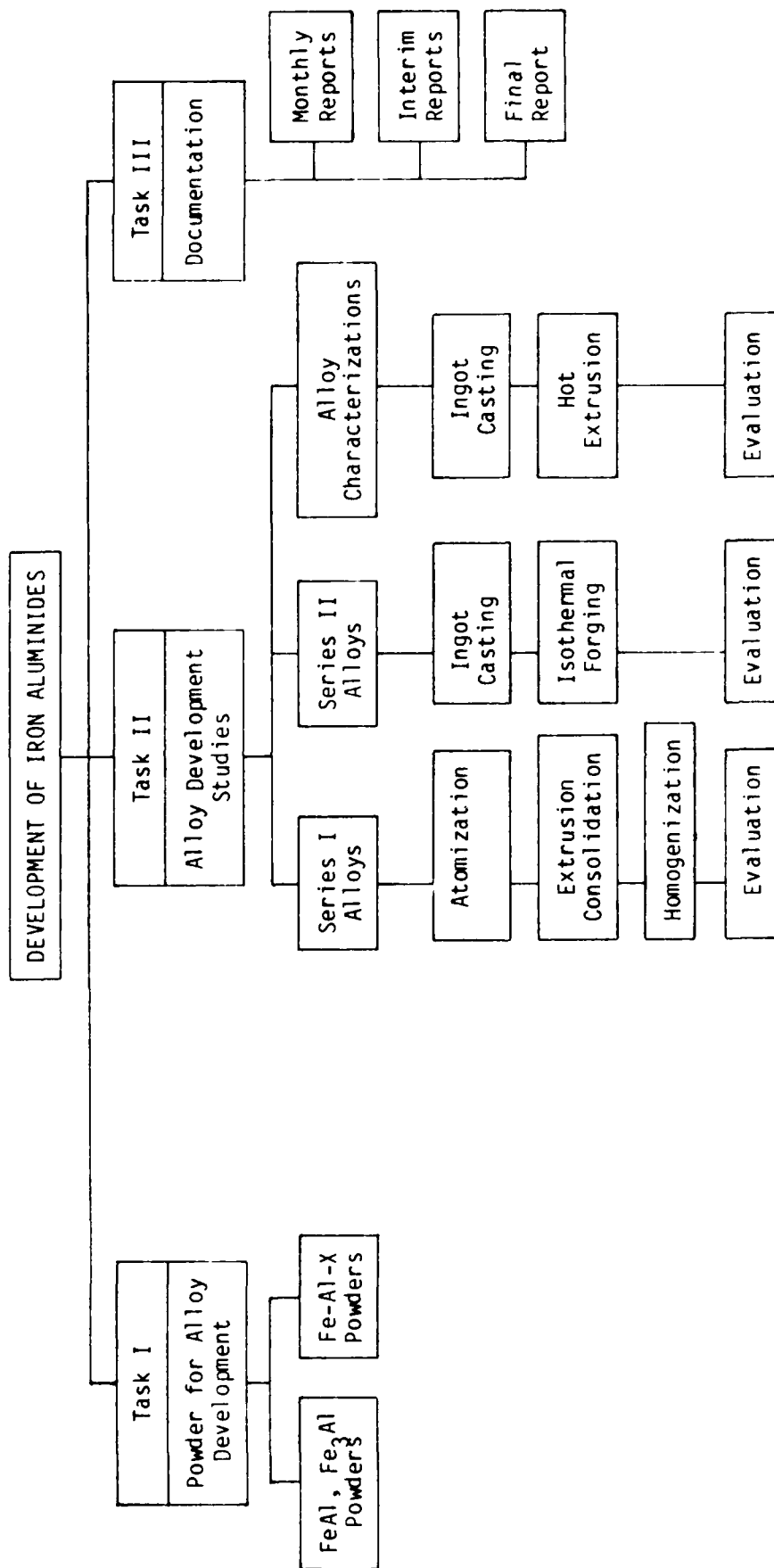


Figure 1. Program Work Breakdown Structure

### 2.2.1 Series I Alloys

For the Series I effort, twenty one alloy compositions (including the  $\text{Fe}_3\text{Al}$  baseline alloy) were produced in powder form and consolidated by hot extrusion. Some of these alloys were blends of PREP powder with gas atomized  $\text{Fe}_3\text{Al}$ , all produced during the Task I portion of this program, and some were solely prealloyed PREP powder.

These alloys were characterized with respect to their microstructure and to the effect the alloy additions had on the critical temperature at which the  $\text{DO}_3\text{-B}_2$  order change occurred. Homogenization heat treatments were developed for the blended alloys and ordering heat treatments were developed for all the alloys.

Screening evaluations included mechanical properties characterization, oxidation testing and workability testing. All evaluations were conducted on material in the extruded, homogenized (where necessary) and fully ordered condition. The mechanical properties characterization included tensile tests at room temperature and  $600^\circ\text{C}$  ( $1112^\circ\text{F}$ ). Oxidation tests included long time exposures in laboratory air at  $816^\circ\text{C}$  ( $1500^\circ\text{F}$ ). Workability tests included isothermal upset forging at  $954^\circ\text{C}$  ( $1750^\circ\text{F}$ ). Metallographic analysis was conducted on selected samples to aid in the interpretation of the results.

### 2.2.2 Series II Alloys

For the Series II effort, fifteen alloy compositions were produced by isothermal forging of cast ingots. These alloys were primarily quaternary compositions and were designed on the basis of the results of the Series I alloys. These alloys were characterized with respect to their microstructure. Screening evaluations were conducted on selected alloys and included four-point bending tests over the temperature range  $600\text{-}700^\circ\text{C}$  ( $1112\text{-}1292^\circ\text{F}$ ).

### 2.2.3 Alloy Characterization

In this portion of the program, a single alloy composition was produced by hot extrusion of cast ingots. This alloy was a quaternary composition and

was designed on the basis of the results of the Series I and II alloys. This alloy was heat treated to obtain the microstructure best suited for optimum performance.

A comprehensive evaluation was conducted on this alloy to characterize its mechanical property behavior and to correlate this behavior with microstructure. The mechanical property tests included tensile, creep rupture, and axial fatigue tests at elevated temperature. Oxidation resistance of the alloy was also characterized. Metallographic analysis was conducted on selected specimens to aid in the interpretation of the mechanical property results.



### 3.0 TASK I - POWDER FOR ALLOY DEVELOPMENT

The objective of this task was to supply iron aluminide powder to AFWAL. The alloy powders were to include FeAl, Fe<sub>3</sub>Al, and twelve ternary alloys based on Fe<sub>3</sub>Al. The FeAl and Fe<sub>3</sub>Al powders were produced by conventional inert gas atomization and sieved into various size fractions to obtain different cooling rates, with smaller particles having faster cooling rates. The ternary alloy powders were produced by the Plasma Rotating Electrode Process (PREP).

#### 3.1 Procurement of FeAl and Fe<sub>3</sub>Al Powders

The Linde Division of Union Carbide Corporation was contracted to produce the inert gas (argon) atomized FeAl and Fe<sub>3</sub>Al powders. A single heat of each of the alloy powders was melted and atomized and the chemical analyses of these two heats are presented in Table I. The following shipment of powder was made to AFWAL.

One container of FeAl powder, -60+140 mesh - 22.7 kg(50 lb)

One container of FeAl powder, -200 mesh - 12.7 kg(28 lb)

One container of Fe<sub>3</sub>Al powder, -60+140 mesh - 18.2 kg(40 lb)

One container of Fe<sub>3</sub>Al powder, -200 mesh - 26.8 kg(59 lb)

Optical metallography of polished cross sections and scanning electron microscopy (SEM) of the FeAl and Fe<sub>3</sub>Al powders were performed to examine the initial microstructure and powder particle characteristics. The powders were examined in size fractions of -60+140 mesh, -140+200 mesh and -200 mesh. Photomicrographs are shown in Figures 2-5 for these powders. For the FeAl alloy, Figures 2-4 show satellite formations (smaller particles attaching themselves to larger particles), particle "capping" (a thin skin formed on solidifying particles as the result of collisions between relatively cool particles and still-molten droplets), and the presence of hollow particles. This alloy is brittle, with numerous examples of grain boundary cracking.

TABLE I

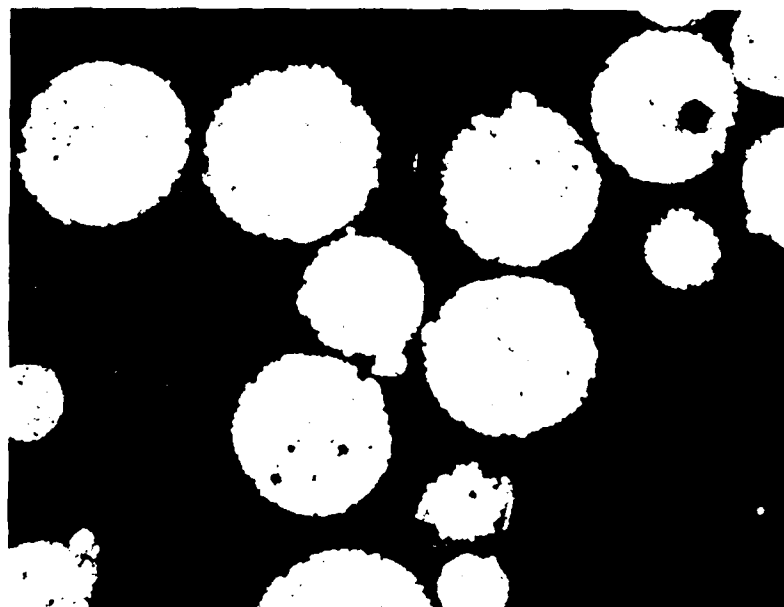
COMPOSITION OF TASK I - INERT GAS ATOMIZED FE-AL POWDERS  
(WEIGHT PERCENT)

---

	$\text{Fe}_3\text{Al}$ (Lot 111381)	$\text{FeAl}$ (Lot 111181)
Fe	85.8	67.9
Al	13.92	31.74
C	0.023	0.017
Co	0.015	0.025
Cr	0.010	0.015
Mo	<0.01	<0.01
Mn	0.085	0.080
Ni	0.021	0.030
Si	0.025	0.045
Ti	<0.01	<0.01
O	0.027	0.026

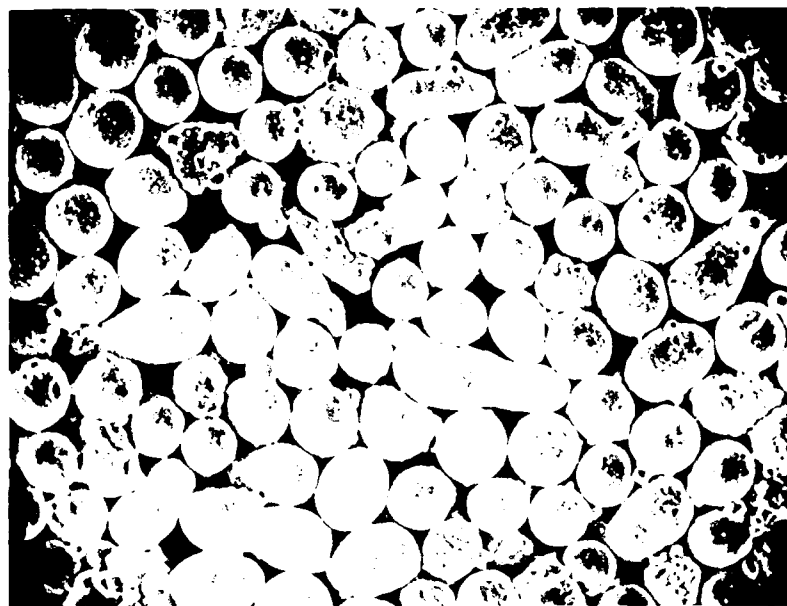


(a)

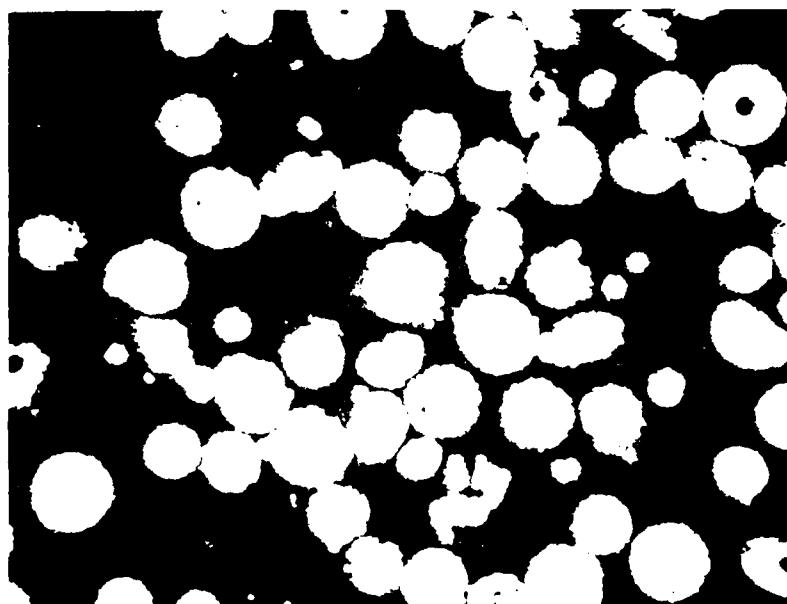


(b)

Figure 2. SEM (a) and light (b) photos of  $-60+140$  mesh size FeAl powder, 100X Magnification.

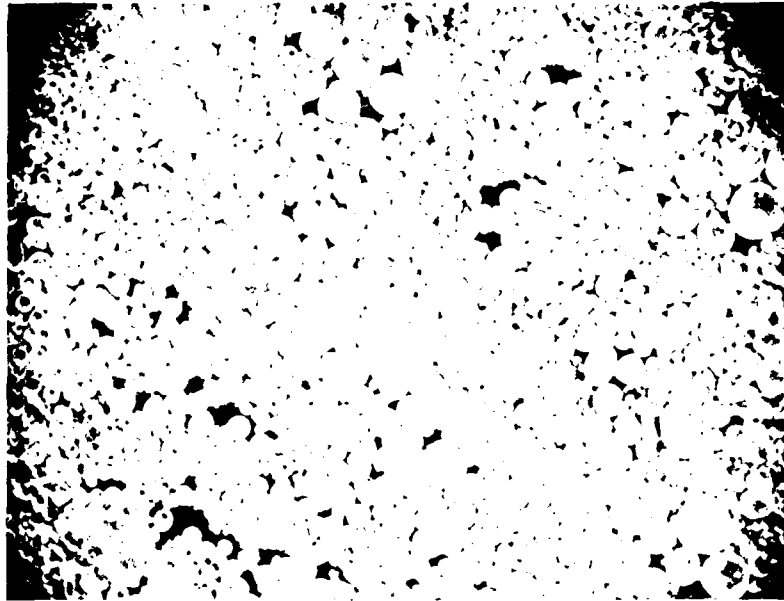


(a)

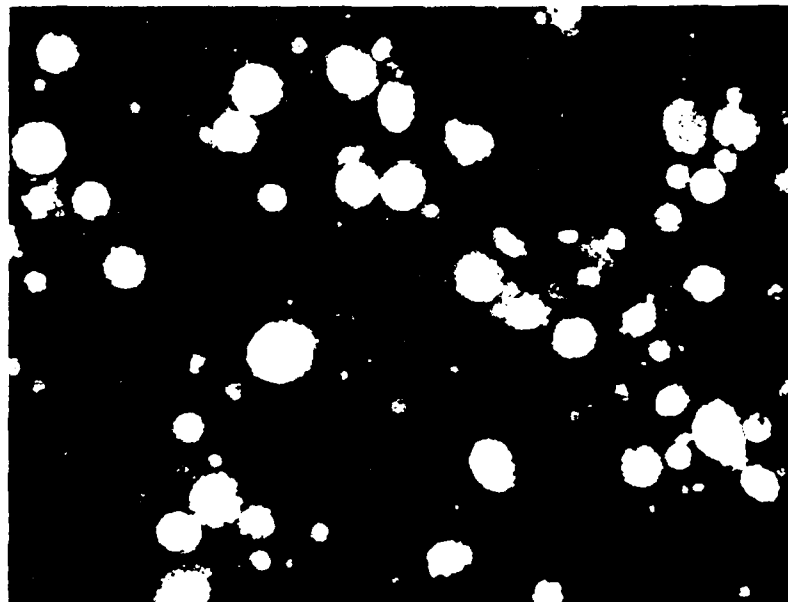


(b)

Figure 3. SEM (a) and light (b) photos of -140+200 mesh size FeAl powder. 100X Magnification.

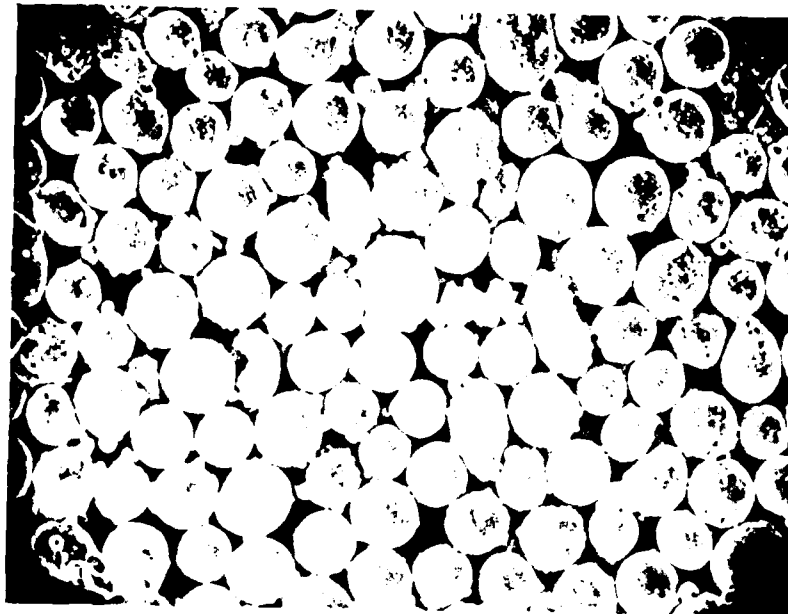


(a)

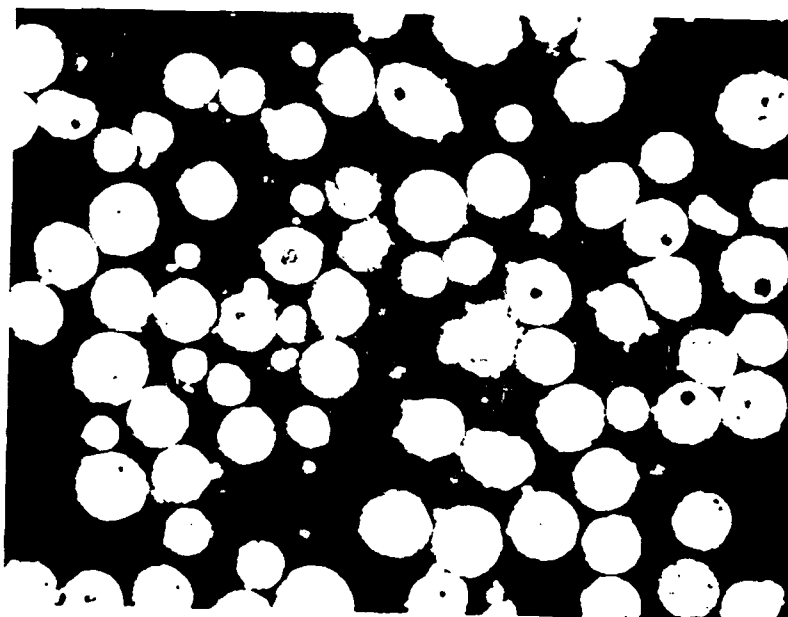


(b)

Figure 4. SEM (a) and Light (b) photos of -200 mesh size FeAl powder. 100X Magnification.



(a)



(b)

Figure 5. SEM (a) and light (b) photos of -140+200 mesh size  $\text{Fe}_3\text{Al}$  powder. 100X Magnification.

This can be observed by the evidence of particle fragments in Figures 2b, 3b, and 4b. There also appears to be a difference in grain structure with particle size. The -140 mesh particles exhibit a finer microstructure than the -60 mesh size particles. However, no chemistry variations were observed by energy dispersive X-ray analysis. Similar general trends were observed in the  $\text{Fe}_3\text{Al}$  powders, Figure 5, particularly the presence of hollow particles and particle "capping".

### 3.2 Procurement of Fe-Al-X Powders

The twelve Fe-Al-X ternary alloy compositions produced as alloy powder by the PREP process are listed in Table II. The final chemistries of the ingot castings used to produce powders are listed in Table III in terms of both weight and atomic percentages. Alloy  $\text{Fe}_{63}\text{Mn}_{12}\text{Al}_{25}$  was off-chemistry as originally cast and a second ingot with the correct chemistry was cast. The castings were machined into stick electrodes for PREP atomization.

At Nuclear Metals, Inc., powder was produced in the short rod rig. Prior to the start of the powder making campaign, the rig was thoroughly cleaned to eliminate the possibility of particle cross-alloy contamination. The twelve alloys listed in Table III were processed sequentially, with chamber cleaning between runs consisting of sweeping and suction cleaning. The chamber was under helium during the PREP runs, but it was exposed to filtered room air during cleaning. Powder was collected in two manners for each run: first, powder was collected in gallon-sized plastic containers while the run was in progress; and second, powder collected during chamber sweeping was bagged in plastic. The former type of powder was sealed under argon, while the latter was exposed to air and possibly contaminated during sweeping and bagging by other alloy powder particles from the previous  $\text{Fe}_3\text{Al}$  alloy runs. The powder yields were low for these alloys, with the Ti-, Si- and V-containing alloys producing chunks as well as powder. The chunks were actually pieces of PREP electrode that broke off due to poor resistance to thermal shock. Grain boundary cracking was evident on many of the stub ends remaining after PREP. Sooting (creation of ultrafine dust) was evident in most alloys, with  $\text{Fe}_{70}\text{Mn}_5\text{Al}_{25}$  alloy causing heavy sooting due to severe casting porosity. The products of the PREP atomization are given in Table IV for these alloys. Due

TABLE II  
TASK I - FE-AL-X ALLOYS

1.  $\text{Fe}_{65}\text{Ti}_{10}\text{Al}_{25}$
2.  $\text{Fe}_{75}\text{Si}_{10}\text{Al}_{15}$
3.  $\text{Fe}_{65}\text{V}_{10}\text{Al}_{25}$
4.  $\text{Fe}_{70}\text{Cr}_5\text{Al}_{25}$
5.  $\text{Fe}_{63}\text{Mn}_{12}\text{Al}_{25}$
6.  $\text{Fe}_{65}\text{Ni}_{10}\text{Al}_{25}$
7.  $\text{Fe}_{70}\text{Cu}_{10}\text{Al}_{20}$
8.  $\text{Fe}_{73}\text{Nb}_2\text{Al}_{25}$
9.  $\text{Fe}_{70}\text{Nb}_5\text{Al}_{25}$
10.  $\text{Fe}_{72}\text{Mo}_3\text{Al}_{25}$
11.  $\text{Fe}_{69}\text{Mo}_6\text{Al}_{25}$
12.  $\text{Fe}_{74}\text{Ta}_1\text{Al}_{25}$



TABLE III  
CHEMICAL COMPOSITION OF TASK I - FE-AL-X ALLOY CASTINGS

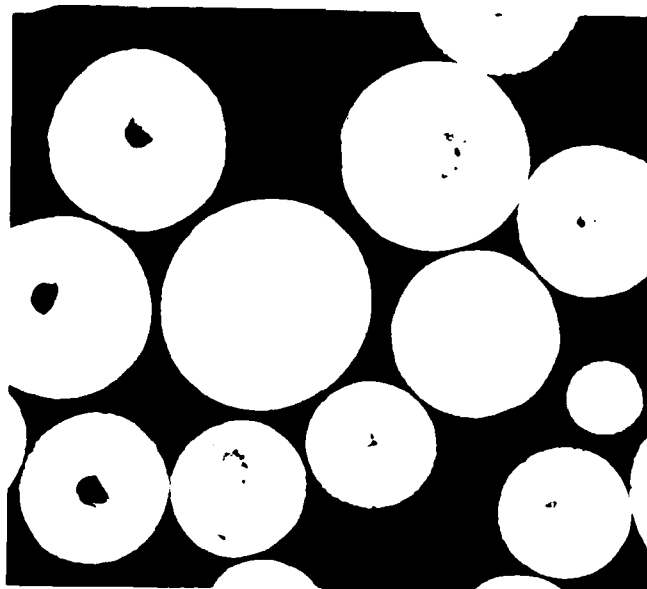
<u>Alloy-Aim</u>	<u>Weight Percentage</u>			<u>Atomic Percentage</u>		
	<u>Fe</u>	<u>Al</u>	<u>X</u>	<u>Fe</u>	<u>Al</u>	<u>X</u>
1. Fe <sub>65</sub> Ti <sub>10</sub> Al <sub>25</sub>	75.8	13.73	10.20	65.28	24.48	10.24
2. Fe <sub>75</sub> Si <sub>10</sub> Al <sub>15</sub>	85.8	8.51	5.45	75.10	15.42	9.49
3. Fe <sub>65</sub> V <sub>10</sub> Al <sub>25</sub>	76.0	14.01	9.84	65.64	25.05	9.32
4. Fe <sub>70</sub> Cr <sub>5</sub> Al <sub>25</sub>	81.2	13.51	5.04	70.87	24.41	4.72
5. Fe <sub>63</sub> Mn <sub>12</sub> Al <sub>25</sub>	80.1	14.19	5.40	69.68	25.55	4.78
5a. Fe <sub>63</sub> Mn <sub>12</sub> Al <sub>25</sub>	72.5	13.63	13.91	63.14	24.58	12.28
6. Fe <sub>65</sub> Ni <sub>10</sub> Al <sub>25</sub>	74.3	13.75	11.74	65.22	24.98	9.80
7. Fe <sub>70</sub> Cu <sub>10</sub> Al <sub>20</sub>	77.2	10.65	11.89	70.38	20.10	9.53
8. Fe <sub>73</sub> Nb <sub>2</sub> Al <sub>25</sub>	83.2	13.46	3.10	73.68	24.67	1.65
9. Fe <sub>70</sub> Nb <sub>5</sub> Al <sub>25</sub>	78.6	13.13	8.04	71.06	24.57	4.37
10. Fe <sub>72</sub> Mo <sub>3</sub> Al <sub>25</sub>	80.6	13.33	5.80	72.24	24.73	3.03
11. Fe <sub>69</sub> Mo <sub>6</sub> Al <sub>25</sub>	75.1	13.16	11.54	68.86	24.98	6.16
12. Fe <sub>74</sub> Ta <sub>1</sub> Al <sub>25</sub>	83.5	13.21	3.08	74.69	24.46	0.85

TABLE IV  
PRODUCTS OF PREP POWDER MAKING OF TASK I - FE-AL-X ALLOYS

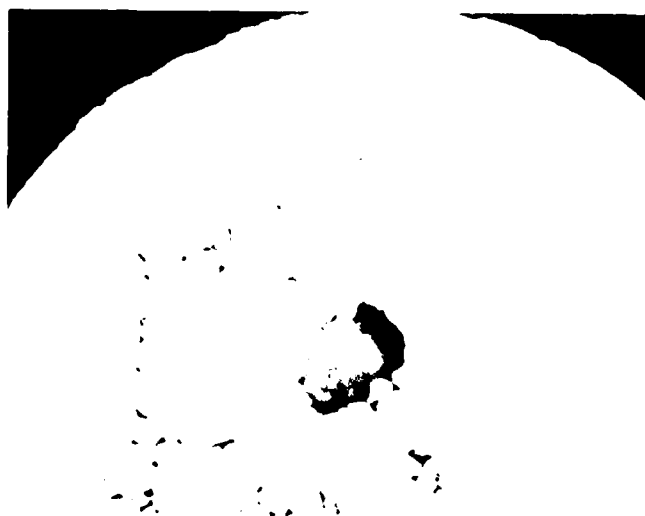
<u>Alloy</u>	<u>Weight of Powder</u>	<u>Weight of Sweep Powder</u>	<u>Weight of Chunks</u>	<u>Weight of Stub Ends</u>
1. Fe <sub>65</sub> Ti <sub>10</sub> Al <sub>25</sub>	2.16 kg	0.07 kg	2.27 kg	2.84 kg
2. Fe <sub>75</sub> Si <sub>10</sub> Al <sub>15</sub>	3.75 kg	0.23 kg	2.16 kg	2.27 kg
3. Fe <sub>65</sub> V <sub>10</sub> Al <sub>25</sub>	2.27 kg	0.23 kg	1.59 kg	1.27 kg
4. Fe <sub>70</sub> Cr <sub>5</sub> Al <sub>25</sub>	6.36 kg	0.11 kg	-	2.61 kg
5. Fe <sub>63</sub> Mn <sub>12</sub> Al <sub>25</sub>	3.30 kg	0.11 kg	-	2.05 kg
5a. Fe <sub>63</sub> Mn <sub>12</sub> Al <sub>25</sub>	5.45 kg	-	-	2.50 kg
6. Fe <sub>65</sub> Ni <sub>10</sub> Al <sub>25</sub>	4.55 kg	0.34 kg	0.68 kg	2.84 kg
7. Fe <sub>70</sub> Cu <sub>10</sub> Al <sub>20</sub>	5.91 kg	0.45 kg	0.05 kg	2.84 kg
8. Fe <sub>73</sub> Nb <sub>2</sub> Al <sub>25</sub>	5.80 kg	0.34 kg	-	2.73 kg
9. Fe <sub>70</sub> Nb <sub>5</sub> Al <sub>25</sub>	5.57 kg	0.34 kg	0.17 kg	3.18 kg
10. Fe <sub>72</sub> Mo <sub>3</sub> Al <sub>25</sub>	5.11 kg	0.34 kg	0.05 kg	3.30 kg
11. Fe <sub>69</sub> Mo <sub>6</sub> Al <sub>25</sub>	5.68 kg	0.51 kg	0.11 kg	2.50 kg
12. Fe <sub>74</sub> Ta <sub>1</sub> Al <sub>25</sub>	5.80 kg	0.34 kg	-	2.95 kg

to the low powder yield, it was decided to use these powders to fulfill the requirements for the Task II - Alloy Development Studies portion of the program.

Samples of the alloy powders were submitted for metallographic examination. Photomicrographs of selected alloys are shown in Figures 6 and 7. Porosity was evident in all alloy powders, both as large centrally located voids as well as finely dispersed interdendritic porosity. Examples of this porosity are shown in Figure 6 for the  $\text{Fe}_{65}\text{V}_{10}\text{Al}_{25}$  alloy. The alloys exhibiting a single phase structure included #1(Ti-10 a/o), #2(Si-10 a/o), #3(V-10 a/o), #4(Cr-5 a/o), #5(Mn-12 a/o), #6(Ni-10 a/o), #7(Cu-10 a/o), #8(Nb-2 a/o), #10(Mo-3 a/o) and #11(Mo-6 a/o). An example of a typical single phase structure is shown in Figure 6, for the 10 a/o V alloy. A second phase was exhibited in the #9(Nb-5 a/o) and #12(Ta-1 a/o) alloys. An example of this structure is shown in Figure 7 for the 5 a/o Nb alloy.

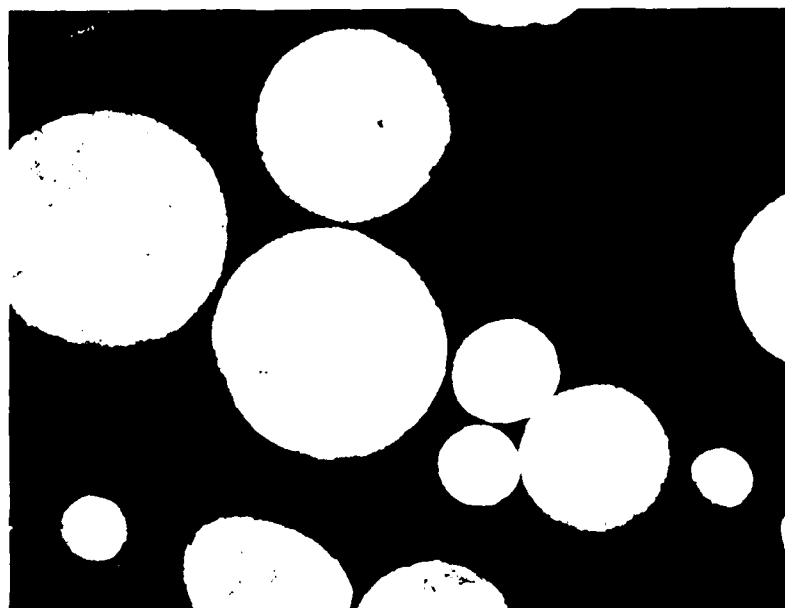


100X

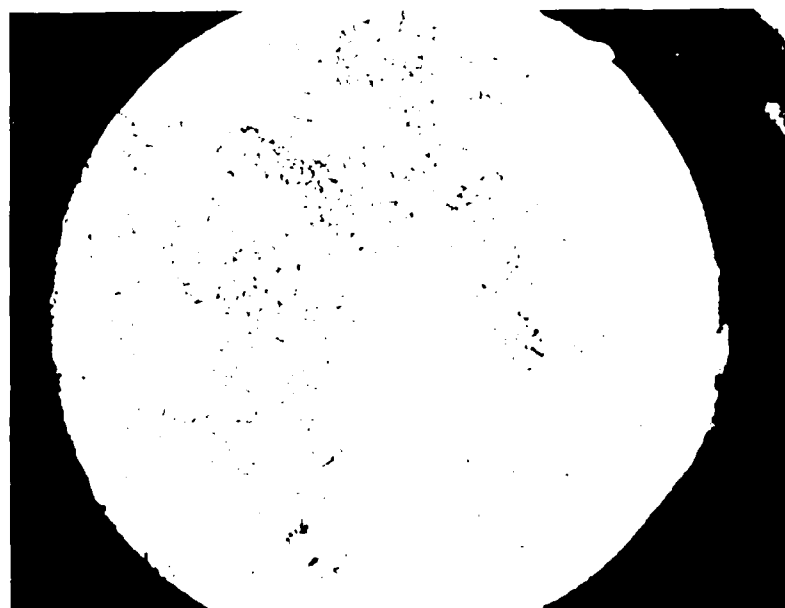


500X

Figure 6. Light photos of PREP Fe-65V-10Al-25 powder showing large central voids and dispersed microporosity.



100X



500X

Figure 7. Light photos of PREP  $\text{Fe}_{70}\text{Nb}_5\text{Al}_{25}$  powder showing presence of second phase precipitates.

#### 4.0 Task II - ALLOY DEVELOPMENT STUDIES

The objective of this task was to characterize the effects of ternary and quaternary alloy additions on  $\text{Fe}_3\text{Al}$ . This was accomplished through a screening evaluation of two experimental series of alloys which involved 21 compositions (including the  $\text{Fe}_3\text{Al}$  as a baseline composition) in the first series and an additional 15 compositions in the second series. As a result of these efforts, an alloy composition was selected for more complete evaluation in the Alloy Characterization portion of this task.

##### 4.1 Series I Alloys

For the Series I effort, twenty one alloy compositions (including the  $\text{Fe}_3\text{Al}$  baseline alloy) were produced in powder form and consolidated by hot extrusion. Some of these alloys were blends of PREP powder with gas atomized  $\text{Fe}_3\text{Al}$ , all produced during the Task I portion of this program and some were solely prealloyed PREP powder. In general, alloy compositions with slow diffusing species, such as Nb, Ta, and Mo, were produced as prealloys. Screening evaluations included mechanical properties characterization, oxidation testing and workability testing.

##### 4.1.1 Alloy Selection

$\text{Fe}_3\text{Al}$  is characterized by a sharp decrease in strength at elevated temperatures. This is due to a phase transformation occurring at a critical temperature  $T_c$ -540 C(1000°F), during which the  $\text{DO}_3$  order is lost. One goal of the alloy design is to increase elevated temperature strength. This may be achieved by increasing  $T_c$  through the addition of alloying elements. To examine the alloying effects on  $\text{Fe}_3\text{Al}$ , transition metals were utilized in the design of the Series I alloys. Elements from Ti through Ni, Zr, Nb, Mo and W substitute for Fe in the  $\text{Fe}_3\text{Al}$  lattice without disrupting the  $\text{DO}_3$  order, although the solubility limits are not known in all cases. Elements Cu, Ge, and Si substitute for Al atoms in the  $\text{DO}_3$  lattice, with Cu and Ge having limited solubility, and Si being completely soluble. On the basis of this general rationale, the Series I alloy compositions listed in Table V were designed with the goal in mind to increase  $T_c$  in order to improve elevated

TABLE V  
TASK II/SERIES I ALLOYS

<u>Alloy</u>	<u>Composition</u>	<u>Method</u>
I-1	$\text{Fe}_{74}\text{Ti}_1\text{Al}_{25}$	Blended $\text{Fe}_3\text{Al}$ and PREP Alloy
I-2	$\text{Fe}_{70}\text{Ti}_5\text{Al}_{25}$	Blended $\text{Fe}_3\text{Al}$ and PREP Alloy
I-3	$\text{Fe}_{70}\text{V}_5\text{Al}_{25}$	Blended $\text{Fe}_3\text{Al}$ and PREP Alloy
I-4	$\text{Fe}_{65}\text{V}_{10}\text{Al}_{25}$	Prealloyed PREP Powder
I-5	$\text{Fe}_{74}\text{Cr}_1\text{Al}_{25}$	Blended $\text{Fe}_3\text{Al}$ and PREP Alloy
I-6	$\text{Fe}_{70}\text{Cr}_5\text{Al}_{25}$	Prealloyed PREP Powder
I-7	$\text{Fe}_{69}\text{Mn}_6\text{Al}_{25}$	Prealloyed PREP Powder
I-8	$\text{Fe}_{63}\text{Mn}_{12}\text{Al}_{25}$	Prealloyed PREP Powder
I-9	$\text{Fe}_{72}\text{Ni}_3\text{Al}_{25}$	Blended $\text{Fe}_3\text{Al}$ and PREP Alloy
I-10	$\text{Fe}_{65}\text{Ni}_{10}\text{Al}_{25}$	Prealloyed PREP Powder
I-11	$\text{Fe}_{73}\text{Nb}_2\text{Al}_{25}$	Prealloyed PREP Powder
I-12	$\text{Fe}_{70}\text{Nb}_5\text{Al}_{25}$	Prealloyed PREP Powder
I-13	$\text{Fe}_{72}\text{Mo}_3\text{Al}_{25}$	Prealloyed PREP Powder
I-14	$\text{Fe}_{69}\text{Mo}_6\text{Al}_{25}$	Prealloyed PREP Powder
I-15	$\text{Fe}_{74}\text{Ta}_1\text{Al}_{25}$	Prealloyed PREP Powder
I-16	$\text{Fe}_{70}\text{Ta}_5\text{Al}_{25}$	Prealloyed PREP Powder
I-17	$\text{Fe}_{72}\text{Cu}_5\text{Al}_{23}$	Blended $\text{Fe}_3\text{Al}$ and PREP Alloy
I-18	$\text{Fe}_{70}\text{Cu}_{10}\text{Al}_{20}$	Prealloyed PREP Powder
I-19	$\text{Fe}_{75}\text{Si}_3\text{Al}_{22}$	Blended $\text{Fe}_3\text{Al}$ and PREP Alloy
I-20	$\text{Fe}_{75}\text{Si}_5\text{Al}_{20}$	Blended $\text{Fe}_3\text{Al}$ and PREP Alloy
Baseline	$\text{Fe}_3\text{Al}$	Gas Atomized Powder

temperature strength retention. As part of this evaluation, it was recognized that the assessment should include the rate and amount of Tc increase as well as a definition of solubility limits and the effects of possible precipitation from solid solution.

The three alloy categories included in the design were:

- 1)  $\text{Fe}_{3-x}\text{T}_x\text{Al}$ , where the transition metal substitutes for Fe to maintain  $\text{DO}_3$  order.
- 2)  $\text{Fe}_3\text{T}_x\text{Al}_{1-x}$ , where the non-transition metal substitutes for both Fe and Al to maintain the  $\text{DO}_3$  order.
- 3)  $\text{Fe}_{3-x}\text{T}_x(\text{AlSi})$ , where Si substitutes for Al at all Si levels and the transition metal substitutes for Fe to maintain the  $\text{DO}_3$  ordered structure.

Certain of the Series I alloys were designed as prealloyed compositions while others were designed as blends of prealloyed Task I compositions with inert gas atomized  $\text{Fe}_3\text{Al}$ . The selection was made on the basis of overall economics regarding the atomization of this large a number of experimental compositions.

#### 4.1.2 Material Procurement/Processing

##### 4.1.2.1 Powder Atomization

The twelve alloys from the Task I portion of this program served as master alloys for certain of the Task II Series I compositions. Additional heats of alloys (Mn-6 a/o and Ta-5 a/o) were melted and cast to make up the remainder of the Series I alloys. These alloys were cast into rod shapes approximately 55 mm (2 inches) in diameter and approximately 150 mm (6 inches) long. These castings were centerless ground and processed into spherical powder by the PREP process employing procedures described previously in Section 3.2. Metallographic analyses conducted on these powders revealed characteristics similar to those of the Task I alloys. Certain of these



characteristics will be discussed in the following section on Hot Extrusion Consolidation as pertaining specifically to various characteristics observed in the as-extruded structures. For the blended compositions, appropriate powders were blended, using -200 mesh  $\text{Fe}_3\text{Al}$  and -40 mesh PREP master alloy powder. For the completely prealloyed compositions, the PREP powders were sieved to remove the +40 mesh fraction prior to use. All sieving and blending was performed in a glove box under a protective argon atmosphere.

#### 4.1.2.2 Hot Extrusion Consolidation

Consolidation of the twenty one Series I alloys was accomplished by hot extrusion. Mild steel tubing with an outer diameter of 6.6 cm (2.6 inches) and an inner diameter of 3.3 cm (1.3 inches) was procured and sectioned into 13.2 cm (5.2 inch) lengths for extrusion cans. The thick wall served to contain the alloy powders. Nose and tail pieces were machined from mild steel bar stock, with an evacuation port being drilled through the center of the nose. Tail pieces were welded onto the thick wall tube prior to powder filling.

Based on input from the AFWAL project engineer, a stainless steel foil liner was inserted into each extrusion container before powder filling. The liner was coated on the outside with magnesia to prevent bonding of the mild steel to the stainless steel. In this manner, excessive tensile stresses induced by cooling due to thermal expansion differences between mild steel and the alloy powders were avoided. A schematic diagram of the extrusion can configuration is shown in Figure 8.

The filled containers were hot degassed and sealed by electron-beam welding of the evacuation hole. The chamber of the electron-beam welder was equipped with a furnace to heat the extrusion cans to  $400^{\circ}\text{C}$  ( $752^{\circ}\text{F}$ ) while the chamber was being evacuated. Once the temperature and a vacuum of  $10^{-4}$  torr were stabilized, the container was sealed. In general, the outgassing rate began to exceed the evacuation rate at a temperature of approximately  $260^{\circ}\text{C}$  ( $500^{\circ}\text{F}$ ).

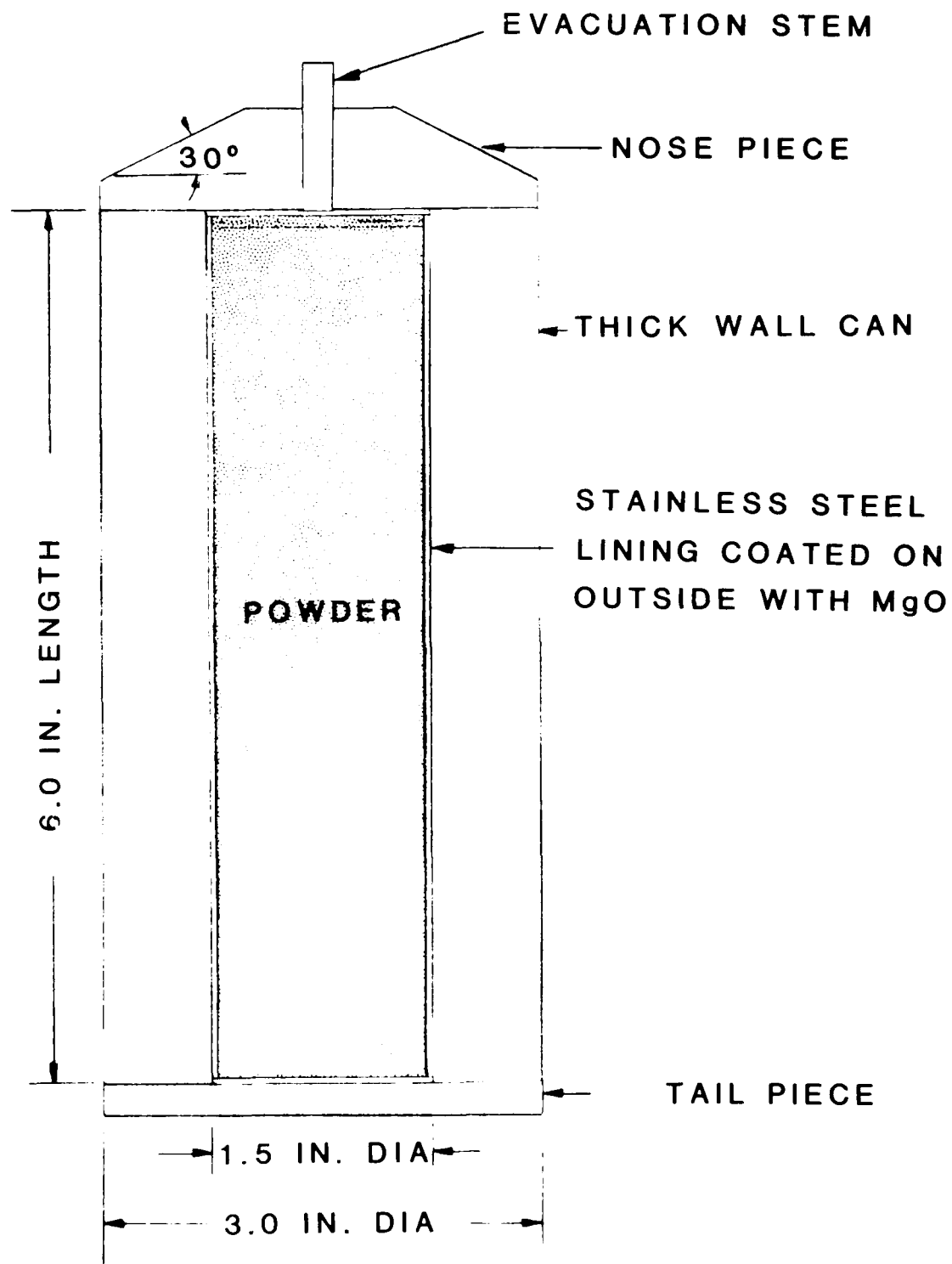


Figure 8. Schematic illustration of extrusion can configuration used for consolidation of Task II/Series I alloy powders.

The extrusion conditions were:

- o Preheat extrusion billet at 1120<sup>0</sup>C (2050<sup>0</sup>F) for 90 minutes
- o Preheat extrusion press container and die 400<sup>0</sup>C (752<sup>0</sup>F)
- o Extrude through a nominal 1.7 cm (0.70 inch) diameter conical die (extrusion reduction ratio- 16:1)
- o Cool extruded rod in sand until black
- o Remove extrusion from sand and air cool to room temperature

The extrusion billets were spray coated with a MgO lubricant prior to preheating. With the exception of the 10 a/o V alloy, the extrusion campaign proceeded without incident. A slight pinging sound was heard during cooling after the extrusion operation, indicating the possibility of cracking. This was confirmed during subsequent metallographic examination of the extrusions. The chemical analyses of the twenty one Series I alloys are presented in Table VI, which includes the aim chemistry for comparison purposes. An error was discovered in the blending of the powders for several of the alloys and in the extrusion can loading for several of the alloys. These errors resulted in a number of quaternary, instead of ternary alloys. This occurred for alloys I-6 (Cr-5 a/o), I-13 (Mo-3 a/o), I-19 (Si-3 a/o) and I-20 (Si-5 a/o). In addition to this, several other ternary alloys were found to be off chemistry with respect to the desired composition. In particular, Alloys I-5 (Cr-1 a/o) and I-14 (Mo-6 a/o) were found to contain less than the intended alloy addition. Preparation of all of these particular alloys was not repeated because it was felt that meaningful information could be derived from these compositions which could be applied to the subsequent Series II alloys.

The initial metallographic analysis conducted on the extruded alloys revealed the presence of particles which appeared to be non-metallic inclusions. The blended alloys, which contained gas-atomized Fe<sub>3</sub>Al powder, in particular, contained large numbers of these particles. Interstitial content analyses were conducted to aid in the possible identification of these constituents and the results are shown in Table VII. The values, however, were somewhat lower than had been anticipated on the basis of the apparent high volume fraction of particles appearing throughout the microstructure. It

TABLE VI  
CHEMICAL COMPOSITION OF TASK II/SERIES I ALLOY EXTRUSIONS

Alloy	Aim	Weight Percentage				Atomic Percentage			
		Fe	Al	X	Y	Fe	Al	X	Y
I-1	Fe <sub>74</sub> Ti <sub>1</sub> Al <sub>25</sub>	85.4	13.74	0.50Ti		74.63	24.86	0.51Ti	
I-2	Fe <sub>70</sub> Ti <sub>5</sub> Al <sub>25</sub>	81.2	13.63	5.15Ti		70.34	24.44	5.21Ti	
I-3	Fe <sub>70</sub> V <sub>5</sub> Al <sub>25</sub>	80.0	13.70	6.08V		69.55	24.66	5.78V	
I-4	Fe <sub>65</sub> V <sub>10</sub> Al <sub>25</sub>	73.2	13.60	13.12V		63.25	24.32	12.43V	
I-5	Fe <sub>74</sub> Cr <sub>1</sub> Al <sub>25</sub>	86.2	12.76	0.49Cr		76.19	23.35	0.47Cr	
I-6	Fe <sub>70</sub> Cr <sub>5</sub> Al <sub>25</sub>	83.0	13.05	3.51Cr	0.47Mo	72.76	23.70	3.31Cr	0.24Mo
I-7	Fe <sub>69</sub> Mn <sub>6</sub> Al <sub>25</sub>	79.5	14.40	6.02Mn		68.87	25.82	5.30Mn	
I-8	Fe <sub>63</sub> Mn <sub>12</sub> Al <sub>25</sub>	72.6	13.08	14.26Mn		63.59	23.72	12.70Mn	
I-9	Fe <sub>72</sub> Ni <sub>3</sub> Al <sub>25</sub>	82.0	13.74	3.98Ni		71.79	24.90	3.31Ni	
I-10	Fe <sub>65</sub> Ni <sub>10</sub> Al <sub>25</sub>	74.6	12.90	12.47Ni		65.92	23.60	10.48Ni	
I-11	Fe <sub>73</sub> Nb <sub>2</sub> Al <sub>25</sub>	83.2	12.82	3.92Nb		74.22	23.67	2.10Nb	
I-12	Fe <sub>70</sub> Nb <sub>5</sub> Al <sub>25</sub>	78.2	12.45	9.29Nb		71.38	23.52	5.10Nb	
I-13	Fe <sub>72</sub> Mo <sub>3</sub> Al <sub>25</sub>	82.5	14.78	0.58Mo	2.12Cr	71.30	26.44	0.29Mo	1.97Cr
I-14	Fe <sub>69</sub> Mo <sub>6</sub> Al <sub>25</sub>	81.1	12.75	4.39Mo		73.69	23.98	2.32Mo	
I-15	Fe <sub>74</sub> Ta <sub>1</sub> Al <sub>25</sub>	84.3	12.87	2.68Ta		75.42	23.84	0.74Ta	
I-16	Fe <sub>70</sub> Ta <sub>5</sub> Al <sub>25</sub>	69.1	11.74	19.02Ta		69.61	24.48	5.91Ta	
I-17	Fe <sub>72</sub> Cu <sub>5</sub> Al <sub>23</sub>	81.9	11.74	6.33Cu		73.28	21.74	4.98Cu	
I-18	Fe <sub>70</sub> Cu <sub>10</sub> Al <sub>20</sub>	77.8	10.03	12.09Cu		71.25	19.02	9.73Cu	
I-19	Fe <sub>75</sub> Si <sub>3</sub> Al <sub>22</sub>	86.3	11.96	1.36Si	0.21Cr	75.71	21.72	2.37Si	0.20Cr
I-20	Fe <sub>75</sub> Si <sub>5</sub> Al <sub>20</sub>	85.9	11.10	2.14Si	0.53Cr	75.55	20.21	3.74Si	0.50Cr
Baseline	Fe <sub>3</sub> Al	87.0	12.86	-		76.57	23.43	-	

# TASK VII

## INTERSTITIAL CONTENT OF TASK II/SERIES I ALLOY EXTRUSIONS

<u>Alloy</u>	<u>Composition</u>	<u>Carbon (ppm)</u>	<u>Oxygen (ppm)</u>	<u>Nitrogen (ppm)</u>
I-1	Fe <sub>74</sub> Ti <sub>1</sub> Al <sub>25</sub>	120	420	13
I-2	Fe <sub>70</sub> Ti <sub>5</sub> Al <sub>25</sub>	130	300	5
I-3	Fe <sub>70</sub> V <sub>5</sub> Al <sub>25</sub>	290	250	13
I-4	Fe <sub>65</sub> V <sub>10</sub> Al <sub>25</sub>	<100	140	16
I-5	Fe <sub>74</sub> Cr <sub>1</sub> Al <sub>25</sub>	<100	270	11
I-6	Fe <sub>70</sub> Cr <sub>5</sub> Al <sub>25</sub>	<100	75	<5
I-7	Fe <sub>69</sub> Mn <sub>6</sub> Al <sub>25</sub>	<100	<5	<5
I-8	Fe <sub>63</sub> Mn <sub>12</sub> Al <sub>25</sub>	100	130	13
I-9	Fe <sub>72</sub> Ni <sub>3</sub> Al <sub>25</sub>	110	160	12
I-10	Fe <sub>65</sub> Ni <sub>10</sub> Al <sub>25</sub>	<100	28	5
I-11	Fe <sub>73</sub> Nb <sub>2</sub> Al <sub>25</sub>	<100	49	5
I-12	Fe <sub>70</sub> Nb <sub>5</sub> Al <sub>25</sub>	<100	160	7
I-13	Fe <sub>72</sub> Mo <sub>3</sub> Al <sub>25</sub>	<100	60	<5
I-14	Fe <sub>69</sub> Mo <sub>6</sub> Al <sub>25</sub>	<100	62	<5
I-15	Fe <sub>74</sub> Ta <sub>1</sub> Al <sub>25</sub>	<100	130	32
I-16	Fe <sub>70</sub> Ta <sub>5</sub> Al <sub>25</sub>	<100	58	6
I-17	Fe <sub>72</sub> Cu <sub>5</sub> Al <sub>23</sub>	<100	320	140
I-18	Fe <sub>70</sub> Cu <sub>10</sub> Al <sub>20</sub>	<100	82	<5
I-19	Fe <sub>75</sub> Si <sub>3</sub> Al <sub>22</sub>	100	300	11
I-20	Fe <sub>75</sub> Si <sub>5</sub> Al <sub>20</sub>	<100	160	11
Baseline	Fe <sub>3</sub> Al	170	120	11

is believed that the inclusions may be principally alumina, which is an extremely stable compound and may not be entirely reduced by the method of analysis, a gas fusion technique using a Leeco Determinator, used for this evaluation.

The as-extruded microstructure of baseline  $\text{Fe}_3\text{Al}$  (transverse section) is shown in Figure 9. This structure is characterized by an equiaxed ASTM 5-6 grain size as well as the presence of large numbers of non-metallic inclusions.

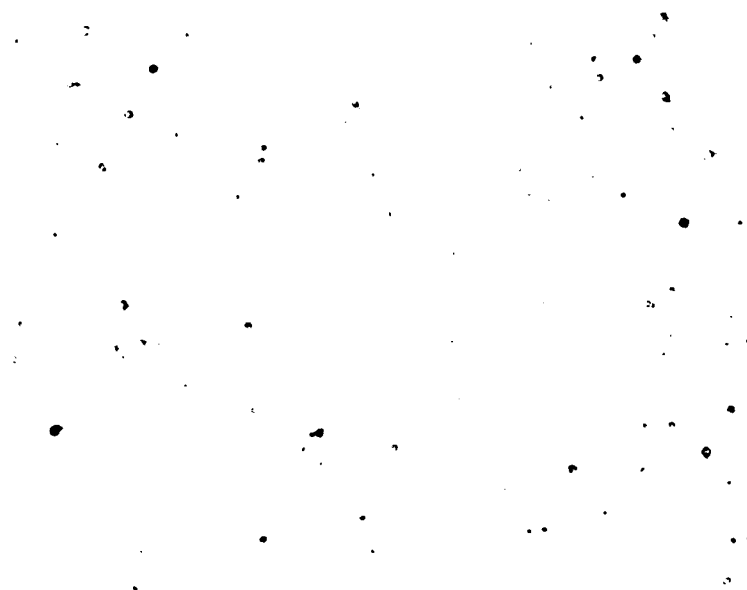
Both of the Ti-containing alloys were prepared by blending, which resulted in a non-homogeneous microstructure. An example of this structure is shown in Figure 10 (transverse section) for the 5 a/o Ti alloy. This degree of non-homogeneity suggests the need for subsequent homogenization heat treatments.

The microstructures of the two V-containing alloys are shown in Figures 11 and 12. The 5 a/o V alloy (Figure 11) was produced by blending and exhibits a non-homogeneous microstructure, suggesting the need for subsequent homogenization heat treatments. A large number of non-metallic inclusions are also evident in this microstructure. The 10 a/o V alloy (Figure 12) was a prealloyed powder and suffered severe cracking during cool down from the extrusion temperature, despite the  $\text{MgO}$  coating. As shown in Figure 12, this cracking was predominantly intergranular in nature.

The Cr-containing alloys displayed unique features upon metallographic examination. In addition to the presence of non-metallic inclusions, regions of light-etching, ghost-like areas were revealed in the structure of the blended 1 a/o Cr alloy, Figure 13. These regions of apparent non-homogeneity did not inhibit the formation of recrystallized grains upon extrusion, as grain boundaries can be observed to continue through the light-etching areas. Furthermore, these light-etching areas are present in the prealloyed 5 a/o Cr alloy, again with grain boundaries being discernable through the areas, Figure 14. The SEM micrograph in Figure 14 indicates that these areas stand above the well etched matrix. Energy dispersive X-ray analysis suggests that these areas may be Cr-depleted.



100X



500X

Figure 9. Light photos of as-extruded Fe<sub>3</sub>Al baseline alloy (transverse section) showing presence of non-metallic inclusions.



100X



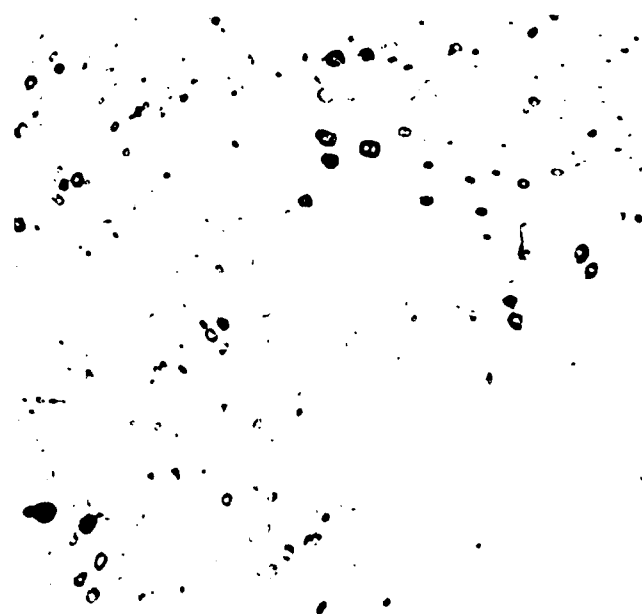
500X

Figure 10. Light photos of as-extruded Ti-5 a/o (Alloy I-2) powder blend (transverse section) showing presence of non-metallic inclusions.





100X



500X

Figure 11. Light photos of as-extruded V-5 a/o (Alloy i-3) powder blend (transverse section) showing presence of non-metallic inclusions and non-homogeneous structure.



100X



200X



500X

Figure 12. Light (100X Magnification) and SEM (200X, 500X Magnification) photos of as-extruded V-10 a/o (Alloy I-4) prealloyed powder (transverse section) showing predominantly intergranular cracking.



100X



500X

Figure 13 (a & b). Light photos of as-extruded Cr-1 a/o (Alloy I-5) powder blend (transverse section) showing presence of non-metallic inclusions and non-homogeneous etching structure.



200X

Figure 13 (c). SEM photo of as-extruded Cr-1 a/o (Alloy I-5) powder blend (transverse section) showing overlapping of continuous grain boundaries by non-homogeneous etching structure.



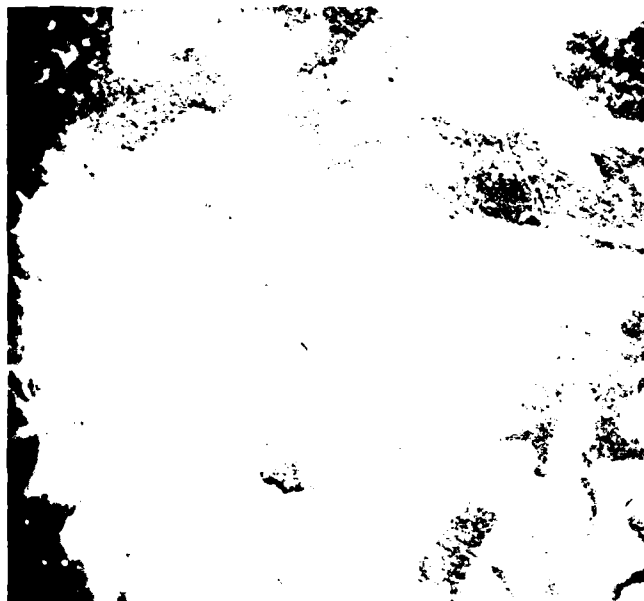
100X

This micrograph shows a transverse section of as-extruded Cr-5 alloy powder. The image displays a distribution of dark, non-metallic inclusions and a non-homogeneous etching structure across the field of view.

500X

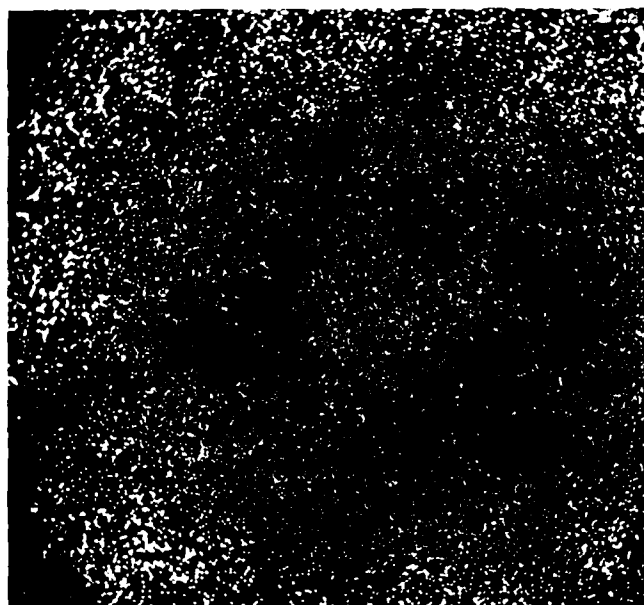
This micrograph provides a higher magnification view of the same material, showing more detail of the non-metallic inclusions and the non-homogeneous etching structure.

Figure 14 (a & b). Light photos of as-extruded Cr-5 a/o (Alloy I-6) prealloyed powder (transverse section) showing presence of non-metallic inclusions and non-homogeneous etching structure.



SEM

200X



Chromium Map

200X

Figure 14 (c & d). SEM and EDAX photos of as-extruded Cr-5 a/o (Alloy 1-6) powder (transverse section) showing areas of chromium depletion.

Both of the Mn-containing alloys were prepared as prealloyed powders. The general characteristics of both extruded microstructures were similar, with each exhibiting an equiaxed grain size with non-metallic inclusions both within the matrix and decorating prior powder particle boundaries. An example of the typical structure is shown in Figure 15 (transverse section) for the 6 a/o alloy. The grain size of the higher Mn-alloy was finer than that of the low Mn-alloy (ASTM 5 vs. ASTM 4-5) and the matrix appeared to contain fewer non-metallic inclusions. The distribution of these non-metallic inclusions appeared to be a function of the dendritic solidification of the PREP powder.

The 3 a/o Ni alloy was prepared as a blend and the as-extruded structure, shown in Figure 16, indicates considerable non-homogeneity and suggests the need for post-extrusion homogenization heat treatments. The 10 a/o Ni alloy was prepared as a prealloyed powder and the as-extruded structure, shown in Figure 17, displays an equiaxed ASTM 6 grain size, with a non-metallic inclusion decoration on the prior powder particle boundaries.

Metallographic analysis of both the Nb-containing alloys revealed that the as-extruded microstructures were characterized by a uniform second phase precipitate. The as-extruded structure of the 2 a/o Nb alloy is shown in Figure 18. Because the low solid solubility of Nb in  $\text{Fe}_3\text{Al}$  resulted in the formation of fine precipitates in the extruded structure, it was of interest to determine whether these particles were present in the PREP powder. As shown in Figure 19, light metallography was unable to resolve the presence of any second phases in the powder. SEM analysis, however, revealed the presence of second phase particles measuring at maximum approximately 2 microns in length and 0.5 microns in width. Figure 20 indicates that these particles were observed both within the grain boundaries as well as within the interdendritic regions of the grains themselves. EDAX analysis indicated that these particles were rich in Nb.

Examination of the as-extruded 5 a/o Nb alloy indicated that the extrusion operation modified the morphology of the second phase precipitates observed in the PREP powder. An example of the as-extruded microstructure is shown in Figure 21. Comparison of this structure with that shown in Figure 22 for the PREP powder reveals that the film type morphology evident in the PREP



100X

This micrograph shows a transverse section of Mn-6 alloy powder at 100X magnification. The image displays a distribution of dark, irregularly shaped non-metallic inclusions scattered across a lighter, granular matrix. These inclusions are primarily located along the boundaries of the powder particles, which appear as a network of fine, interconnected lines.

500X

This micrograph shows a transverse section of Mn-6 alloy powder at 500X magnification. The image provides a more detailed view of the powder particles and the non-metallic inclusions. The particles are smaller and more distinct than in the 100X view, and the inclusions are more clearly visible as dark, elongated features along the particle boundaries.

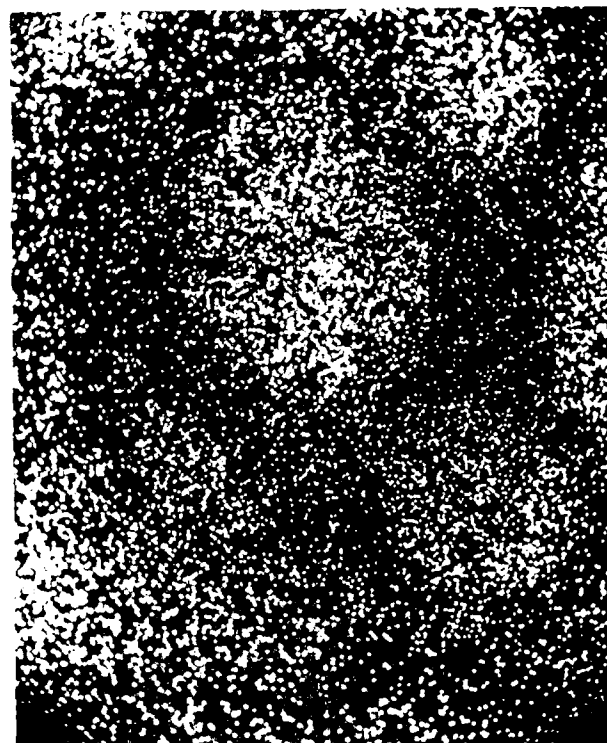
Figure 15. Light photos of as-extruded Mn-6 a/o (Alloy I-7) prealloyed powder (transverse section) showing non-metallic inclusions decorating prior particle boundaries.





SEM

200X



Nickel Map

200X



100X

Figure 16. SEM, 100X and 200X magnification of fractured surface of powder metallurgy 304 stainless steel. The fracture surface is highly irregular and textured, with many sharp edges and deep, jagged cracks.



100X



500X

Figure 17. Light photos of as-extruded Ni-10 a/o (Alloy I-10) prealloyed powder (transverse section) showing non-metallic inclusions decorating prior particle boundaries.

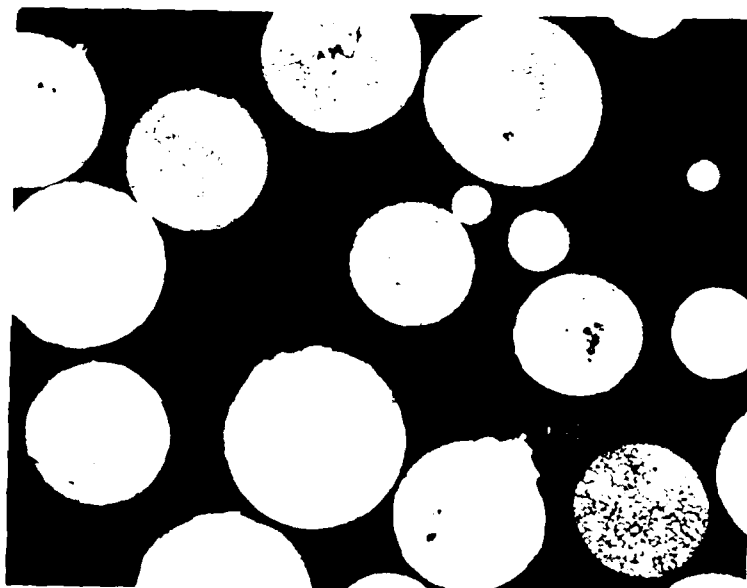


100X



500X

Figure 18. Light photos of as-extruded Nb-2 a/o (Alloy I-11) prealloyed powder (transverse section) showing presence of second phase precipitate particles.

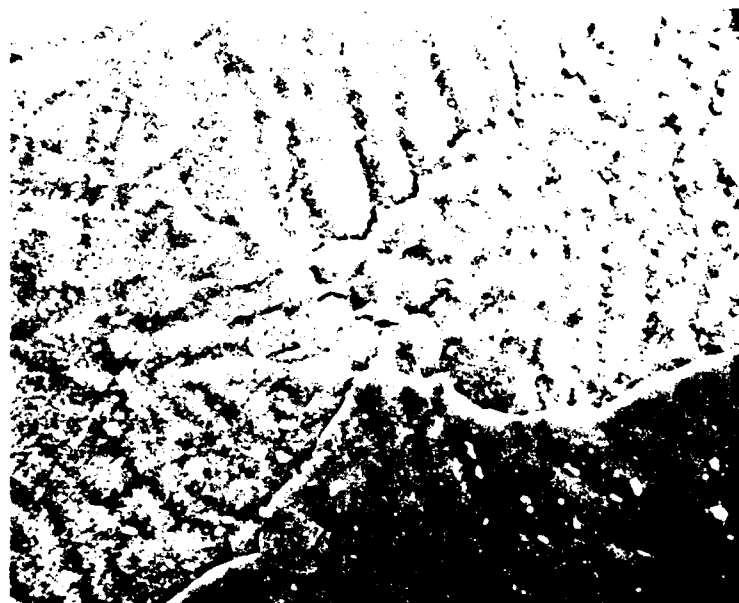


(a) 100X

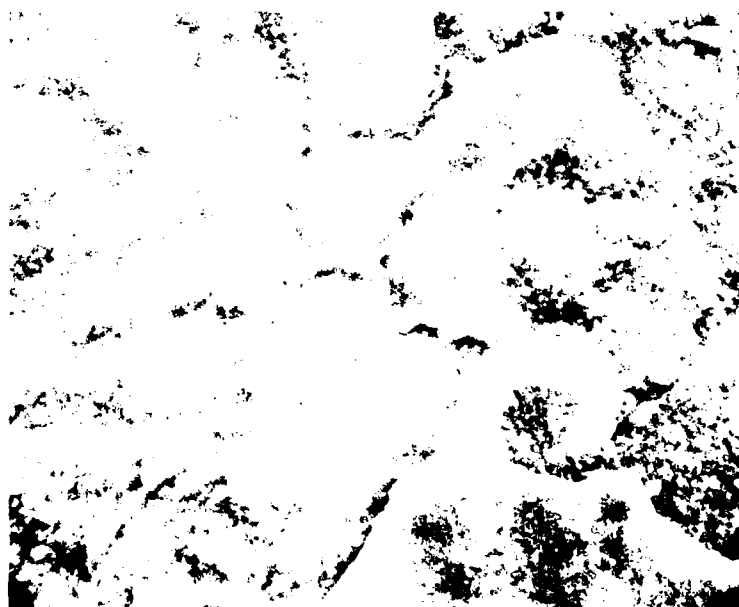


(b) 500X

Figure 19. Light photos of PREP Nb-2 a/o (Alloy I-11) powder.

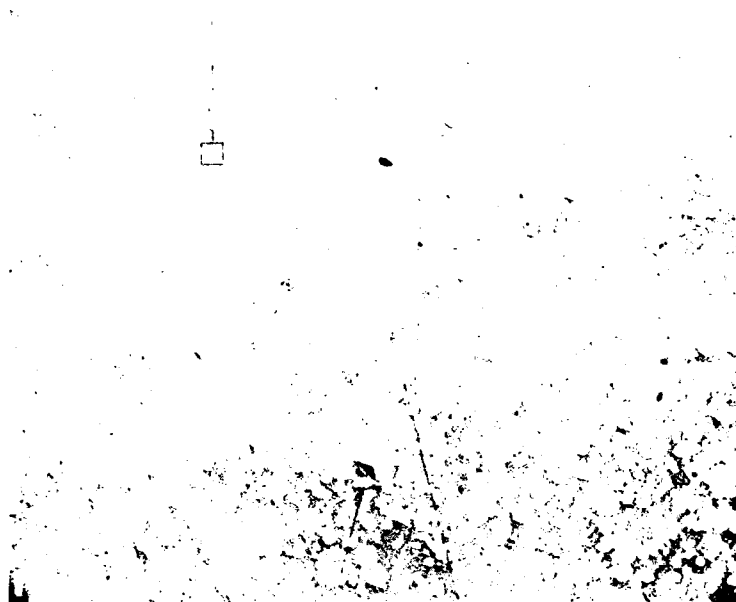


(a) 2000X Magnification

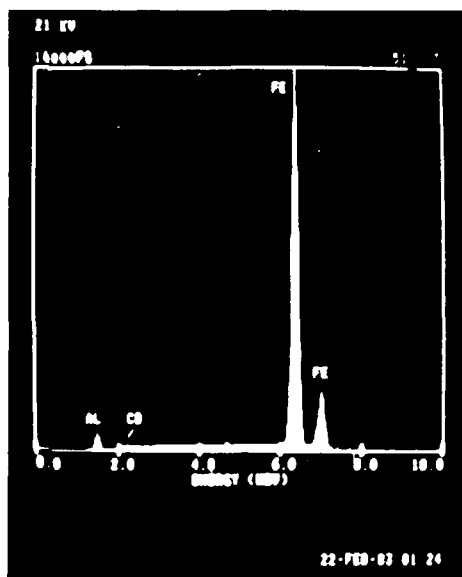


(b) 5000X Magnification

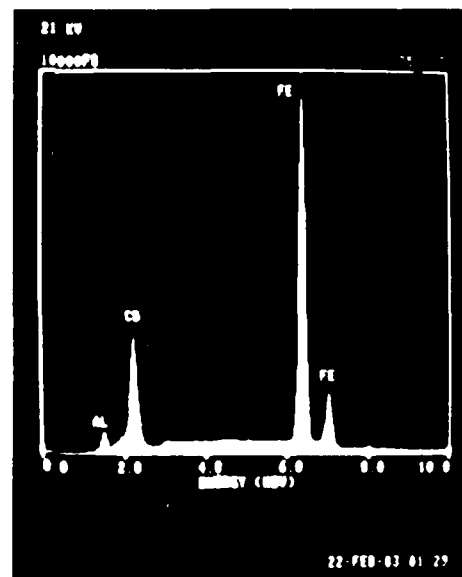
Figure 20. SEM photos of PREP Nb-2 a/o (Alloy I-11) powder showing presence of second phase precipitate particles in grain boundary and interdendritic regions.



(a) SEM Photo at 1000X Magnification



(b) EDAX Analysis of Matrix Region



(c) EDAX Analysis of Precipitate

Figure 21. SEM and EDAX photos of as-extruded Nb-5 a/o (Alloy I-12) prealloyed powder (transverse section).



(a) 2000X Magnification



(b) 5000X Magnification

Figure 22. SEM photos of PREP Nb-5 a/o (Alloy 1-12) powder showing presence of second phase precipitate particles and continuous films.

powder was modified to a discrete particle type morphology during extrusion. The discrete particles (1-3 microns in diameter) are uniformly distributed and are quite high in Nb, as shown by the EDAX analysis also included in Figure 21. Analysis of the dark appearing microconstituent in Figure 21a indicated this to be a region of microporosity filled with mounting compound. The presence of the Nb rich particles suggests that this alloy could potentially be strengthened by precipitation hardening.

The two Mo-containing alloys were produced as prealloys and exhibited significantly different microstructures. The structure of the 3 a/o Mo alloy, shown in Figure 23, exhibited a highly non-uniform attack during etching, indicating chemical inhomogeneity. The presence of Cr was observed, as was established by the chemical analyses reported in Table VI. The microstructural features of this alloy are similar in respects to those observed in the 5 a/o Cr alloy, shown previously in Figure 14. This may reflect the fact that the 3 a/o Mo alloy is, in fact, a quaternary, with only 0.3 a/o Mo and 2 a/o Cr. The 6 a/o Mo alloy, shown in Figure 24, exhibited a homogeneous structure, with an equiaxed ASTM 4 grain size.

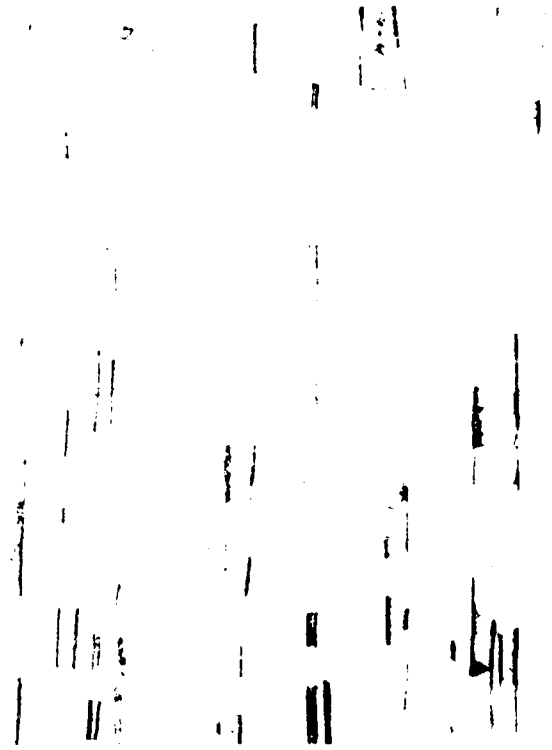
Analysis of the Ta-containing alloys indicated that the solubility limit was exceeded by increasing the Ta level from 1 a/o to 5 a/o. The as-extruded microstructure of the 1 a/o Ta alloy, shown in Figure 25, exhibits a particle-free matrix, with considerable evidence of prior powder particle decoration. Analysis of the as-extruded microstructure of the 5 a/o Ta alloy indicated that similar to the 5 a/o Nb alloy, a change occurred in the second phase particle morphology during extrusion of the PREP powder. Specifically, the film type morphology changed to a discrete type morphology. As shown in Figure 26, however, the 5 a/o Ta alloy exhibited a duplex type of structure. This included the discrete type particles as well as the larger irregularly shaped particles which were retained from the PREP powder shown in Figure 27. EDAX confirmed that both types of precipitates were rich in Ta, with a somewhat higher concentration in the larger particles. The shape of the large particles suggests that they were retained from the cast structure of the master metal ingot electrodes used for the PREP process. It would seem unlikely that modification of the extrusion parameters would be effective in altering the morphology of these larger particles.





Transverse

100X



Longitudinal

100X



Transverse

200X

Figure 23. Light (100X Magnification) and SEM (200X Magnification) photos of as-extruded Mo-3 a/o (Alloy I-13) prealloyed powder showing presence of non-homogeneous etching structure.

100X

500X



200X

Figure 24. Light (100X, 500X Magnification) and SEM (200X Magnification) photos of as-extruded Mo-6 a/o (Alloy I-14) prealloyed powder (transverse section).



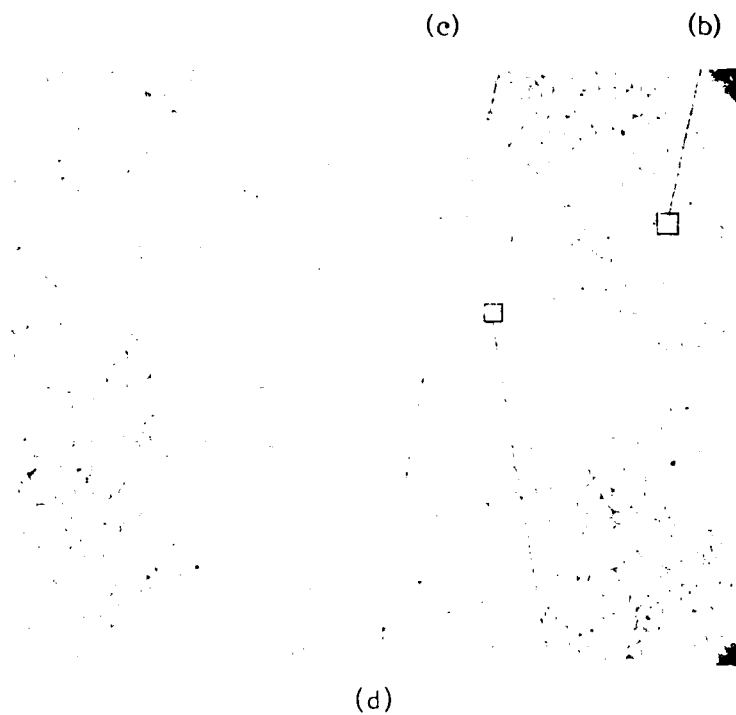
100X

500X

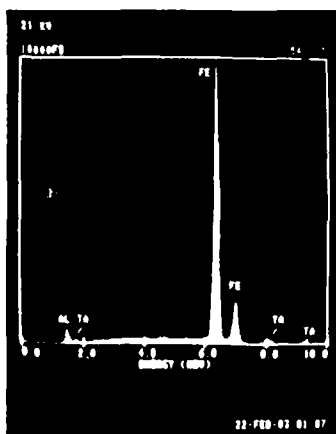


200X

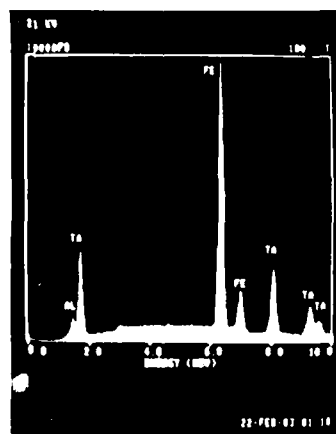
Figure 25. Light (100X, 500X Magnification) and SEM (200X Magnification) photos of as-extruded Ta-1 a/o (Alloy I-15) prealloyed powder (transverse section) showing presence of non-metallic inclusions decorating prior particle boundaries.



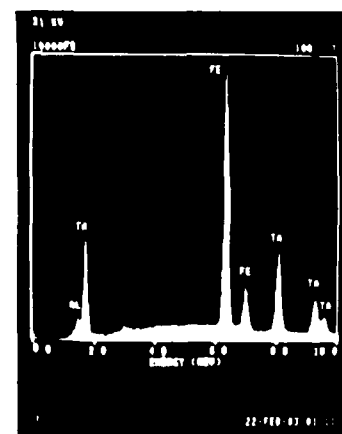
(a) SEM Photo at 1000X Magnification



(b) EDAX Analysis of Matrix Region



(c) EDAX Analysis of Fine Precipitate



(d) EDAX Analysis of Large Particle

Figure 26. SEM and EDAX photos of as-extruded Ta-5 a/o (Alloy 1-16) prealloyed powder (transverse section).



(a) 2000X Magnification



(b) 5000X Magnification

Figure 27. SEM photos of PREP Ta-5 a/o (Alloy I-16) prealloyed powder showing presence of duplex second phase particle distribution.

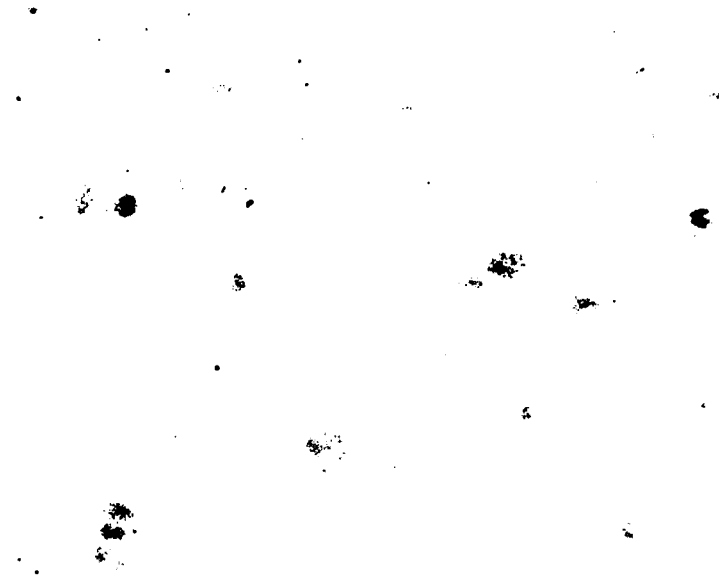
Analysis of the Cu-containing alloys indicated that both alloys exhibited an equiaxed grain size of approximately ASTM 6-7. The 5 a/o Cu alloy was free of second phase particles. The 10 a/o Cu alloy, however, exhibited a fine dispersion of a second phase as well as a film along the grain boundaries, Figure 28. As shown in the high magnification SEM photo in Figure 29a, the grain boundary regions exhibited a film type precipitate as well as a precipitate free zone adjacent to the grain boundary. EDAX analysis was conducted on this structure and the results are also presented in Figure 29. Analysis of the grain interior (including the matrix and fine precipitates) compared to the precipitate free zone suggested a slight depletion of Cu in the precipitate free zone. The grain boundary film appeared to be enriched in Cu compared to the precipitate free zone, but was approximately comparable to the Cu content in the grain interior.

Both of the Si-containing alloys were prepared as blends and both exhibited similar microstructures in the as-extruded condition. An example of this structure for the 3 a/o Si alloy is shown in Figure 30. This alloy exhibited an equiaxed ASTM 5 grain size and a dispersion of non-metallic inclusion particles.

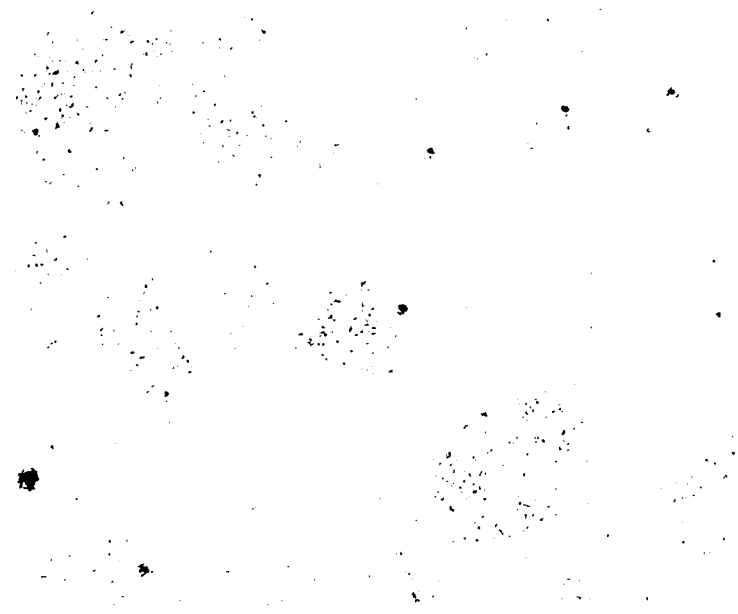
#### 4.1.2.3 Summary of SRL Studies

TRW was teamed with Systems Research Laboratories, Inc. (SRL) on this program with SRL responsible for in-depth metallographic characterization of alloys under study. The SRL efforts are presented in detail in Appendix I. A summary of their findings is presented in this section and includes homogenization studies, a screening of the  $DO_3$ -B2 transition temperatures ( $T_c$ ) for the various alloys as well as a characterization of the precipitation behavior of the Nb containing alloys.

Homogenization of selected blended alloys (5 a/o Ti, 3 a/o Ni), and the prealloyed 3 a/o Mo alloy, which was also found to contain Cr, was achieved via a  $1100^{\circ}\text{C}$  ( $2012^{\circ}\text{F}$ ) hold for 168 hours (1 week). Chemical homogeneity was confirmed and abnormal grain growth was not observed in the alloys tested.

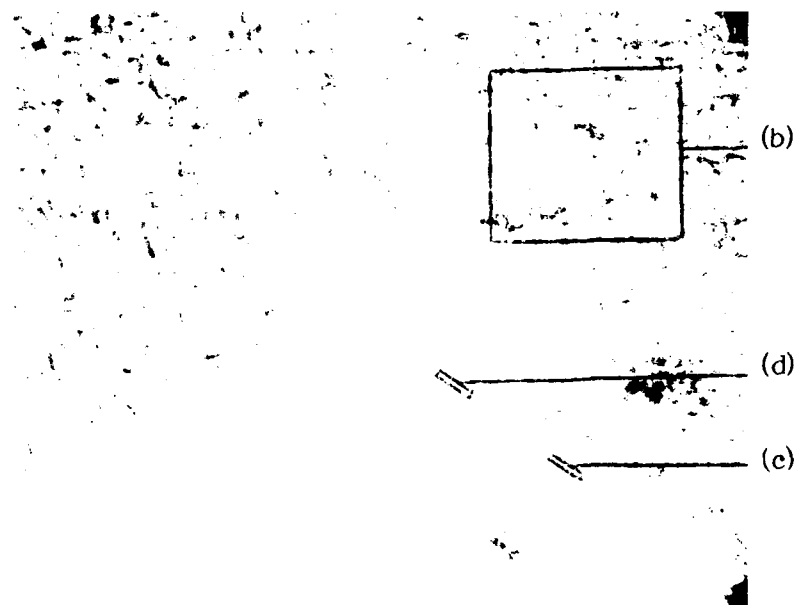


(a) 100X

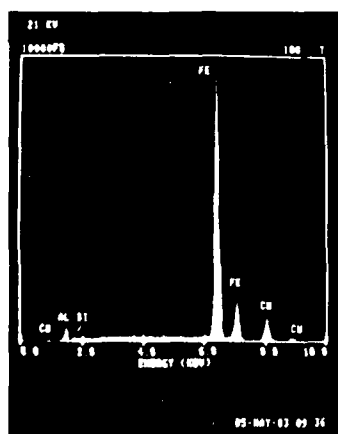


(b) 500X

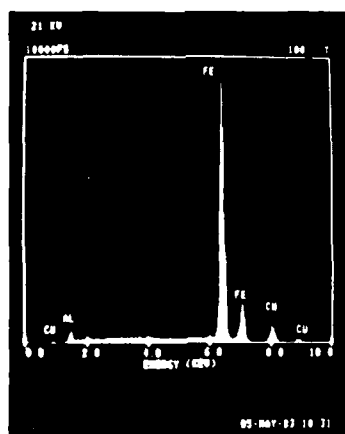
Figure 28. Light photos of as-extruded Cu-10 a/o (Alloy I-18) prealloyed powder (transverse section).



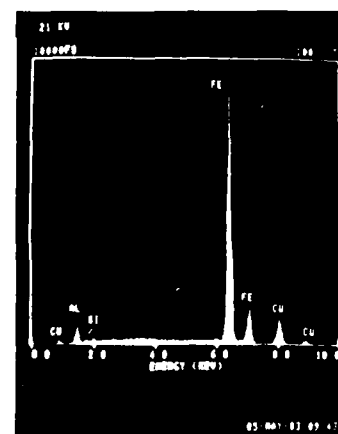
(a) SEM Photo at 5000X Magnification



(b) EDAX Analysis of Grain Interior



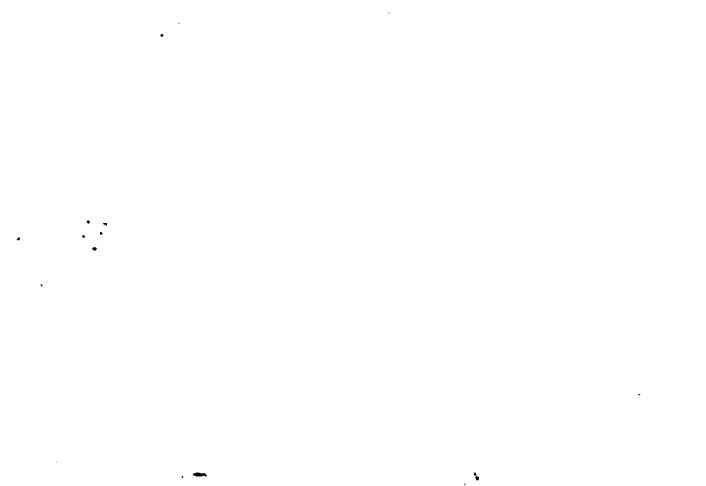
(c) EDAX Analysis of Precipitate Free Zone



(d) EDAX Analysis of Grain Boundary Film

Figure 29. SEM and EDAX photos of as-extruded Cu-10 a/o (Alloy I-18) prealloyed powder (transverse section).





100X



500X

Figure 30. Light photos of as-extruded Si-3 a/o (Alloy I-19) powder blend (transverse section) showing presence of non-metallic inclusions.

Studies were conducted to establish the effect of the additions on the transition temperature of the  $\text{Fe}_3\text{Al}$  baseline alloy. These efforts included a determination of whether  $T_c$  was higher or lower than  $600^\circ\text{C}$  ( $1112^\circ\text{F}$ ) and, in cases where  $T_c$  was higher, to determine the approximate temperature range within which  $T_c$  might fall. The results indicated that a number of additions increase  $T_c$  above  $600^\circ\text{C}$  ( $1112^\circ\text{F}$ ).  $T_c$  increases were observed for the 5 a/o Ti alloy, the 5 a/o Cr alloy, the 6 a/o Mn alloy, the 12 a/o Mn alloy, the 10 a/o Ni alloy, the 3 a/o Mo alloy, the 3 a/o Si alloy and the 5 a/o Si alloy. The greatest increase in  $T_c$  was observed in the 5 a/o Si alloy, with the  $T_c$  falling within the range  $700\text{--}725^\circ\text{C}$  ( $1292\text{--}1337^\circ\text{F}$ ) for this alloy. There was little correlation, however, between  $600^\circ\text{C}$  ( $1112^\circ\text{F}$ ) tensile strength and changes in  $T_c$  values. This suggested that factors other than the stabilization of the  $\text{DO}_3$  phase to a higher temperature control high temperature strength in these alloys.

Characterization of the precipitation behavior of the Nb containing alloys indicated that these systems offer potential for increased strength at elevated temperature compared to the  $\text{Fe}_3\text{Al}$  baseline alloy. The strength increase was thought to be associated with the precipitation of a uniform distribution of coherent second phase particles. This phase was metastable with respect to the equilibrium phase having a chemistry  $\text{Fe}_{56}\text{Al}_{19}\text{Nb}_{25}$ . The equilibrium phase was found to be isostructural with the known  $\text{Fe}_2\text{Nb}$  phase. While the limit of thermal stability for this phase was not established, there does appear to be significant potential to exploit this phase for significant strength improvements in these alloy systems.

#### 4.1.2.4 Homogenization Studies

As shown in Table V, eight of the twenty-one Series I alloy compositions were prepared by a powder blending approach in which prealloyed powder was mixed with gas atomized  $\text{Fe}_3\text{Al}$  to produce the desired compositions. Due to the nature of the hot extrusion consolidation operation, the bar stock was cooled too rapidly to achieve satisfactory elemental diffusion and, hence, there was insufficient homogenization of the alloying additions. Homogenization heat treatments were, thus, investigated for the blended alloys. In addition to the blended alloys, homogenization was also applied to the 5 a/o Cr and 3 a/o

Mo prealloyed compositions, because of inadvertent mixing during extrusion billet canning resulting in the non-homogeneous structures discussed previously in Section 4.1.2.2. The objective of the homogenization studies was to develop heat treatments resulting in microstructures suitable for the subsequent alloy evaluations.

On the basis of studies conducted at SRL, the initial homogenization efforts included heat treatments in argon at  $1100^{\circ}\text{C}$  ( $2012^{\circ}\text{F}$ ) for 168 hours (1 week) followed by cooling in air. These treatments were conducted on several selected alloy compositions. Examination of these specimens after the homogenization treatment indicated that a satisfactory distribution of the alloying elements was achieved. This was determined from the results of EDAX analyses conducted at various locations in different grains across the cross section of specimens prepared from the heat treated material.

In spite of this success in achieving homogenization, certain microstructural features observed in the heat treated material suggested that  $1100^{\circ}\text{C}$  ( $2012^{\circ}\text{F}$ )/168 hours may not be a desirable homogenization treatment. These features included the occurrence of abnormal grain growth resulting in a relatively small number of very large (up to 3000 microns) grains throughout the microstructure. An example of this type of structure is shown in Figure 31 for the 5 a/o Cr alloy. It was anticipated that this large a grain size would not offer attractive strength properties. Another feature also shown in this figure is the occurrence of porosity in the structure. this is thought to be thermally induced porosity (tip) which is caused by the coalescence of residual inert gases which are present in hollow powder particles as well as absorbed on particle surfaces. while the exact effects of tip upon the strength properties of  $\text{Fe}_{3}\text{Al}$  alloys is not well documented, it was thought desirable to maintain as low a tip level as possible in these structures consistent with adequate homogenization.

Because of these results, subsequent studies were conducted at lower temperatures in order to achieve satisfactory homogenization, but eliminate the condition of abnormal grain growth and minimize the occurrence of tip in the microstructure. for this work, the 1 a/o cr and the 3 a/o ni alloys were given a 168 hour (1 week) treatment at  $1000^{\circ}\text{C}$  ( $1832^{\circ}\text{F}$ ) in argon, followed by cooling in air.

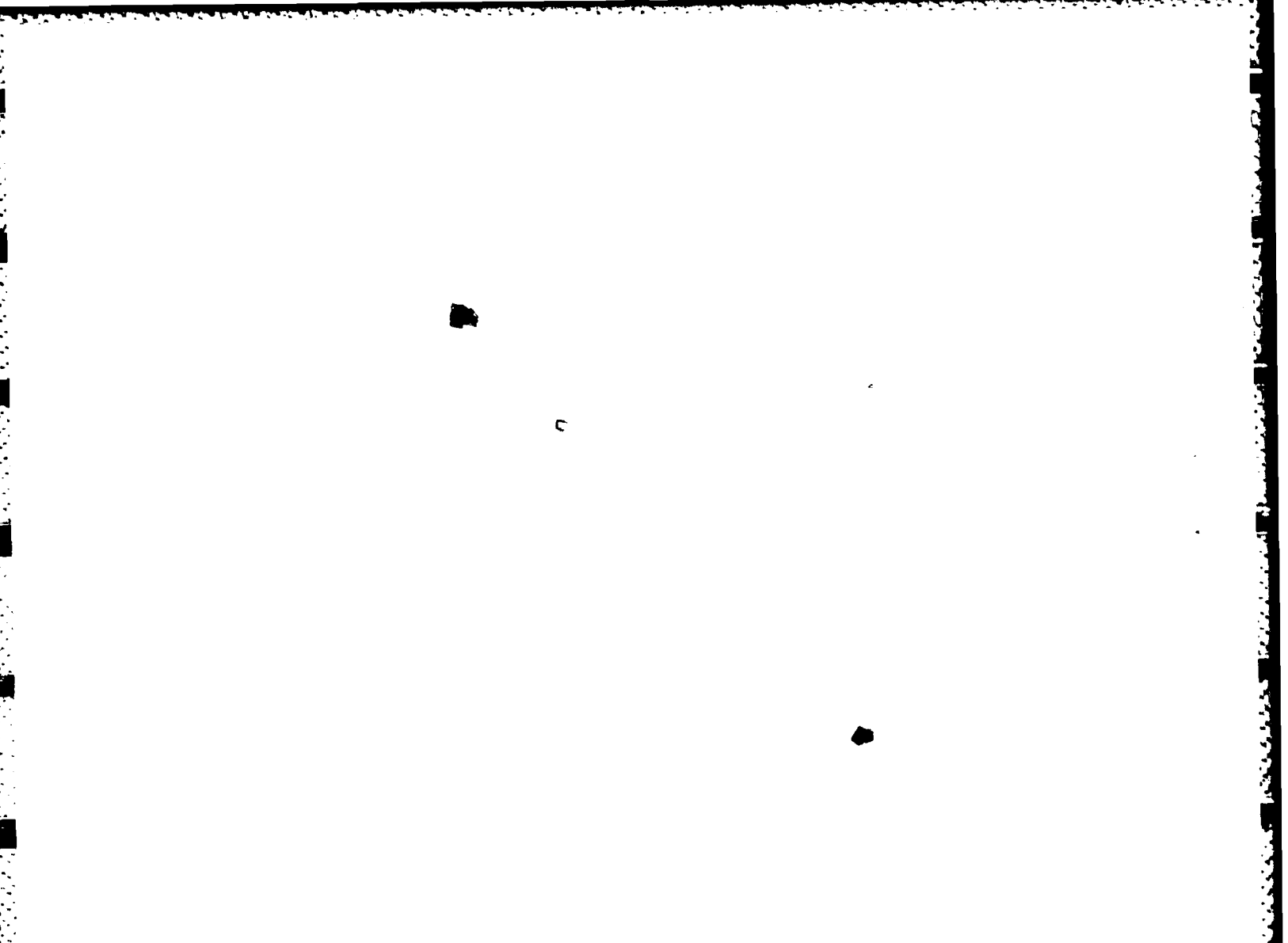



Figure 31. Light photo of Cr-5 a/o (Alloy I-6) prealloyed powder homogenized 168 Hours at 1100°C (2012°F). 100X Magnification.


EDAX analyses of these alloys indicated that the 1000°C (1832°F) treatment was successful in homogenizing the elemental distribution throughout the microstructure. This was established by analysis at various locations in different grains throughout the cross section of the specimens. Microstructural analysis indicated that the alloys homogenized at 1000°C (1832°F) did not exhibit excessive grain growth during the treatment. An example of this is shown for the 1 a/o Cr alloy in Figure 32, which displays an equiaxed grain size of approximately ASTM 4-7 (average size of 50 microns). This is essentially unchanged from that exhibited in the as-extruded material. TIP was observed in both alloys, but was reduced in both pore size and volume fraction with respect to that observed after the higher temperature heat treatment.

Samples of each blended alloy were then exposed to 1000°C (1832°F) for one week and examined for chemical homogeneity using Electron Dispersive Spectroscopy (EDS). These included the blends of prealloyed powder with argon atomized Fe<sub>3</sub>Al and the accidental blends of prealloyed Cr/Mo containing powders. All of the alloys, except the 3 a/o Ni composition, were shown to be homogenized. This evaluation included analysis of a minimum of five different grains, along an arbitrary line through a polished metallographic specimen and comparison of the height of characteristic X-ray peaks of the alloying elements. Light metallographic analysis indicated that the average as-extruded grain size and grain size distribution were not measurably altered by this heat treatment. Thermally induced pores observed in the as-polished surfaces were generally less than 25 microns in diameter. This lack of abnormal grain growth and excessive TIP, as compared to homogenized samples at 1100°C (2012°F), suggested that the alloys were acceptable for subsequent evaluations.

The 3 a/o Ni alloy still exhibited significant chemical inhomogeneity with respect to nickel after the 1000°C (1832°F)/one week thermal treatment. An additional heat treatment was, therefore, investigated, including an exposure at 1050°C (1922°F) for one week. EDS analysis indicated that this heat treatment produced sufficient chemical homogeneity without causing TIP or abnormal grain growth.



(a) 100X Magnification



(b) 500X Magnification

Figure 32. Light photos of Cr-1 a/o (Alloy I-5) powder blend homogenized 168 Hours at 1000<sup>0</sup>C (1832<sup>0</sup>F).

#### 4.1.3 Screening Evaluations

Screening evaluations were conducted on the twenty-one Series I alloys which included tensile tests, oxidation tests, and workability tests. The results of these screening evaluations are presented in the following sections.

##### 4.1.3.1 Tensile Test Results

The program objective included the development of alloy modifications based on  $\text{Fe}_3\text{Al}$  which offer improved room temperature ductility and high temperature strength compared to the baseline alloy. Tensile screening tests were performed at room temperature and  $600^\circ\text{C}$  ( $1112^\circ\text{F}$ ). The blended alloys were homogenized with the appropriate heat treatment, as discussed in Section 4.1.2.4, followed by a 24-hour hold at  $500^\circ\text{C}$  ( $932^\circ\text{F}$ ), recommended by SRL to ensure that complete  $\text{DO}_3$  ordering was achieved. Prealloys were given only the ordering heat treatment following extrusion. A schematic diagram of the test specimen configuration is shown in Figure 33. Single tests were conducted at each test temperature and the results which are summarized in Tables VIII and IX include ultimate tensile strength, 0.2% offset yield strength, percent elongation and percent reduction of area. These data are plotted in bar graph form in Figure 34, showing the effect that each alloying addition had upon the most critical properties of the baseline material. These properties are elevated temperature yield strength and room temperature yield strength and ductility. Subsequent to testing, one-half of each specimen was mounted and examined to aid in the interpretation of the data.

##### 4.1.3.1.1 $\text{Fe}_3\text{Al}$ Baseline Alloy

The unalloyed  $\text{Fe}_3\text{Al}$  baseline material exhibited an ultimate tensile strength of approximately 894 MPa (129.7 Ksi) and a yield strength of 674 MPa (97.7 Ksi) with ductility values of less than 8% at room temperature. Examination of the failed test specimen revealed that there was little deformation of the grains and that separation occurred primarily along the grain boundaries. Some evidence of cracking along slip lines was also observed. An example of this structure is shown in Figure 35 which displays the region near the fracture surface at two different magnifications. The

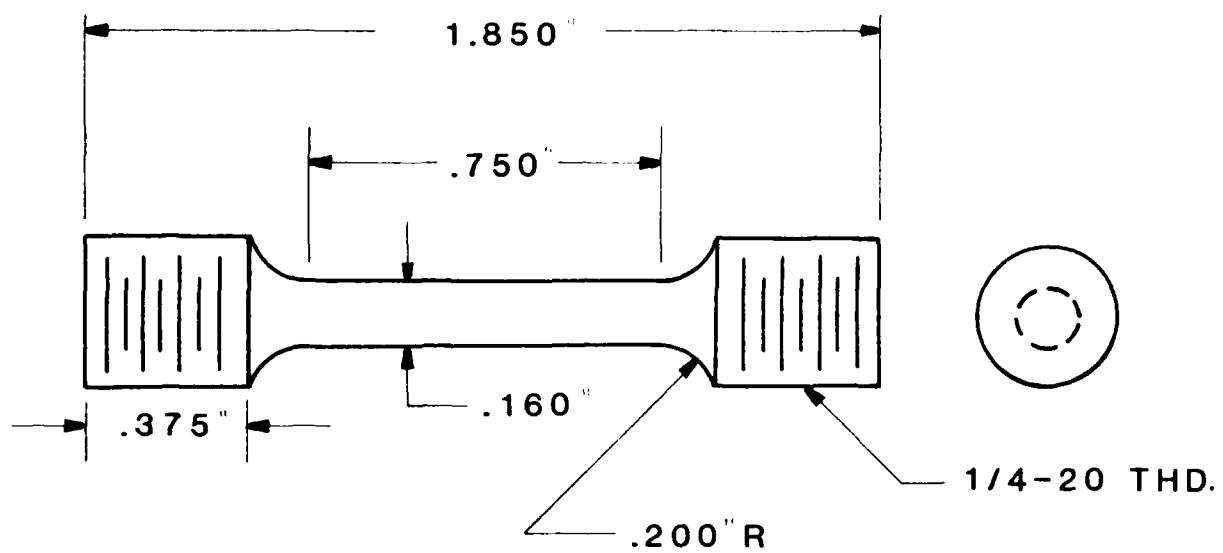


Figure 33. Schematic Illustration of Tensile Test Specimen Configuration.



TABLE VIII

## ROOM TEMPERATURE TENSILE DATA FOR TASK II/SERIES I ALLOYS

Alloy	Composition	Ultimate Tensile Strength		0.2% Yield Strength		% Elongation	% Reduction Area
		(MPa)	(Ksi)	(MPa)	(Ksi)		
I-1	Fe <sub>74</sub> Ti <sub>1</sub> Al <sub>25</sub>	878	127.4	725	105.2	1.4	3.1
I-2	Fe <sub>70</sub> Ti <sub>5</sub> Al <sub>25</sub>	785	113.9	736	106.8	0.5	1.8
I-3	Fe <sub>70</sub> V <sub>5</sub> Al <sub>25</sub> (1)						
I-4	Fe <sub>65</sub> V <sub>10</sub> Al <sub>25</sub> (1)						
I-5	Fe <sub>74</sub> Cr <sub>1</sub> Al <sub>25</sub>	926	134.3	743	107.7	1.7	3.7
I-6	Fe <sub>70</sub> Cr <sub>5</sub> Al <sub>25</sub>	638	92.5	261	37.8	4.8	6.2
I-7	Fe <sub>69</sub> Mn <sub>6</sub> Al <sub>25</sub> (2)	463	67.2	250	36.3	3.4	3.8
		(2) 624	90.5	260	37.7	5.2	3.7
I-8	Fe <sub>63</sub> Mn <sub>12</sub> Al <sub>25</sub> (2)	283	41.0	230	33.3	1.9	0.7
		(2) 46	6.6	46	6.6	-	-
I-9	Fe <sub>72</sub> Ni <sub>3</sub> Al <sub>25</sub> (2)	494	71.7	494	71.7	0.2	-
I-10	Fe <sub>65</sub> Ni <sub>10</sub> Al <sub>25</sub>	647	93.9	647	93.9	0	0
I-11	Fe <sub>73</sub> Nb <sub>2</sub> Al <sub>25</sub>	1106	160.4	881	127.7	1.7	3.1
I-12	Fe <sub>70</sub> Nb <sub>5</sub> Al <sub>25</sub> (3)	1127	163.5	1049	152.1	-	-
		(3) 1265	183.4	1052	152.5	0.4	0.6
I-13	Fe <sub>72</sub> Mo <sub>3</sub> Al <sub>25</sub>	294	39.8	219	31.8	1.1	2.5
I-14	Fe <sub>69</sub> Mo <sub>6</sub> Al <sub>25</sub>	205	29.7	205	29.7	0	0
I-15	Fe <sub>74</sub> Ta <sub>1</sub> Al <sub>25</sub>	1049	152.1	818	118.7	3.1	5.5
I-16	Fe <sub>70</sub> Ta <sub>5</sub> Al <sub>25</sub>	1299	188.4	938	136.1	1.8	3.1
I-17	Fe <sub>72</sub> Cu <sub>5</sub> Al <sub>23</sub>	945	137.1	898	130.3	0.3	1.0
I-18	Fe <sub>70</sub> Cu <sub>10</sub> Al <sub>20</sub>	985	142.9	840	121.8	12.1	19.5
I-19	Fe <sub>75</sub> Si <sub>3</sub> Al <sub>22</sub> (2)	271	39.3	271	39.3	0.3	-
I-20	Fe <sub>75</sub> Si <sub>5</sub> Al <sub>20</sub> (2)	312	45.3	312	45.3	0.1	-
Baseline	Fe <sub>3</sub> Al	894	129.7	674	97.7	4.7	6.7

(1) Alloy Not Tested

(2) Specimen Failed in Radius

(3) Specimen Failed in Thread Section

TABLE IX

600°C (1112°F) TENSILE DATA FOR TASK II/SERIES I ALLOYS

Alloy	Composition	Ultimate Tensile Strength		0.2% Yield Strength		% Elongation	% Reduction Area
		(MPa)	(Ksi)	(MPa)	(Ksi)		
I-1	Fe <sub>74</sub> Ti <sub>1</sub> Al <sub>25</sub>	305	44.2	302	43.8	44.0	72.6
I-2	Fe <sub>70</sub> Ti <sub>5</sub> Al <sub>25</sub>	259	37.6	252	36.6	45.2	71.3
I-3	Fe <sub>70</sub> V <sub>5</sub> Al <sub>25</sub> (1)						
I-4	Fe <sub>65</sub> V <sub>10</sub> Al <sub>25</sub> (1)						
I-5	Fe <sub>74</sub> Cr <sub>1</sub> Al <sub>25</sub>	359	52.0	354	51.3	42.2	71.6
I-6	Fe <sub>70</sub> Cr <sub>5</sub> Al <sub>25</sub>	277	40.1	273	39.6	69.4	93.7
I-7	Fe <sub>69</sub> Mn <sub>6</sub> Al <sub>25</sub>	330	47.8	263	38.1	64.6	83.3
I-8	Fe <sub>63</sub> Mn <sub>12</sub> Al <sub>25</sub>	269	39.0	201	29.2	44.0	65.4
I-9	Fe <sub>72</sub> Ni <sub>3</sub> Al <sub>25</sub>	299	43.4	288	41.8	21.0	34.8
I-10	Fe <sub>65</sub> Ni <sub>10</sub> Al <sub>25</sub>	529	76.7	395	57.3	12.6	13.2
I-11	Fe <sub>73</sub> Nb <sub>2</sub> Al <sub>25</sub>	508	72.7	419	60.8	38.3	60.6
I-12	Fe <sub>70</sub> Nb <sub>5</sub> Al <sub>25</sub>	523	75.9	434	63.0	39.5	59.1
I-13	Fe <sub>72</sub> Mo <sub>3</sub> Al <sub>25</sub>	350	50.7	339	49.2	43.1	88.5
I-14	Fe <sub>69</sub> Mo <sub>6</sub> Al <sub>25</sub>	471	68.3	364	52.8	4.0	4.4
I-15	Fe <sub>74</sub> Ta <sub>1</sub> Al <sub>25</sub>	370	53.7	370	53.7	38.3	77.9
I-16	Fe <sub>70</sub> Ta <sub>5</sub> Al <sub>25</sub>	476	69.1	453	65.7	31.1	57.5
I-17	Fe <sub>72</sub> Cu <sub>5</sub> Al <sub>23</sub>	171	24.8	171	24.8	0.8	0.7
I-18	Fe <sub>70</sub> Cu <sub>10</sub> Al <sub>20</sub>	175	25.4	170	24.6	1.1	3.0
I-19	Fe <sub>75</sub> Si <sub>3</sub> Al <sub>22</sub>	603	87.4	603	87.4	16.1	38.0
I-20	Fe <sub>75</sub> Si <sub>5</sub> Al <sub>20</sub>	582	84.4	531	77.0	13.9	14.5
Baseline	Fe <sub>3</sub> Al	215	31.2	211	30.6	69.3	78.9

(1) Alloy Not Tested

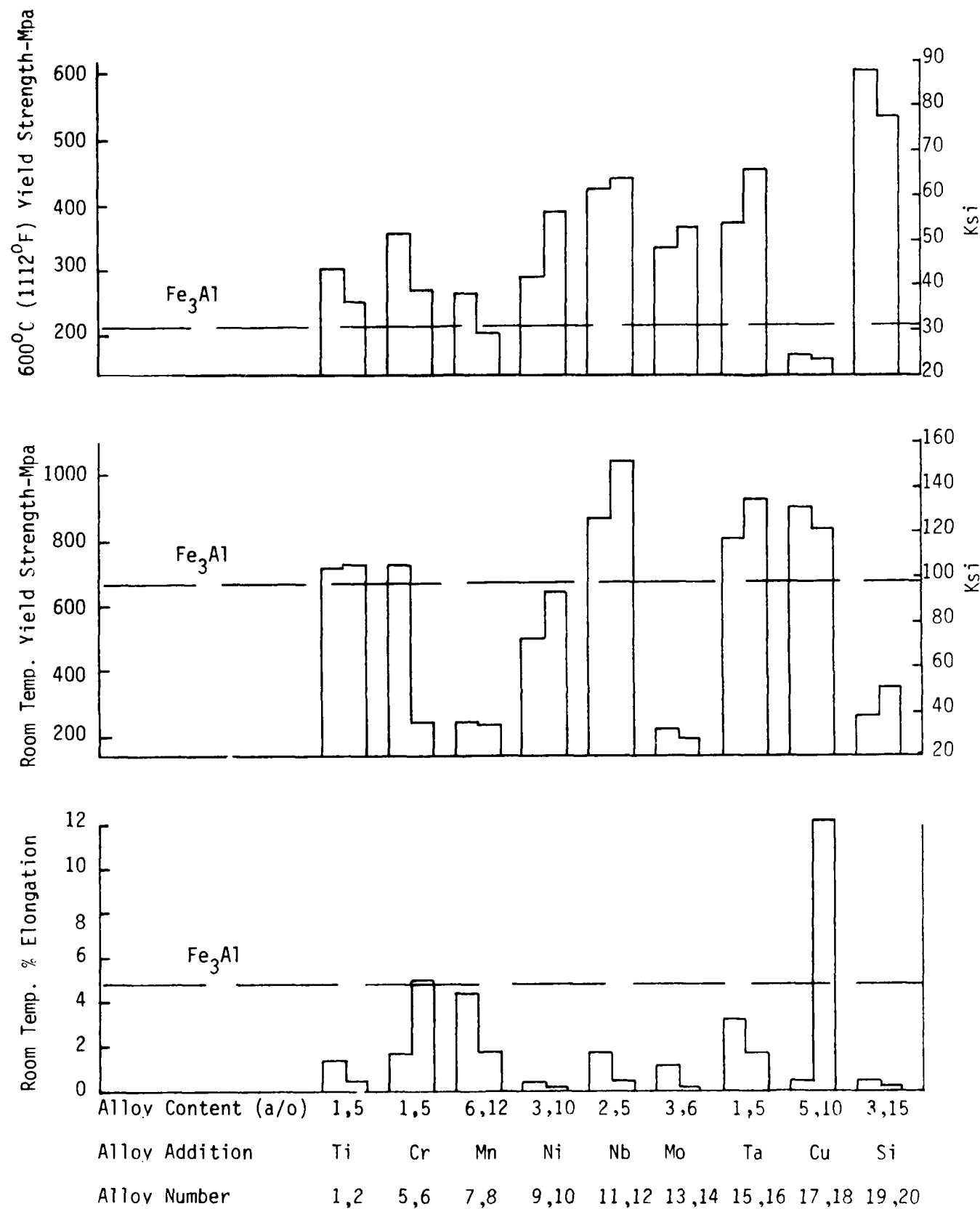


Figure 34 Summary of Task II/Series I tensile data.



(a) 100X Magnification



(b) 500X Magnification

Figure 35. Light photos of  $\text{Fe}_3\text{Al}$  failed room temperature tensile test specimen showing structure near the fracture surface.

effect of the impurity particles in the structure could not be established, but it was observed that secondary cracking did not appear to be associated with these particles.

This material exhibited an ultimate tensile strength of 215 MPa (31.2 Ksi), a yield strength of 211 MPa (30.6 Ksi) and ductility values in the range 70-80% at 600°C (1112°F). Extensive deformation of grains was observed near the fracture surface as well as separation along grain boundaries to form large void areas. An example of this structure is shown in Figure 36 for regions near the fracture surface as well as for regions within the specimen grips. The high elongation and reduction of area values indicated that the material exhibited high ductility in spite of the presence of non-metallic inclusion impurities.

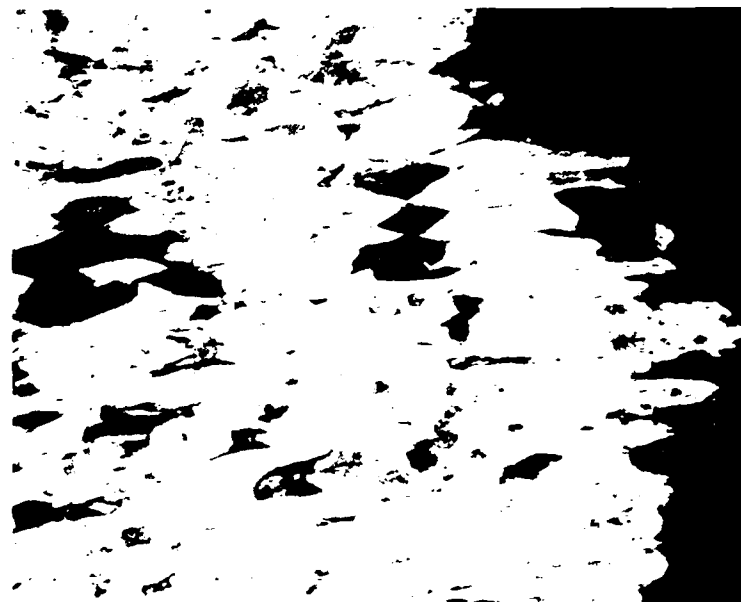
In the following sections, discussions are presented relative to the tensile properties of the other various Series I alloys. All tensile failures, unless stated otherwise, were similar in appearance to the baseline Fe<sub>3</sub>Al material shown in Figures 35 (room temperature) and 36 (600°C (1112°F)).

#### 4.1.3.1.2 Ti-Containing Alloys

Titanium additions were found to be significantly detrimental to room temperature ductility and afforded only moderate gains in elevated temperature strength as compared to the baseline material. The room temperature elongation was reduced more than three-fold by the 1 a/o Ti addition, and nearly ten-fold by the 5 a/o Ti addition. Yield strength at 600°C (1112°F) was increased by 43% in the case of the 1 a/o Ti addition, and by 20% in the 5 a/o alloy.

#### 4.1.3.1.3 V-Containing Alloys

Tensile testing was not conducted on the two V-containing alloys. This decision was made on the basis of the cracking observed upon extrusion of the 10 a/o V alloy (discussed previously in Section 4.1.2.2) and its poor performance during oxidation testing (to be described in Section 4.1.3.2). It was not thought that testing of the lower V-content alloy (5 a/o) would



(a) Fracture Area



(b) Grip Area

Figure 36. Light photos of Fe<sub>3</sub>Al failed 600°C (1112°F) tensile test specimen showing structure near the fracture surface and the grip area. 100X Magnification.

provide useful information for the design of the subsequent second series of alloys.

#### 4.1.3.1.4 Cr and Mo-Containing Alloys

The analysis of the effect of Cr and Mo alloy additions on  $\text{Fe}_3\text{Al}$  was complicated by the inadvertent mixing of Cr and Mo prealloyed powders prior to extrusion of Alloys I-6 and I-13. As shown in Table VI, chemical analyses of the extrusions indicated that the compositions of the four Cr and/or Mo alloys studied were actually:

Alloy I-5	0.5 a/o Cr
Alloy I-6	3.31 a/o Cr with 0.24 a/o Mo
Alloy I-13	1.97 a/o Cr with 0.29 a/o Mo
Alloy I-14	2.3 a/o Mo

It was assumed that the small amounts of Mo present in alloys I-6 and I-13 would have only slight effects upon the tensile properties. The single alloy which contained only Mo (Alloy I-14) exhibited a large (73%) increase in  $600^\circ\text{C}$  ( $1112^\circ\text{F}$ ) yield strength, but had nil ductility at room temperature. Cr, at the 3.3 a/o level, appeared to be a moderate strengthener (29% increase in yield strength) at  $600^\circ\text{C}$  ( $1112^\circ\text{F}$ ), while maintaining a room temperature tensile ductility equivalent to the baseline  $\text{Fe}_3\text{Al}$  alloy. Metallographic examination of failed test specimens revealed that localized abnormal grain growth occurred in the other Cr plus Mo alloy (Alloy I-13). As shown in Figure 37, the grip section of the room temperature tensile specimens exhibited equiaxed grains of approximately 100 microns in diameter; however, the microstructure near the fracture surface reveals grains as large as 2000 microns. The presence of only 1-2 grains in the gage section would be expected to limit ductility and this was, in fact, observed. No cause was found for the ductility loss shown by the low Cr alloy (Alloy I-5).

#### 4.1.3.1.5 Mn-Containing Alloys

The room temperature tensile results indicated that Mn additions to the baseline alloy resulted in the degradation of both strength and ductility

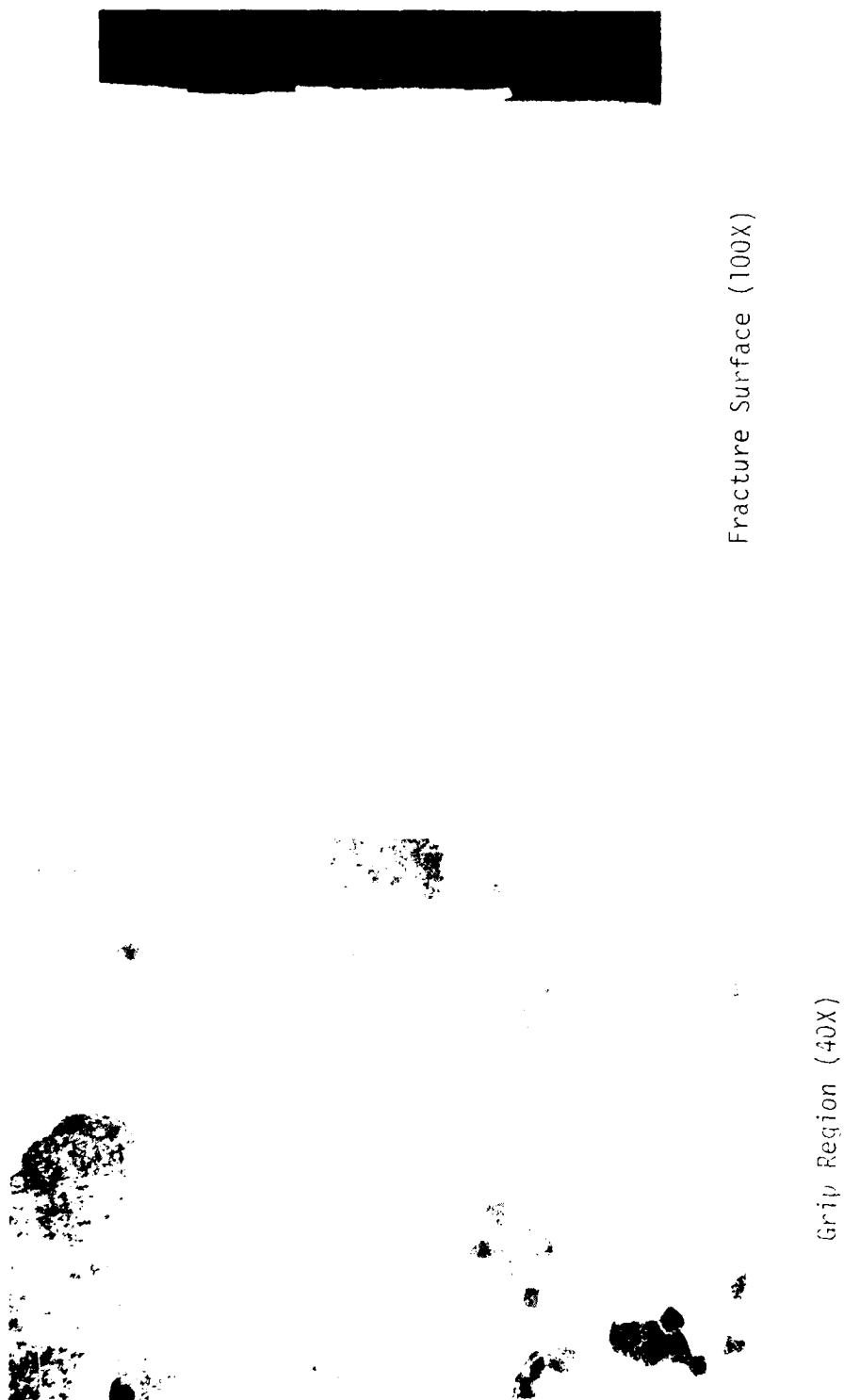


Figure 37. Light photos of Mo-3 a/o (Alloy I-13) failed room temperature tensile test specimen showing localized abnormal grain growth.



properties. The degree of degradation increased with an increase in Mn content. The 600°C (1112°F) tensile results indicated that Mn at the 6 a/o level was more effective in improving the high temperature strength of the baseline alloy. This alloy exhibited an improvement of approximately 111% in yield strength compared to unalloyed Fe<sub>3</sub>Al and the ductility levels were comparable. At the higher Mn level, some increase in yield strength was observed compared to Fe<sub>3</sub>Al, but to less than one-half the amount seen in the lower Mn alloy. The high temperature ductility values, however, were inferior to both the low Mn alloy as well as the baseline alloy. Analysis of the failed test bars revealed microstructural features similar to those presented in Figures 35 and 36 for the baseline alloy.

#### 4.1.3.1.6 Ni-Containing Alloys

The Ni addition to Fe<sub>3</sub>Al at the 10 a/o level resulted in some loss in ultimate tensile strength and an equivalent yield strength compared to the baseline material at room temperature. There was, however, no measurable ductility. Examination of the failed test specimen revealed microstructural features significantly different from those found in the Fe<sub>3</sub>Al alloy. An example of this structure near the fracture surface is shown in Figure 38. In particular, the secondary cracking was observed to be primarily transgranular, compared to the grain boundary separation observed in Fe<sub>3</sub>Al at room temperature, Figure 35.

At 600°C (1112°F) the strength values increased significantly compared to the baseline alloy, with yield strength being double and ultimate strength being almost triple that of Fe<sub>3</sub>Al. Ductility, on the other hand, was significantly reduced, by approximately 85%, with the 10 a/o Ni addition. Similar to the room temperature situation, examination of the failed test specimen revealed microstructural features significantly different from those found in the baseline alloy. An example of the structure is shown in Figure 39 for regions near the fracture surface as well as for regions within the specimen grips. Comparison with the structure displayed in Figure 36 for the Fe<sub>3</sub>Al indicates that the grains in the Ni-containing alloy exhibited little deformation during this high temperature tensile test. The grains near the fracture surface are similar in shape to those in the grip area and

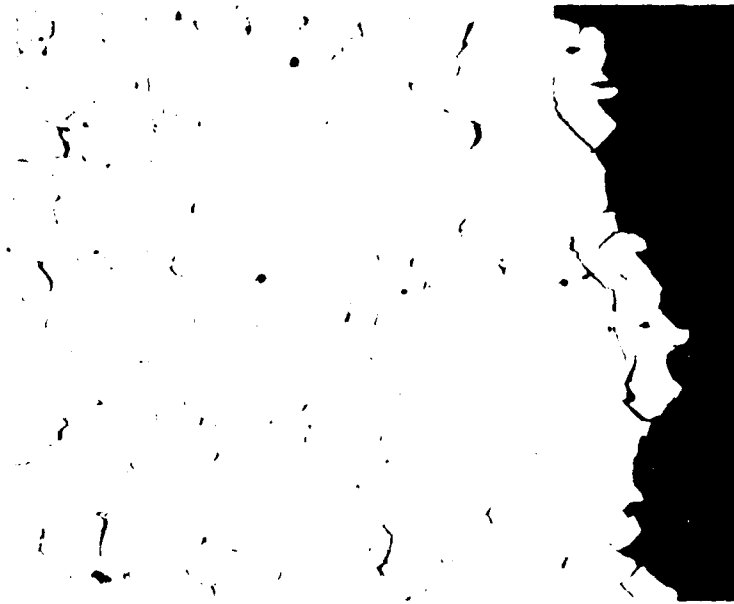


(a) 100X Magnification.



(b) 500X Magnification

Figure 38. Light photos of Ni-10 a/o (Alloy I-10) failed room temperature tensile test specimen showing structure near the fracture surface.



(a) Fracture Area



(b) Grip Area

Figure 39. Light photos of Ni-10 a/o (Alloy I-10) failed  $600^{\circ}\text{C}$  ( $1112^{\circ}\text{F}$ ) tensile test specimen showing structures near the fracture surface and grip area. 100X Magnification.

considerable evidence of secondary cracking along grain boundaries was observed adjacent to the fracture surface. These results indicate that the flow stress in the individual Ni alloy grains is much higher than in the  $\text{Fe}_3\text{Al}$ .

The blended Ni-containing alloy, at the 3 a/o level, exhibited behavior similar to the higher Ni-content alloy. Elevated temperature yield strength was increased somewhat (37%) over the baseline alloy, but not to the same degree (87%) of the 10 a/o Ni alloy. Similarly, room temperature ductility was also drastically reduced at the 3 a/o Ni level.

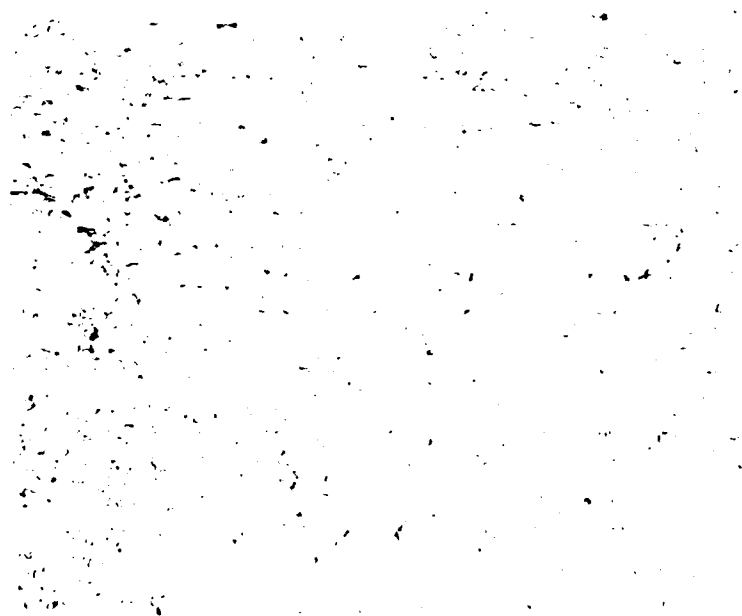
#### 4.1.3.1.7 Nb-Containing Alloys

At the 2 a/o Nb level, the room temperature yield strength was approximately 23% higher than the baseline  $\text{Fe}_3\text{Al}$ , but the ductility values were approximately half those of the baseline. While the strength values for the higher Nb alloy were superior to those of the lower Nb alloy, interpretation of the data was made difficult by the fact that the higher Nb specimens failed in the threaded portions of the specimens. This suggests the possibility of notch sensitivity in this material.

The  $600^\circ\text{C}$  ( $1112^\circ\text{F}$ ) tensile results indicated little significant difference in strength properties between the two Nb-containing alloys. Both the ultimate tensile strength and the yield strength were improved compared to the baseline, in that both strength values more than doubled. The ductility values for both alloys were also similar, but were reduced compared to  $\text{Fe}_3\text{Al}$ . These alloys exhibited similar tensile properties in spite of the differences in their microstructures. The lower Nb content alloy exhibited a larger grain size and less of a volume fraction Nb-rich precipitate distribution than the higher Nb alloy. An example of the microstructures of these alloys near the fracture surfaces is shown in Figure 40. Some grain deformation can be observed in Figure 40a for the 2 a/o alloy while both alloys exhibited evidence of separation along the interfaces between the matrix and the precipitate particles. The similarity in tensile properties suggests that little contribution to strength was provided by the precipitate phases in the size and distribution displayed in Figure 40. The strengthening effects in the Nb alloys can, thus, be attributed principally to solid solution



(a) Alloy 11



(b) Alloy 12

Figure 40. Light photos of Nb-2 a/o (Alloy I-11) and Nb-5 a/o (Alloy I-12) failed 600°C (1112°F) tensile test specimens showing structure near the fracture area. 500X Magnification.

strengthening. As was pointed out in the discussion of the SRL results in Section 4.1.2.3, some potential does exist in these alloys for enhanced strengthening by heat treating to produce a coherent precipitate phase.

#### 4.1.3.1.8 Ta-Containing Alloys

The room temperature properties indicated that at the 1 a/o Ta level, the yield strength was approximately 21% higher than the baseline and the ductility was comparable to the baseline. The 5 a/o Ta alloy exhibited a strength increase of about 39% over the baseline, but was approximately half as ductile.

The Ta alloys exhibited the same property trends at 600°C (1112°F) as were observed at room temperature, in that the higher Ta alloy exhibited higher strength, but lower ductility than the lower Ta alloy. At the higher Ta level, strengths were more than double those for Fe<sub>3</sub>Al, but with only one-half the ductility. Metallographic examination of the high temperature tensile test specimens indicated that the structure of the low Ta alloy was similar to that presented in Figure 36 for the baseline alloy, while the structure for the high Ta alloy was similar to that presented in Figure 40b for the 5 a/o Nb alloy. The low Ta alloy exhibited no second phase precipitation, but did exhibit grain deformation near the fracture surface accompanied by separation along the grain boundaries to form large void areas. The high Ta alloy exhibited extensive second phase precipitation as well as separation along the interfaces between the matrix and the Ta rich particles, including the larger particles retained from the powder production process. Because of the presence of these large particles, there appears to be little likelihood that significant change in the particle morphology can be achieved for this particular composition by heat treatment.

#### 4.1.3.1.9 Cu-Containing Alloys

The room temperature tensile properties of the 10 a/o Cu alloy exhibited a 24% increase in yield strength coupled with a 150% increase in ductility. The presence of a film at the grain boundaries and a precipitate free zone near the grain boundaries are most likely responsible for this large increase

in ductility. The major effect of the Cu addition at high temperature was a significant (95%) reduction in ductility. Examination of the failed test specimen indicated that grains in this alloy exhibited little deformation during testing and that separation occurred along the grain boundaries. An example of this structure is shown in Figure 41. The presence of the Cu rich film resulted in premature failure along the grain boundary areas.

The blended 5 a/o Cu alloy exhibited behavior similar to that seen previously for the prealloyed 10 a/o Cu alloy, with the exception that the room temperature ductility was significantly inferior to that of both the baseline as well as the 10 a/o alloy.

#### 4.1.3.1.10 Si-Containing Alloys

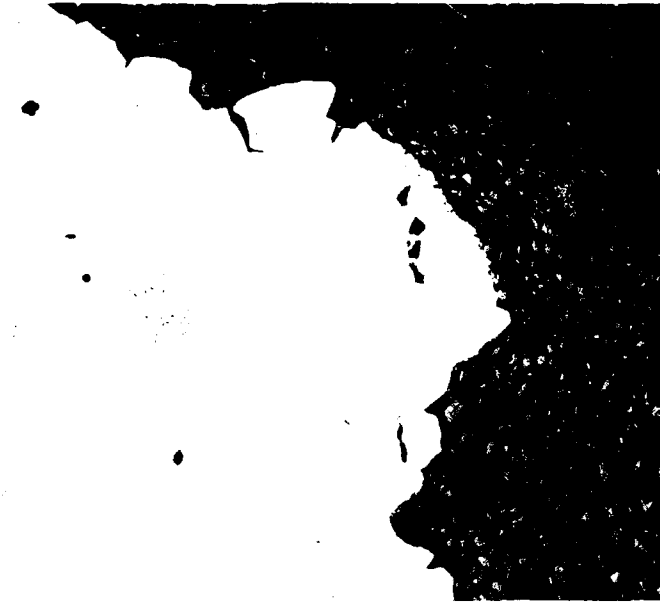
The two blended Si-containing alloys exhibited nearly identical tensile properties. While Si additions provided the greatest strength enhancement at 600°C (1112°F) (nearly a three-fold increase in yield strength compared to Fe<sub>3</sub>Al), this was accompanied by nil ductility at room temperature for both alloys.

#### 4.1.3.1.11 Summary of Tensile Test Results

The Series I alloys exhibited either single or two-phase microstructures. The two-phase alloys included the Nb, Ta, and Cu-containing alloys. All other additions resulted in single-phase microstructures.

##### 4.1.3.1.11.1 Two-Phase Alloys

Both Nb-containing alloys exhibited a distribution of Nb-rich particles (typically 1-3 microns in diameter) which were traced back to precipitate films found between dendrite arms in the individual powder particles. The relative coarseness of these precipitates apparently prevented the second phase from providing significant strengthening as evidenced by the similar strength values of the two Nb-containing alloys, although the volume fractions of the second-phase particles were significantly different. As a solid solution strengthening addition, Nb resulted in significant yield strength



(a) Fracture Area

(b) Grip Area

Figure 41. Light photos of Cu-10 a/o (Alloy 1-18) failed  $600^{\circ}\text{C}$  ( $1112^{\circ}\text{F}$ ) tensile test specimen showing structures near the fracture surface and grip areas. 100X Magnification.



increases at elevated temperature (105%). Room temperature ductility was reduced from 3-10 fold. Two thread failures in the 5 a/o Nb alloy indicated that a notch sensitivity problem may exist.

The Ta-containing alloys behaved somewhat similarly. The 5 a/o alloy exhibited a bi-modal distribution of precipitates. The 1-3 micron particles were observed, as in the Nb alloys, as well as larger elongated particles which were traced to the cast electrode bar used to produce the PREP powder. This suggests that gross segregation occurred on solidification of the bar, and there was insufficient superheat during the PREP process to melt these regions. Therefore, the Ta rich regions were spun off the stick in a solid or semi-solid state and were frozen within the powder particles. The low (1 a/o Ta) alloy, apparently, did not exceed the solid solubility limit and, thus, was tested as a single-phase alloy. This afforded a comparison of the effect of the solid solution strengthening capability of Ta. It was shown that Ta is a potent strengthener (with a 115% yield strength increase exhibited by the high Ta alloy) at elevated temperatures and, more importantly, did not cause as significant a loss (33%) in room temperature ductility as was observed for the Nb-containing alloys. This combination of properties was unique among the prealloys tested.

Both Cu-containing alloys exhibited poor elevated temperature properties which can be attributed to weakened grain boundaries.

#### 4.1.3.1.11.2 Single-Phase Alloys

The single-phase alloys, as a group, exhibited, with a few exceptions, either substantial high temperature strength improvement or acceptable room temperature ductility, but not both. The 6 a/o Mn alloy was one of the exceptions in that it exhibited a 25% increase in yield strength at 600°C (1112°F) while maintaining attractive elongation at room temperature. The 12 a/o Mn alloy was weaker and less ductile than the 6 a/o alloy. However, both alloys exhibited a greater than two-fold drop in room temperature strength as compared to the baseline alloy.

Mo was shown to dramatically increase the elevated temperature strength over the baseline, but, at least at the 2.3 a/o level, resulted in nil ductility. As in other nil ductility alloys, this alloy exhibited premature tensile failure at room temperature. Therefore, the room temperature ultimate strength was lower than the 600<sup>0</sup>C (1112<sup>0</sup>F) ultimate strength.

Cr at the 2-3 a/o level along with small amounts of Mo (0.2-0.3 a/o) was shown to enhance elevated temperature yield strength somewhat (29%) while maintaining the inherent room temperature ductility of the baseline. This was the only alloy, besides the 6 a/o Mn alloy, which did not exhibit reduced room temperature ductility compared to the baseline alloy.

#### 4.1.3.2 Oxidation Results

Oxidation testing was performed on the Series I alloys to determine if any of the alloying additions significantly degraded the inherent oxidation resistance of the baseline Fe<sub>3</sub>Al. The evaluation was performed in two runs. The first run included all the prealloyed extrusions which did not require homogenization heat treatments, but were given the 500<sup>0</sup>C (932<sup>0</sup>F)/24 hour ordering heat treatment. The second run included all the alloys which were not chemically homogeneous in the as-extruded condition. These alloys were exposed to the homogenization heat treatments described previously in Section 4.1.2.4 and then the ordering heat treatment prior to the initiation of testing. The specimens in both runs were identical and consisted of a right circular cylinder 0.66 cm (0.25 inch) in diameter by 1.3 cm (0.5 inch) high. Samples were weighed on a laboratory analytical balance with a precision of nominally 0.0002 grams before and after exposure to static laboratory air in a box furnace held at 816<sup>0</sup>C (1500<sup>0</sup> F).

During the first run, all specimens were removed from the furnace and reweighed at 24, 96, 240, and 480 hours. The intent of this evaluation was to determine the parabolic weight constant for each alloy and compare it with that of the baseline. However, only a few alloys demonstrated parabolic weight gains. Most of the alloys, including the baseline Fe<sub>3</sub>Al, showed weight losses. For these reasons, parabolic rate constants were not computed, and the second oxidation screening run, conducted on the blended alloys, was

AD-A168 578

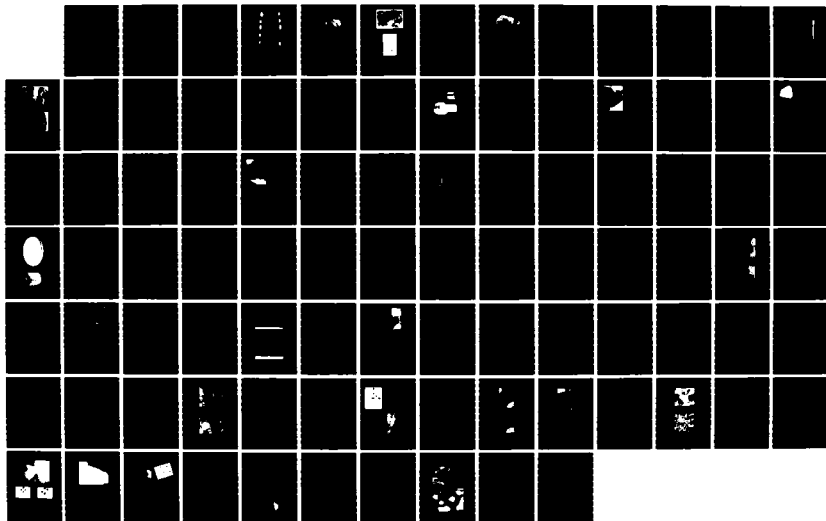
DEVELOPMENT OF IRON ALUMINIDES(U) TRW MATERIALS AND  
MANUFACTURING CENTER EUCLID OH G C CULBERTSON ET AL.  
MAR 86 ER-8215-6 AFMIL-TR-85-4155 F33615-81-C-5155

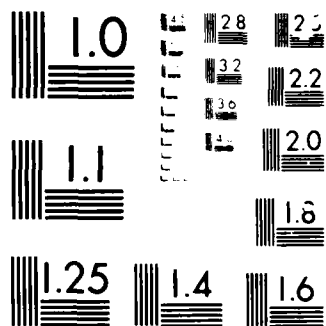
2/2

UNCLASSIFIED

F/G 11/6

NL





Mr. Robert

1977

limited to a single weighing after a 240 hour hold at 816<sup>0</sup>C (1500<sup>0</sup>F) in static laboratory air.

The data for both runs is tabulated in Table X and includes the results for the 240 hour exposure. The 1 a/o Cr and 3 a/o Si alloys were not tested because of material shortages. The 3 a/o Ni alloy was not tested because of the delays in the establishment of the proper homogenization heat treatment for this particular alloy. Since alloys containing greater amounts of these particular elemental additions did not exhibit a degradation in oxidation resistance compared to the baseline, it was assumed that the alloys which were not tested would have behaved similarly.

A photograph of the prealloyed samples after 96 hours exposure to 816<sup>0</sup>C (1500<sup>0</sup>F) is shown in Figure 42 and indicates the relative oxidation resistance of the prealloyed specimens. The 10 a/o V alloy was degraded rapidly, while the other alloys, including the baseline, evidence little or no oxidation reaction products. This observation was supported by the weight gain data, Table X, which indicated that most of the alloys exhibited weight changes which were comparable to the baseline alloy.

Figure 43 compares the alloy containing 5 a/o Ti to the 10 a/o V alloy and to the baseline. In this photograph, the Ti alloy is shown after 240 hours exposure while the V alloy and the baseline are shown after 480 hours. The V alloy has undergone catastrophic oxidation with the result that little sound, unoxidized, material remains. Apparently, V at this level not only prevents the formation of a coherent alumina film, but accelerates the oxidation kinetics as well. The Ti alloy exhibited a thick scale and a large increase in weight. The specimen surface was analyzed by SEM/EDS, and as shown in Figure 44, was found to be principally iron oxide. It appears that Ti, at the 5 a/o level, prevents the formation of a coherent alumina layer. The baseline alloy, shown in Figure 43, was representative of the alloys which did not experience significant weight changes.

Alloy I-14 (actual Mo content of 2.3 a/o) experienced a moderate weight loss (-3 mg/cm<sup>2</sup>) which was related to a slight increase in the amount of scale observed on the specimen surface as compared to the baseline material.

TABLE X

## OXIDATION RESULTS FOR TASK II/SERIES I ALLOYS

Alloy	Composition	Specific Weight Change (10 <sup>-3</sup> g/cm <sup>2</sup> ) After 10-day (240 Hours) Exposure to 816 °C (1500 °F) Laboratory Air
I-1	Fe <sub>74</sub> Ti <sub>1</sub> Al <sub>25</sub>	0.0
I-2	Fe <sub>70</sub> Ti <sub>5</sub> Al <sub>25</sub>	+9.6
I-3	Fe <sub>70</sub> V <sub>5</sub> Al <sub>25</sub>	Not Tested
I-4	Fe <sub>65</sub> V <sub>10</sub> Al <sub>25</sub>	Decomposed
I-5	Fe <sub>74</sub> Cr <sub>1</sub> Al <sub>25</sub>	Not Tested
I-6	Fe <sub>70</sub> Cu <sub>5</sub> Al <sub>25</sub>	-0.25
I-7	Fe <sub>69</sub> Mn <sub>6</sub> Al <sub>25</sub>	-0.71
I-8	Fe <sub>63</sub> Mn <sub>12</sub> Al <sub>25</sub>	-0.96
I-9	Fe <sub>72</sub> Ni <sub>3</sub> Al <sub>25</sub>	Not Tested
I-10	Fe <sub>65</sub> Ni <sub>10</sub> Al <sub>25</sub>	+0.25
I-11	Fe <sub>73</sub> Nb <sub>2</sub> Al <sub>25</sub>	-0.47
I-12	Fe <sub>70</sub> Nb <sub>2</sub> Al <sub>25</sub>	-0.03
I-13	Fe <sub>72</sub> Mo <sub>3</sub> Al <sub>25</sub>	-0.13
I-14	Fe <sub>69</sub> Mo <sub>6</sub> Al <sub>25</sub>	-3.03
I-15	Fe <sub>74</sub> Ta <sub>1</sub> Al <sub>25</sub>	-0.67
I-16	Fe <sub>70</sub> Ta <sub>5</sub> Al <sub>25</sub>	+0.32
I-17	Fe <sub>72</sub> Cu <sub>5</sub> Al <sub>23</sub>	-1.80
I-18	Fe <sub>70</sub> Cu <sub>10</sub> Al <sub>20</sub>	-0.19
I-19	Fe <sub>75</sub> Si <sub>3</sub> Al <sub>22</sub>	Not Tested
I-20	Fe <sub>75</sub> Si <sub>5</sub> Al <sub>20</sub>	-0.06
Baseline	Fe <sub>3</sub> Al	-0.35

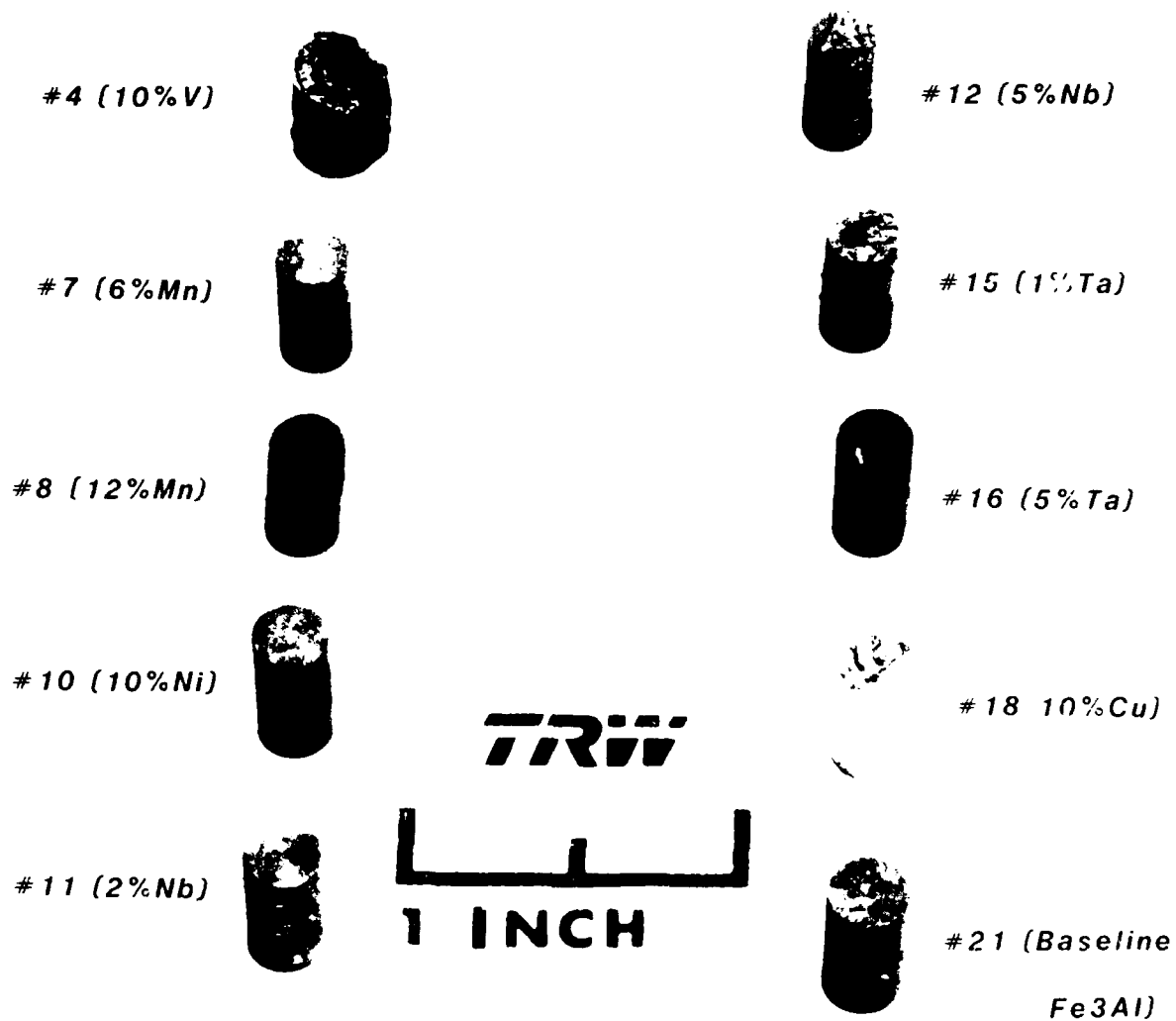


Figure 42. Photograph of prealloyed Task I/Series I Alloys after exposure to 816°C (1500°F) Air for 96 Hours.



Alloy	Fe <sub>3</sub> Al (No. 21)	5 at Ti (No. 2)	10 at V (No. 4)
Time	430 Hrs.	240 Hrs.	430 Hrs.

Figure 43. Photograph of selected Task I/Series I Alloys showing effect of alloying additions on oxidation resistance after exposure to 816°C (1500°F) Air. 2X Magnification.



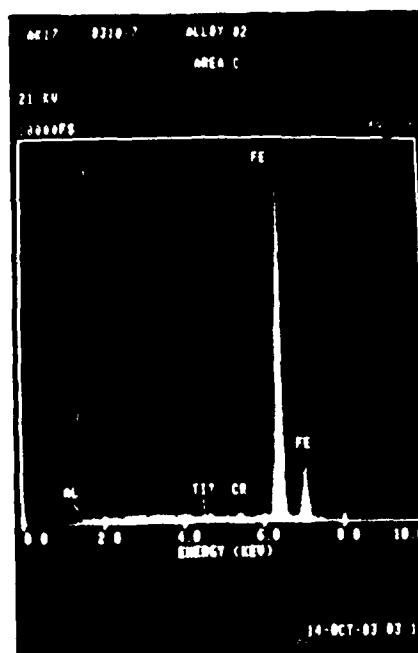


Figure 44. SEM and EDAX photos of Ti-5 a/o (Alloy 1-2) after 240 hour exposure to 816°C (1500°F) Air. 16x Magnification.

The degradation of oxidation resistance is much less for this alloy than for either the 5 a/o Ti or the 10 a/o V alloys.

In summary, dramatic changes in oxidation behavior were observed for only two alloys. Only the 5 a/o Ti and the 10 a/o V alloys exhibited extensive oxidation. The only other alloy not emulating the oxidation behavior of  $\text{Fe}_3\text{Al}$  was Alloy I-14 (actual Mo content of 2.3 a/o). Apparently Ti and V, when present in sufficient quantities, prevent the formation of a coherent aluminum oxide layer. Mo alloys may exhibit similar characteristics, but to a far lesser degree.

#### 4.1.3.3 Workability Results

In order to determine the effect of alloy additions on the workability of  $\text{Fe}_3\text{Al}$ , samples of extruded plus ordered prealloys and extruded plus homogenized and ordered blends were upset forged. A sample of each alloy was machined into a barrel shape and isothermally forged between unlubricated flat platens at  $954^\circ\text{C}$  ( $1750^\circ\text{F}$ ) and at a strain rate of 8 inch/inch/second in vacuum. The preform configuration and an as-forged specimen are shown in Figure 45. These parameters were selected as representative of typical forging conditions employed within industry and were intended to offer a preliminary indication of the relative workability of the various alloys. The work was performed by Deformation Control Technology using an MTS apparatus located at the University of Pittsburgh.

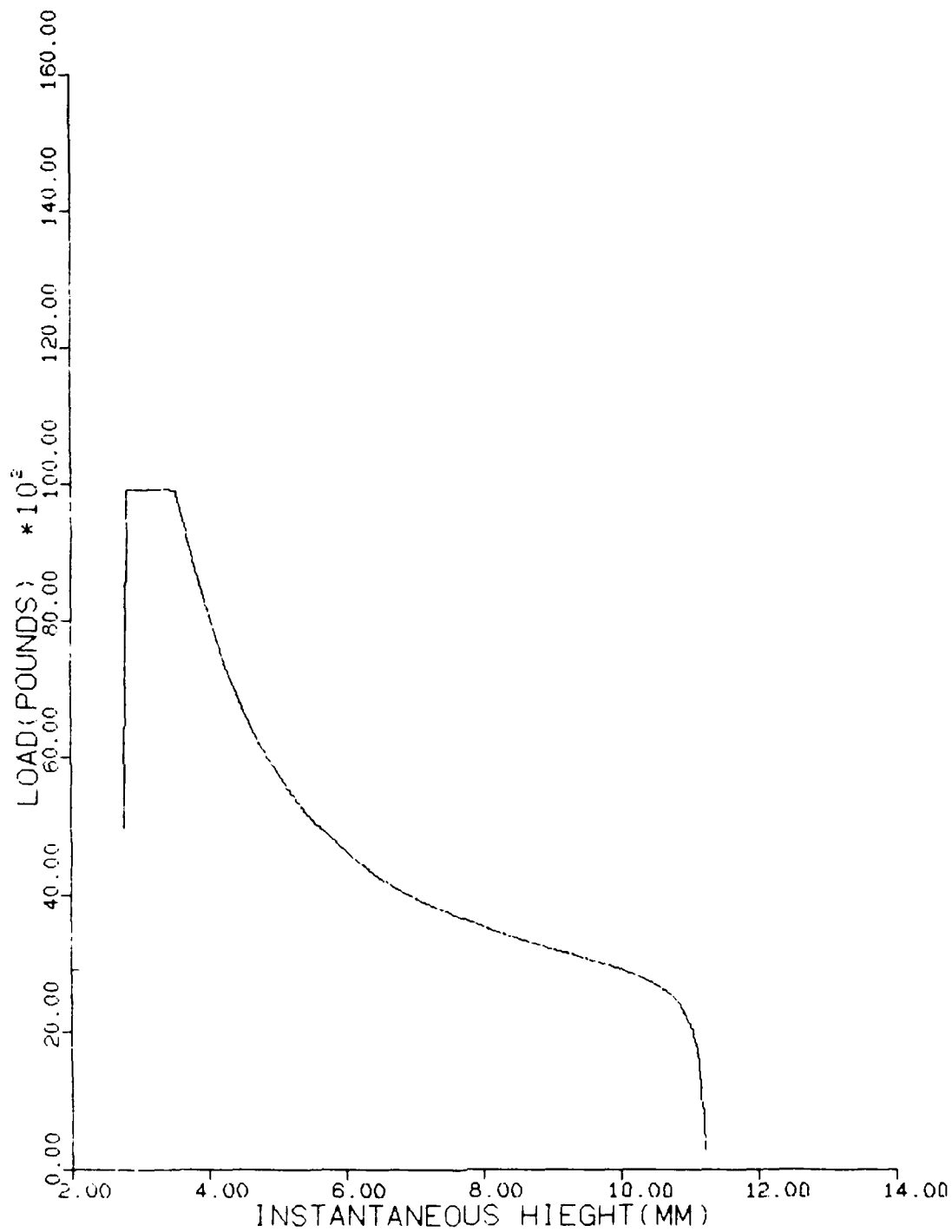
Each test generated a plot of applied load versus cylinder height for the alloy. A typical plot is shown in Figure 46 for the 2 a/o Nb alloy. Each compact was evaluated metallographically to establish the extent of cracking as an aid in the interpretation of the results.

Deformation studies were conducted in two lots with the initial studies being conducted on the prealloyed compositions and subsequent studies being conducted on the blended alloys. Microstructural examination of the upset, prealloyed specimens revealed that small amounts of residual steel extrusion can remain on portions of some specimens. This made it necessary to reduce the diameter of the extruded bar approximately 10% in order to ensure that all



(Approx. 4.2X)

Figure 45. Photograph of Fe<sub>3</sub>Al forging preform and as-forged specimen.



F 11

Figure 46. Load versus height curve for Nb-2 a/o (Alloy I-11) for deformation at 954°C (1750°F) and 8/second strain rate.

of the can had been removed prior to homogenization of the blended materials. This, in turn, resulted in slightly smaller samples and a reduced load carrying capability which was considered during computation of the deformation loads.

The data gathered during both sets of tests are summarized in Table XI. Note that those alloys exhibiting very low tensile ductility at elevated temperature (10 a/o Ni, 5 a/o Cu, 10 a/o Cu, and 3 a/o Si) were omitted from the evaluations because poor workability was anticipated. The load to deform the samples 10% in height was determined from the applied load versus cylinder height plots. This load can be considered as being proportional to a relative flow stress since the two lots were normalized with respect to the different sample sizes. The deformation loads indicated that for this particular test temperature, 954<sup>0</sup>C (1750<sup>0</sup>F), the alloys could be grouped into three categories.

The first category included single-phase alloys (1 a/o Ti, 5 a/o Ti, 5 a/o Cr, 6 a/o Mn, 12 a/o Mn, and 3 a/o Mo) which all deformed 10% underloads less than or similar to the baseline Fe<sub>3</sub>Al alloy. This corresponded well with the elevated temperature tensile data which indicated that all of these alloys exhibited approximately the same ultimate tensile strength as the baseline.

The second category included the 6 a/o Mo, 1 a/o Ta, and 5 a/o Si alloys, which deformed 10% at loads 33-50% higher than the baseline alloy. Again, this data corresponded well with the elevated temperature data. The group of alloys included three of the most potent elevated temperature solid solution strengthening alloy additions (Mo, Ta, and Si, respectively) of the Series I compositions.

The third category included second phase containing 2 a/o Nb, 5 a/o Nb, and 5 a/o Ta, which deformed 10% at loads approximately twice that of the baseline. These data also agreed with the tensile data for these two-phase alloys.

A relative workability ranking was made on the basis of the prevalence and size of the cracks observed along the circumference of the forged compacts relative to the baseline alloy. This ranking is also included in Table XI. A

TABLE XI

WORKABILITY RESULTS FOR TASK II/SERIES I ALLOYS  
ISOTHERMALLY FORGED AT 954°C (1750°F) AND 8/SECOND

Alloy	Composition	Load to Upset Sample Heights 10%		External Cracking (Relative to Baseline)
		Kg	Pounds	
I-1	Fe <sub>74</sub> Ti <sub>1</sub> Al <sub>25</sub>	502	1106	Similar
I-2	Fe <sub>70</sub> Ti <sub>5</sub> Al <sub>25</sub>	631	1389	Similar
I-3	Fe <sub>70</sub> V <sub>5</sub> Al <sub>25</sub>	(1)		-
I-4	Fe <sub>65</sub> V <sub>10</sub> Al <sub>25</sub>	(1)		-
I-5	Fe <sub>74</sub> Cr <sub>1</sub> Al <sub>25</sub>	(2)		-
I-6	Fe <sub>70</sub> Cr <sub>5</sub> Al <sub>25</sub>	591	1302	Worse
I-7	Fe <sub>69</sub> Mn <sub>6</sub> Al <sub>25</sub>	755	1662	Similar
I-8	Fe <sub>63</sub> Mn <sub>12</sub> Al <sub>25</sub>	681	1500	Similar
I-9	Fe <sub>72</sub> Ni <sub>3</sub> Al <sub>25</sub>	(3)		-
I-10	Fe <sub>65</sub> Ni <sub>10</sub> Al <sub>25</sub>	(4)		-
I-11	Fe <sub>73</sub> Nb <sub>2</sub> Al <sub>25</sub>	1323	2913	Similar
I-12	Fe <sub>70</sub> N <sub>5</sub> Al <sub>25</sub>	1353	2981	Similar
I-13	Fe <sub>72</sub> Mo <sub>3</sub> Al <sub>25</sub>	654	1441	Worse
I-14	Fe <sub>69</sub> Mo <sub>6</sub> Al <sub>25</sub>	1039	2289	Similar
I-15	Fe <sub>74</sub> Ta <sub>1</sub> Al <sub>25</sub>	926	2040	Much Worse
I-16	Fe <sub>70</sub> Ta <sub>5</sub> Al <sub>25</sub>	1407	3100	Worse
I-17	Fe <sub>72</sub> Cu <sub>5</sub> Al <sub>23</sub>	(4)		-
I-18	Fe <sub>70</sub> Cu <sub>10</sub> Al <sub>20</sub>	(4)		-
I-19	Fe <sub>75</sub> Si <sub>3</sub> Al <sub>22</sub>	(4)		-
I-20	Fe <sub>75</sub> Si <sub>5</sub> Al <sub>20</sub>	1021	2249	Similar
Baseline	Fe <sub>3</sub> Al	681	1500	Baseline

(1) Not Tested - Alloy cracked as extruded

(2) Not Tested - Material shortage

(3) Not Tested - Homogenization delays

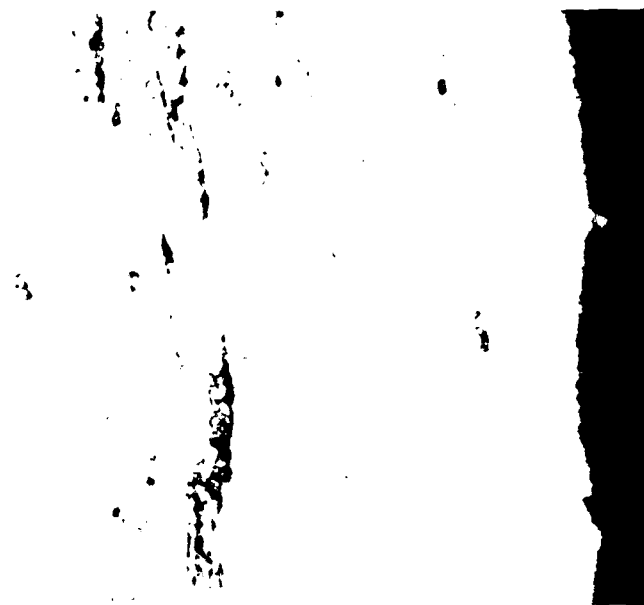
(4) Not Tested - Very low 600°C (1112°F) tensile ductility

"similar" ranking was given to those alloys exhibiting cracks similar to those observed on the baseline compacts. These cracks were typically 0.002-0.01 cm (0.001-0.005 inch) in width.

A "worse" ranking was given to those alloys exhibiting more cracks per unit of surface area or a similar number of cracks which were significantly larger than observed on the baseline samples. These were cracks typically larger than 0.01 cm (0.005 inch) wide. The cause of this increased cracking could, in most cases, be traced to microstructural features not found in the baseline material. The cause of cracking in the 5 a/o Ta alloy was related to the presence of large second phase particles. Figure 47 shows that cracks are associated with the interfaces between these particles and the matrix. The cause of the cracking in alloy I-13 (a Cr + Mo containing alloy) was related to the presence of a few very large grains in this alloy. This microstructural feature was caused by localized abnormal grain growth during the homogenization heat treatment.

The single "much worse" ranking was applied to the 1 a/o Ta alloy which exhibited a large number of very large cracks. These cracks were 0.07-0.13 cm (0.030-0.060 inch) wide. Microstructural examination indicated that this single phase alloy contained more than the usual amount of oxide stringers. Figure 48 displays sections both transverse and longitudinal to the forging direction. Cracks can be observed opening up along the oxide stringers. These stringers did not significantly affect the tensile results presumably because the tensile tests were performed with the loading axis parallel to the extrusion (and, therefore, stringer) orientation. During the upset forging, however, the circumference of the sample was loaded in tension perpendicular to the stringer orientation resulting in extensive cracking.

In summary, the workability results indicated that the deformation loads of the various alloys were a strong function of composition. For a number of alloys, the loads required to accomplish a 10% deformation were generally similar to that for the baseline Fe<sub>3</sub>Al alloy. For alloys containing potent solid solution strengthening additions (Mo, Ta, and Si), the deformation loads were increased by approximately 33-50% compared to the baseline. For the two phase alloys (2 a/o Nb, 5 a/o Nb, and 5 a/o Ta), deformation loads were double



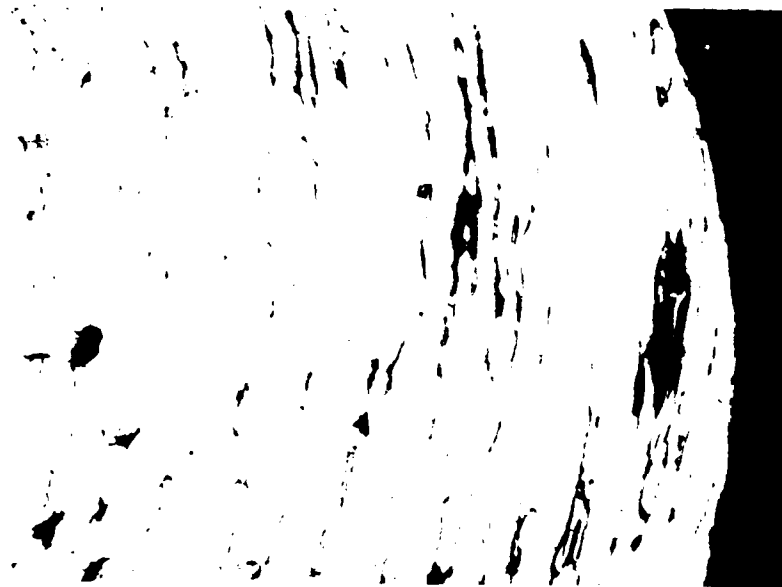
(500X)

Figure 47. Light photo of Ta-5 a/o (Alloy I-16) hot deformation specimen (longitudinal section) showing cracking near precipitate/matrix interface.





(a) (100X)



(b) (100X)

Figure 48. Light Photos of Ta-1 a/o (Alloy I-15) hot deformation specimen (a-transverse section, b-longitudinal section) showing cracking associated with non-metallic inclusion stringers.

that for the baseline alloy. A workability ranking was made relative to the cracking tendency observed in the baseline alloy and, in general, the alloy additions did not significantly alter the workability characteristics. In those instances where the workability was degraded, it was possible to identify microstructural features not present in the baseline alloy as the probable cause for the degradation. These microstructural features included the presence of large second phases (in the 5 a/o Ta alloy), abnormally large grains (in the Cr + Mo alloys), as well as extensive oxide stringer formations (in the 1 a/o Ta alloy).

#### 4.1.4 Series I Summary

The Series I alloy studies included twenty alloys in addition to the baseline material, Fe Al. These included ternary additions of ten elements at two levels each, as shown in Table VI. Note that four of the alloys were actually quaternary due to inadvertent mixing of the powders prior to the hot extrusion consolidation operation. Screening evaluations including oxidation, workability, and tensile property tests were conducted on these alloys.

For the oxidation testing, samples were held at 816°C (1500°F) 480 hours in laboratory air. Visual and weight gain results indicated that only two alloys (5 a/o Ti and 10 a/o V) exhibited significant degradation compared to the baseline alloy.

Workability testing, involving upset isothermal forging at 954°C (1750°F) indicated that none of the alloying additions adversely affected the workability of the baseline material. However, microstructural features such as stringers of inclusions and large second phase particles overshadowed compositional differences in a few alloys.

The prime objective of this program was to enhance the elevated temperature strength of the baseline alloy without degrading the room temperature ductility. The results of tensile testing performed both at room temperature and at 600°C (1112°F) are shown in Tables VIII and IX. Room temperature ductility was generally sacrificed for superior elevated temperature strength in the case of alloys containing Mo, Ni, or Si.

Quaternary alloys containing Mo and Cr showed promise in that usable ductility was maintained at room temperature while elevated temperature strength was enhanced. The two phase alloys (Nb and Ta) also showed improved elevated temperature strength while maintaining some of the baseline ductility. This strengthening apparently was due primarily to solid solution effects since the properties could not be related to the volume fraction of precipitates. This indicated that a potential exists for further strengthening via refinement of the precipitate size. Researchers at SRL determined that the 2 a/o Nb alloy could indeed be further strengthened by heat treatment. The SRL heat treatment consisted of a solution treatment with a water quench, plus a aging treatment.

#### 4.2 Series II Alloys

For the Series II effort, fifteen alloy compositions were produced by isothermal forging of cast ingots. These alloys were primarily quaternary compositions and were evaluated by four-point bending tests.

##### 4.2.1 Alloy Selection

Based on the Series I evaluations, fifteen additional compositions, as shown in Table XII, were selected for further evaluation in Series II. These were primarily quaternary alloys, and included combinations of one of the non-embrittling additions with one of the strengthening additions, with the intent of achieving both enhanced elevated temperature strength and acceptable room temperature ductility. These Series II alloys were grouped into three categories, (Cr series, Ta series, and Nb series), each designed to evaluate a specific area of interest.

The Cr series was intended to be wholly single phase quaternaries. Cr did not show a tendency to embrittle the baseline (as long as abnormal grain growth is avoided) and Mo was shown to provide solid solution strengthening at elevated temperature. The principal objective was to bracket the optimal ratio of Cr to Mo in terms of elevated temperature strength and room temperature ductility.

TABLE XII  
TASK II/SERIES II ALLOYS

(Atomic Percentage)

<u>Alloy</u>	<u>Chromium Series - Single Phase</u>
II-1	Fe - 25 Al - 1 Cr - 1 Mo
II-2	Fe - 25 Al - 1 Cr - 2 Mo
II-3	Fe - 25 Al - 4 Cr - 1 Mo
II-4	Fe - 25 Al - 4 Cr - 2 Mo
	<u>Tantalum Series - Single-Phase</u>
II-5	Fe - 25 Al - 0.75 Ta - 1 Mo
II-6	Fe - 25 Al - 0.75 Ta - 2 Mo
II-7	Fe - 25 Al - 0.75 Ta - 0.50 Nb
II-8	Fe - 25 Al - 2 Ta
	<u>Niobium Series - Two-Phase</u>
II-9	Fe - 25 Al - 1 Nb - 2 Cr
II-10	Fe - 25 Al - 1 Nb - 0.50 Ta
II-11	Fe - 25 Al - 1 Nb - 1 Ta
II-12	Fe - 25 Al - 1 Nb - 2 V
II-13	Fe - 25 Al - 2 Nb - 1 Cr
II-14	Fe - 25 Al - 2 Nb - 0.50 Ta
II-15	Fe - 25 Al - 2 Nb - 1 V

The Ta series was intended to evaluate the solid solution strengthening potential of Ta-Mo and Ta-Nb additions, based on the high elevated temperature strength of the single phase Ta alloy of Series I. Nb and Mo additions to this ternary would be expected to further enhance elevated temperature strength. The single ternary alloy (2 a/o Ta) was intended to evaluate an alloy with Ta content intermediate between the two alloys studied in Series I. This was necessary because the leaner (1 a/o Ta) alloy was single phase and the richer (5 a/o Ta) alloy contained large amounts of second phase which could not be solutioned via heat treatment.

The Nb series was intended to result in essentially two phase alloys. The 2 a/o Nb alloy was found to have significant precipitation potential. However, it was established that the strengthening phase was metastable at 700°C (1292°F). The Cr, Ta, and V additions were selected in order to evaluate their effect on precipitate stability as well as mechanical properties. Other work at AFWAL has shown that small additions of V have been shown to impart ductility to iron aluminides. The Series I results suggested that Cr may have a similar effect.

#### 4.2.2 Material Procurement/Processing

##### 4.2.2.1 Ingot Casting/Homogenization

In order to evaluate the Series II compositions, new test stock was produced. It was determined that producing test stock by casting ingots and forging these ingots to refine the microstructure was more expedient in terms of time and cost than the P/M process routing used for Series I. While the P/M routing would be expected to produce a more refined microstructure in terms of grain size and the size and distribution of any second phase, it was anticipated that by proper selection of Thermo-Mechanical Processing (TMP) parameters, the cast plus forge routing would produce a satisfactory structure. The process, thus, selected included casting small ingots, enhancing their chemical homogeneity via heat treatment, and upset forging to refine the microstructure.

Materials were procured to produce the Series II alloys and casting molds were prepared using standard aerospace investment casting mold preparation procedures. The charge compositions (by weight) are listed in Table XIII. A 1 kg (2.2 lb) total charge was used for each alloy. The charge was placed in a ceramic crucible in a vacuum induction furnace. The chamber was evacuated to 30 microns, backfilled with argon, and re-evacuated to 30 microns, after which power was applied to the induction coil. The charge temperature was monitored optically and with a shielded thermocouple. After 15-20 minutes of heating, the charge typically had reached 1610-1620°C (2930-2950°F). The molten charge was held in this superheated condition for five minutes while inductive stirring was taking place in order to improve homogeneity of the melt. The melt was then poured into a cold ceramic mold. The temperature at time of pour was typically 1600-1605 C (2910-2920 F). Use of both the five minute hold and the use of a cold mold were developed during initial casting trials. It was determined that the charge was not fully homogenized without the five minute hold as evidenced by unmelted portions of the charge found in the castings. Using a preheated mold caused casting pipe (shrinkage porosity) to extend well beyond the riser and resulted in unusable ingots. The ceramic mold, a typical casting, and the resultant forging preform after removal of the riser and finish machining are shown in Figure 49. The vacuum induction melted ingots were homogenized for 1000°C (1832°F)/1 week prior to the isothermal forging operations.

#### 4.2.2.2 Isothermal Forging

Isothermal forging was selected as the most suitable hot working method on the basis of prior experience at AFWAL with the iron aluminide alloys. In order to evaluate forgeability, the effects on microstructure, and establish forging parameters, subscale forging trials were performed prior to committing larger sections of the castings to forging. Subscale forging specimens 1.0 cm (0.4 inch) in diameter and height were EDM machined from sound sections of the riser of each alloy.

TABLE XIIICHARGE WEIGHTS FOR TASK II/SERIES II ALLOYS (GRAMS)

<u>Alloy</u>	<u>Fe</u>	<u>Al</u>	<u>Other</u>	
II-1	832.1	137.7	Cr 10.6	Mo 19.6
II-2	814.1	136.6	Cr 10.5	Mo 38.8
II-3	799.8	138.0	Cr 42.6	Mo 19.6
II-4	782.0	136.9	Cr 42.2	Mo 38.9
II-5	818.7	135.0	Ta 27.2	Mo 19.2
II-6	801.0	133.9	Ta 26.9	Mo 38.1
II-7	822.7	135.6	Ta 27.3	FeNb 14.4
II-8	797.3	131.9	Ta 70.8	
II-9	811.5	137.9	FeNb 29.4	Cr 21.3
II-10	816.8	135.9	FeNb 29.0	Ta 18.2
II-11	801.1	134.2	FeNb 28.7	Ta 36.0
II-12	806.1	137.9	FeNb 29.4	Fe 28.3
II-13	794.4	136.7	FeNb 58.4	Cr 10.5
II-14	789.4	134.9	FeNb 57.6	Ta 18.1
II-15	790.8	136.8	FeNb 58.4	Fe 14.0

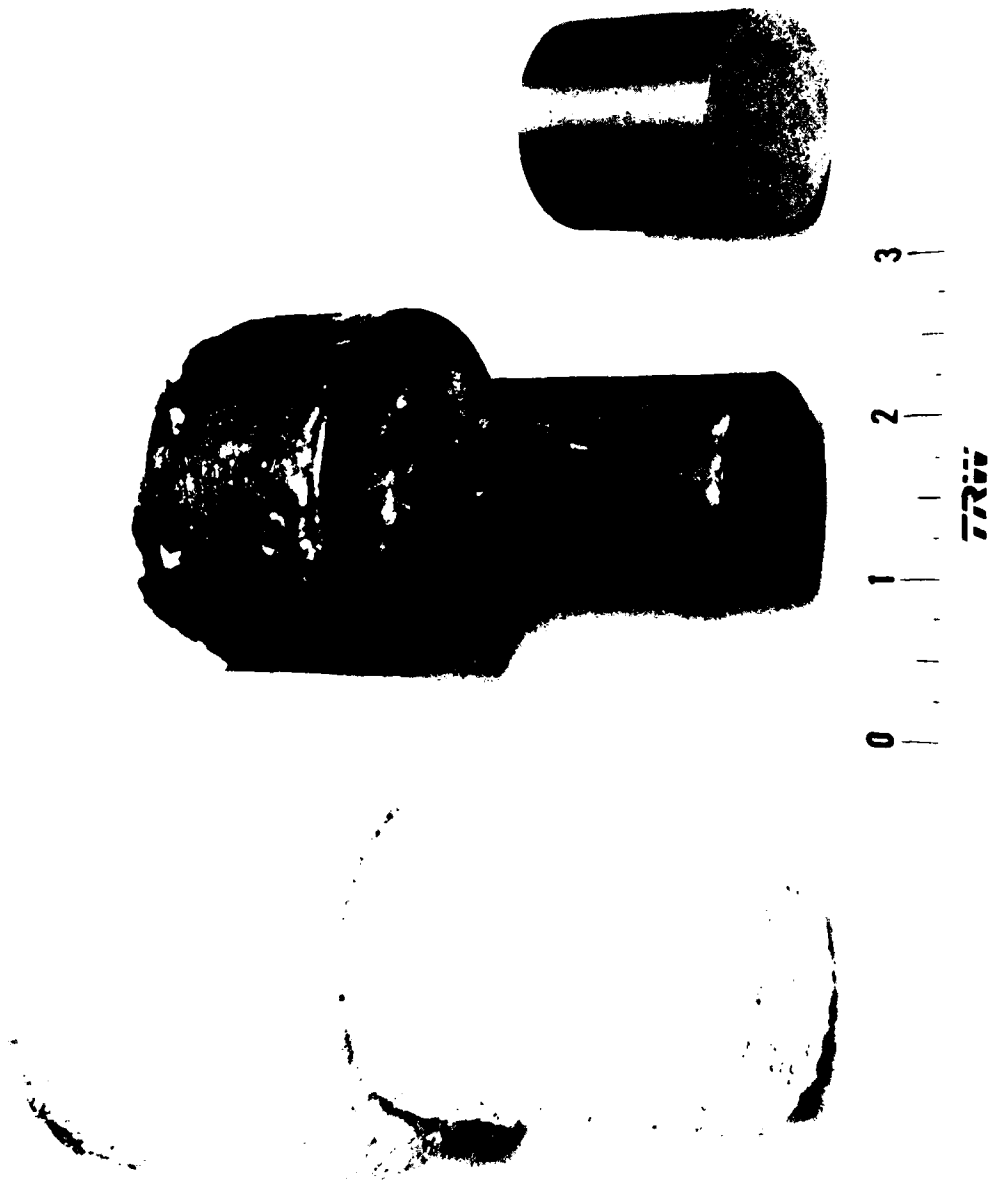


Figure 49. Photograph of ceramic mold (left) used to cast ingot (center) which was machined into a forging preform (right) for the Task II/ Series I alloy studies.



#### 4.2.2.2.1 Forging Results

Forging was performed between flat internally heated IN-100 dies placed in a 54,400 kg (60 ton) Baldwin Testing Machine. This equipment offered the capability for controlled, variable cross-head speed. Specimens were coated on all surfaces with a glass/graphite forging lubricant. Each specimen was heated to 595°C (1100°F) for 5-10 minutes in air as a pre-heat operation to preserve the integrity of the forging lubricant.

After pre-heating, each specimen was placed on the heated dies, which had been heated to the 954°C (1750°F) forging temperature. Once the temperature of the specimen was nominally the same as the dies (as determined visually by color), ram contact was made with the workpiece and a small pre-load of approximately 23 kg (50 lb) was applied. The specimen was monitored with an optical pyrometer to determine temperature equivalence with dies. Once the temperature was equivalent, the pre-load was maintained for another 1-2 minutes to ensure temperature uniformity throughout the sample.

A cross-head speed of 0.03 cm/min (0.015 inch/min) was used throughout the forging trials. This is equivalent to a strain rate of 0.04/min. Initial trials indicated that a 6:1 (83%) reduction in height was possible in one blow, but that the forging load increased exponentially during the last portion of the forging. In addition, small surface cracks were observed on the circumference of compacts forged in a single blow. The cause of the load increase was determined to be excessive depletion of the lubricant. In all subsequent trials, the specimens were upset approximately 2:1 (50%), cleaned, re-lubricated, and finish forged in a second blow. This resulted in lower, more practical loads and less cracking of the forgings. Maximum forging loads typically varied between 362-996 kg (800-2200 lb) for the first blow and between 4525-8145 kg (10,000-18,000 lbs) for the second blow.

#### 4.2.2.2.2 Microstructural Evaluation

The processing sequence discussed in the preceding section was performed in order to develop process routings that would result in fine-grained structures suitable for mechanical property testing. It was anticipated that

the alloys would either undergo dynamic recrystallization during forging or recrystallization during subsequent isothermal annealing at higher temperatures. It was also anticipated that the forging would refine the size of second phase precipitates (if any) and cause them to become more homogeneously dispersed than in the cast structure. Once the second phase was well dispersed, it might then be possible to create coherent precipitates via a solution and age heat treatment.

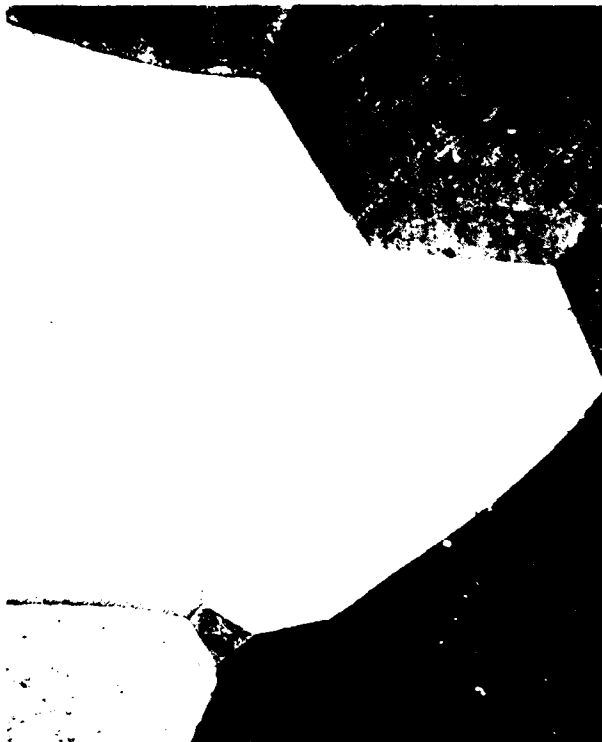
#### 4.2.2.2.1 Cr Series

The Cr series, which included various ratios of Cr and Mo additions to the baseline material, was characterized by single phase alloys. A representative example of this series was alloy II-1 (1 a/o Cr, 1 a/o Mo). The as-cast structure, shown in Figure 50, was characterized by a very large grain size, approximately 0.2 cm (0.08 inch) in diameter.

The structure of alloy II-1 forged at 954°C (1750°F) is shown in Figure 51a. Note that although the grains have been severely deformed, the grain size was not changed. Typical grains measured 1 cm x 0.02 cm (0.4 inch x 0.0008 inch). The microstructure after application of a heavier etch is shown in Figure 51b. This shows that smaller, lightly etched, grains are present within the larger unrecrystallized grains. X-ray diffraction analysis suggested that the smaller grains were actually defined by low angle grain boundaries. Similar structures were observed in all of the alloys after forging at 954°C (1750°F) when exposed to the heavy etch, although only the lightly etched structure is shown in most of the figures. This textured structure is not considered optimal for improved mechanical properties performance. There was no discernable difference between the microstructures of the four alloys in the Cr series.

#### 4.2.2.2.2 Ta Series

The intent of the alloy design of this series was to create single phase alloys, but the degree of solid solubility of the refractory metals in the baseline material was not precisely known. All four Ta series alloys exhibited two phase structures, although the volume fraction of the second



40X (polarized light)

100X

500X

Figure 50. Light photos of as-cast Cr-1 a/o, Mo-1 a/o (Alloy II-1) ingot showing coarse grain size.

(a)

100X

500X

(b)

Figure 51. Light photos of as-forged Cr-1 a/o, Mo-1 a/o (Alloy II-1) sub-size specimen isothermally forged at 554°C (1750°F) and 6:1 height reduction (longitudinal section) showing structure after normal etch (a) and heavy etch (b).

phase varied. Two examples of this series are discussed, alloy II-5 (0.75 a/o Ta, 1 a/o Mo) and alloy II-8 (2 a/o Ta).

Alloy II-5 in the as-cast condition is shown in Figure 52. The grain size and shape were similar to that of the alloys in the Cr series. A small amount of second phase was observed at grain boundaries and within the grains.

In the as-forged condition, alloy II-5 contained a small amount of second phase as shown in Figure 53. These second phase particles were principally composed of Ta-Mo-Fe, as determined by EDS, and amount of about 1 volume percent of the structure. The preferential partitioning of Mo in the second phase relative to the matrix was somewhat unexpected, since Mo alone does not form a second phase. The particles range from 5-15 microns in diameter.

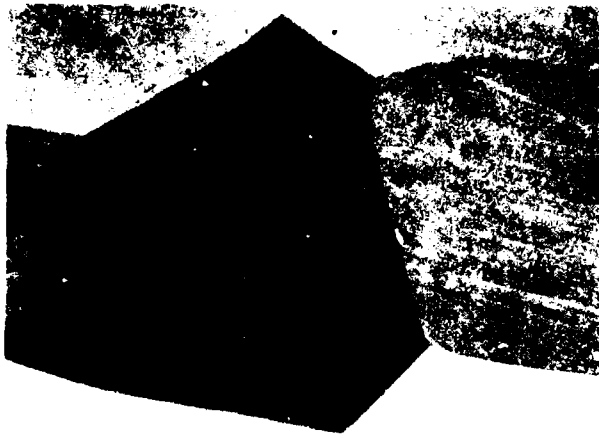
Alloy II-8 in the as-cast condition is shown in Figure 54. The grain size is consistent with the other alloys. The second phase is concentrated at grain boundaries, but is also present to a lesser extent within grains.

After isothermal forging, alloy II-8 exhibited large deformed grains and relatively evenly distributed second phase particles as shown in Figure 55. These particles are aligned perpendicular to the forging direction and typically measure 15 x 1 microns. EDS indicated that these particles are principally of Fe-Ta composition and amount to about 20 volume per cent of the structure.

#### 4.2.2.2.3 Nb Series

It was expected that all of the alloys in the Nb series would contain second phase particles, due to the limited solid solubility of refractory metals in the baseline alloy. It was also anticipated that solution and age heat treatments would be necessary subsequent to forging in order to fully utilize the precipitation strengthening potential of these alloys.

The Nb series was, in general, characterized by the same large grains observed in all the alloys. As expected, all six alloys contained second phase particles and the amount of second phase was directly related to the refractory metal (Nb + Ta) content.



40X (polarized light)

100X

500X

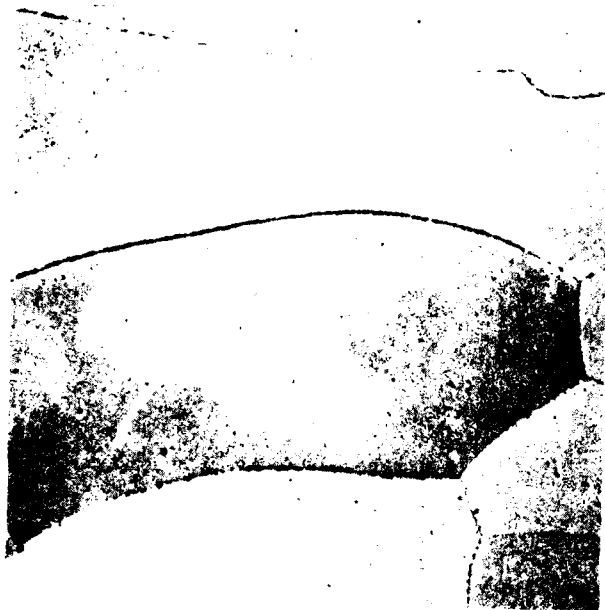
Figure 1. A series of three photographs showing the same mineral specimen at increasing magnifications: 40X (polarized light), 100X, and 500X. The images illustrate the crystal's morphology and internal features at different scales.



100X

500X

Figure 53. Light photos of as-forged Ta-0.75 a/o, Mo-1 a/o (Alloy II-5) sub-size specimen isothermally forged at 954°C (1750°F) and 6:1 height reduction (longitudinal section).



40X (polarized light)

100X

500X

Figure 50. Micrograph of as-cast Ta-2 alloy (Alloy 11-8) ingot showing coarse grain structure.





100X

500X

Figure 55. Light photos of as-forged Ia-2 a/o (Alloy II-8) sub-size specimen isothermally forged at 954°C (1750°F) and 6:1 height reduction (longitudinal section).

Alloy II-9 (1 a/o Nb, 2 a/o Cr) and alloy II-12 (1 a/o Nb, 2 a/o V) exhibited similar structures. The as-cast structure of alloy II-9 is shown in Figure 56. Note the large grains and the presence of second phase particles distributed throughout the grains as opposed to concentration at the grain boundaries. After isothermal forging, Figure 57, alloy II-9 exhibited the same large deformed grains observed in other alloys and second phase particles which amounted to about 10 volume per cent. EDS indicated that the second phase was principally composed of Nb-Fe.

Alloy II-11 (1 a/o Nb, 1 a/o Ta), alloy II-13 (2 a/o Nb, 1 a/o Cr), and alloy II-15 (2 a/o Nb, 1 a/o V) were observed to exhibit microstructures very similar to each other. Alloy II-15 was representative of this group within the Nb series and its cast structure is shown in Figure 58. Note the grain size and the large amount of second phase both at grain boundaries and within the grains. After forging, Figure 59, the second phase was aligned perpendicular to the forging direction. These second phase particles are typically 2 microns wide by 15 microns long and amount to about 20 volume percent. EDS indicates that they are principally Nb-Fe, which indicates that V, like Cr, tended to remain in solution in the matrix. Note that the heavy etch, as employed for alloy II-1, Figure 51, delineated a sub-structure of low angle grain boundaries within the large deformed grains.

The remaining two alloys in the series, alloy II-10 (1 a/o Nb, 0.5 a/o Ta) and alloy II-14 (2 a/o Nb, 0.5 a/o Ta) exhibited microstructures and volume fractions of second phase which correlated well with their respective refractory metal content.

#### 4.2.2.3 Grain Refinement Studies

Grain refinement studies were conducted on the assumption that the large grains and/or textured structure observed in the as-forged structures would be unsuitable for mechanical properties testing. On the premise that the forging conditions selected for the initial sub-size forgings did not impart sufficient strain energy into the alloys to cause fine grain recrystallization, additional isothermal forging trials were performed at



40X (polarized light)

100X

500X

Figure 56. Light photos of as-cast Nb-1 a/o, Cr-2 a/o (Alloy 11-9) ingot showing coarse grain size.

100X

500X

Figure 5/ . Light photos of as-forged Nb-1 d/o<sub>2</sub> Cr-2 d/g (Alloy II-9) sub-size specimen isothermally forged at 954°C (1750°F) and 6:1 height reduction (longitudinal section).



40X (polarized light)

100X

500X

Figure 58. Light photos of as-cast Nb-2 a/o, V-1 a/o (Alloy II-15) ingot showing coarse grain size.



100X (light etch)

100X (heavy etch)



500X (heavy etch)

Figure 59. Light photos of as-forged Nb-2 a/o, V-1 a/o (Alloy II-15) sub-size specimen isothermally forged at 954°C (1750°F) and 6:1 height reduction (longitudinal section).

lower temperatures. For this effort, sub-size specimens 0.9 cm (0.375 inch) in diameter by 0.9 cm (0.375 inch) high of each alloy were isothermally forged at 730°C (1350°F) and 790°C (1450°F) at a constant strain rate of 0.04/min. Forging was halted when the load on the dies reached 8,160 kg (18,000 lbs.), which had been determined to be the safe limit of the ceramic insulation which backed up the forging dies. This generally corresponded to a reduction in height of approximately 6:1.

The single phase alloys exhibited similar forging response at both forging temperatures. The as-cast grain size was severely deformed and there were smaller grains present within the larger unrecrystallized grains. An example of this type of microstructure for alloy II-4 (4 a/o Cr, 2 a/o Mo) is shown in Figure 60a in the as-forged condition. Recrystallization annealing treatments were investigated in order to produce a more uniform grain size throughout the forgings. These recrystallization anneals were conducted in the temperature range 730°C (1350°F) - 1120°C (2050°F). These treatments indicated that a one hour exposure at 954°C (1750°F) resulted in the most uniform grain size throughout the forgings. An example of this recrystallized grain size for alloy II-4 (4 a/o Cr, 2 a/o Mo) is shown in Figure 60b. The average grain diameter is approximately 375 microns. There was little appreciable difference between the microstructures of the four alloys in the Cr series. While it was realized that these grain sizes were significantly larger than observed in the powder metallurgy alloys of the first series (as shown in Figure 9 for the baseline Fe<sub>3</sub>Al alloy) they were refined compared to the as-cast ingot and their distribution was homogeneous.

In general, the isothermal forging response of the two phase alloys was similar at both forging temperatures. The microstructures were also similar to those of the 954°C (1750°F) forgings in that large deformed grains were observed, which also contained smaller sub-grains. It was noted, however, that the sub-grains appeared somewhat smaller in the lower temperature forgings.

(a) as-forged

(b) after one hour at 984° (1,300°F)

Figure 60 Light photos of cross section of 1000-psi (411a, 1141) high-speed steel, as-forged and after one hour at 984° (1,300°F) and cooling to room temperature, 1000 Magnification.



An example of the as-forged structure for alloy II-15 (2 a/o Nb, 1 a/o V) forged at 730°C (1350°F) is shown in Figure 61. A comparison of this structure with that presented in Figure 59 for the same alloy isothermally forged at 954°C (1750°F) suggests a more refined size in the small sub-grain structure. As a general comment as related to these two phase structures, all the alloys contained second phase particles and the amount of the second phase was related to the refractory metal content. As will be discussed in more detail in Section 4.2.3.2 describing the material preparation efforts for the Series II screening evaluation, solution treatment studies were conducted on selected two-phase alloys in order to develop a dispersion of coherent second phase particles in order to take advantage of the precipitation strengthening potential of these alloys.

#### 4.2.3 Screening Evaluations

Screening evaluations were conducted on selected alloys of the Series II group which included elevated temperature four-point bend testing. The details of these screening evaluations are presented in the following sections.

##### 4.2.3.1 Alloy Selection

The Series II alloys selected for the screening evaluations are listed in Table XIV. Included in the table are the aim chemistries as well as the analyzed results. These results indicated that the actual chemistries met the aim with the exception of alloy II-15, which had less than the desired 1 a/o V.

The rationale for the alloy selection was based upon several considerations. First, it was desired to evaluate an alloy in each particular series (Cr, Ta, and Nb as originally planned and shown in Table XII) with the greatest strengthening potential compared to the baseline Fe<sub>3</sub>Al composition. Second, on the basis of on-going studies of precipitate behavior being conducted at AFWAL/SRL, it was desired to evaluate an alloy with at least a 2 a/o amount of precipitate forming addition to optimize the amount of coherent second phase in the microstructure.



(a) 100X

(b) 500X

Figure 61 Light photos of as-forged Nb-2, V-1 alloy (Alloy 11-13) sub-size specimen isothermally formed at 730°C [1350°F] and 611 height reduction.

TABLE XIV

CHEMICAL COMPOSITION OF TASK II/SERIES II  
ALLOYS SELECTED FOR SCREENING EVALUATIONS

<u>ALLOY</u>	<u>AlM</u>	<u>WEIGHT PERCENTAGE</u>				<u>ATOMIC PERCENTAGE</u>			
		<u>Fe</u>	<u>Al</u>	<u>X</u>	<u>Y</u>	<u>Fe</u>	<u>Al</u>	<u>X</u>	<u>Y</u>
II-4	Fe-25Al-4Cr-2Mo	79.03	13.03	3.97	3.97	70.2	24	3.8	2
II-8	Fe-25Al-2Ta	80.9	11.97	7.13	---	75	23	2	--
II-13	Fe-25Al-2Nb-1Cr	81.16	13.74	4.04	1.06	71.8	25.1	2.1	1
II-15	Fe-25Al-2Nb-1V	81.84	13.63	4.13	0.4	72.4	25	2.2	0.4

On this basis, alloy II-4 (4 a/o Cr, 2 a/o Mo) was chosen from the single phase Cr series as having greatest strengthening potential. Alloy II-8 (2 a/o Ta) was chosen from the Ta series to maximize refractory content. Alloys II-13 (2 a/o Nb, 1 a/o Cr) and II-15 (2 a/o Nb, 1 a/o V) were chosen to maximize refractory content as well as on the basis of studies in progress at AFWAL that Cr and V additions do not significantly degrade ductility.

#### 4.2.3.2 Material Preparation

The purpose of the sub-size isothermal forging/grain refinement efforts was to establish forging parameters for the eventual scale-up to provide material for the screening evaluations. As stated previously, the sub-size forging specimens were prepared from sound sections of the riser portion of the vacuum induction melted ingot of each alloy. The scale-up forging work was done on forging preforms machined from the ingots as shown in Figure 49.

The same isothermal forging procedures were used for each of the four alloys selected for the screening evaluations. The starting stock size was 3.6 cm (1.4 inch) in diameter by 3.8 cm (1.5 inch) high. The forging was performed at 730°C (1350°F) in a 678,733 kg (750 ton) vacuum hydraulic press using flat Mo-TZM dies with boron nitride/graphite lubricant. A constant strain rate of 0.06/min was used and the workpiece was soaked at temperature for 1-1/2 hours prior to deformation. A reduction in height of 6:1 was achieved and a full-size forging, along with a forging preform, is shown in Figure 62.

On the basis of the grain refinement studies conducted on the sub-size specimens, a recrystallization anneal heat treatment was applied to the alloy II-4 forging. This anneal consisted of a one hour exposure at 954°C (1750°F).

On the basis of studies conducted at AFWAL/SRL on the precipitation behavior of the Ta and Nb containing alloys it was established that full precipitate solutioning could be achieved in alloys II-8, II-13, and II-15.

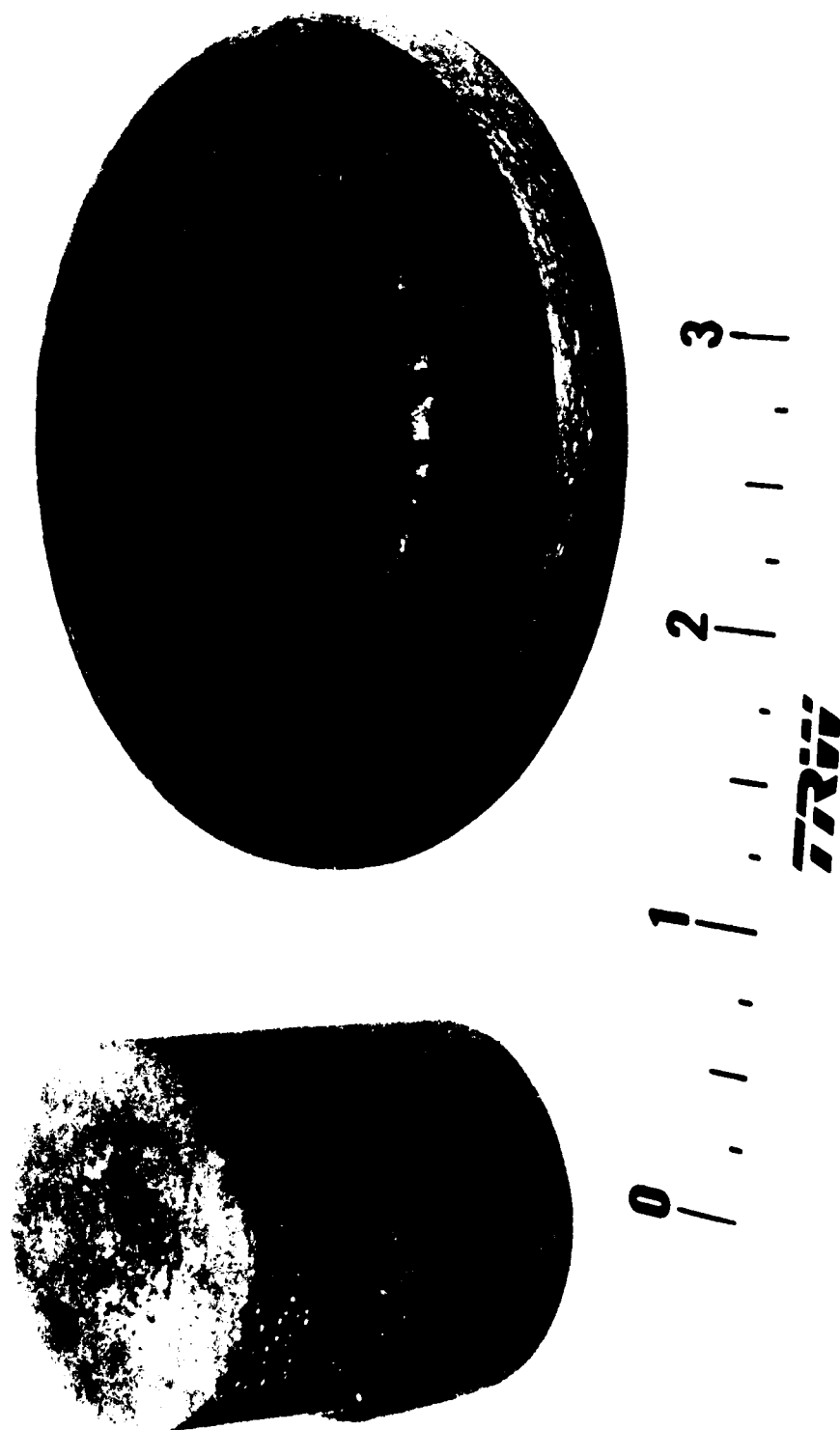


Figure 62 Photograph of typical Series II full-size preform pancake isothermally forged at 730°C (1350°F) and 6:1 height reduction.

This had been established on the basis of studies conducted on small metallographic specimens sectioned from the sub-size forgings. This solution treatment included a 30 minute exposure at 1250°C (2282°F) followed by a quench in agitated water. Upon application of this solution treatment to the full size forgings, however, severe quench cracks were observed throughout the forgings. The degree of quench cracking was so severe that specimens could not be machined from the forgings. This indicated that the vacuum induction melting/isothermal forging processing approach developed for these particular alloys would not be able to exploit the strengthening potential suggested by the precipitation behavior in small section sizes.

#### 4.2.3.3 Test Results

As a result of the quench cracking problem with alloys II-8, II-13, and II-15, testing was conducted only on the II-4 alloy. This evaluation included elevated temperature four-point bend tests conducted on specimens 0.3 cm (0.125 inch) x 0.6 cm (0.250 inch) x 2.9 cm (1.125 inch) in size. The results of these tests are presented in Table XV and include the yield strength (elastic limit) at 600°C (1112°F), 650°C (1202°F) and 700°C (1292°F). For comparison purposes, the yield strength results for the baseline Fe<sub>3</sub>Al alloy at 600°C (1112°F) generated as part of the Series I testing and the yield strength results of Fe-35Al-4Cr-2Mo generated at AFWAL are also included in Table XV.

The results indicate that the II-4 alloy offers significant improvement in yield strength capability at 600°C (1112°F) compared to the baseline Fe<sub>3</sub>Al composition. The yield strength of the II-4 alloy was approximately 2.5 times that of Fe<sub>3</sub>Al. These results confirm the potent solid solution strengthening capability of Cr and Mo additions to Fe<sub>3</sub>Al identified in the Series I alloy testing. The yield strength of the I-13 alloy (0.3 a/o Mo, 2 a/o Cr) was approximately 1.6 times that of Fe<sub>3</sub>Al at 600°C (1112°F). The increased Cr and Mo additions in alloy II-4 (4 a/o Cr, 2 a/o Mo) resulted in improved solid solution strengthening.

TABLE XV

YIELD STRENGTH RESULTS FOR TASK II/SERIES II ALLOYS (1)

<u>ALLOYS</u> <sup>(2)</sup>	<u>600°C (1112°F)</u>	<u>650° (1202°F)</u>	<u>700°C (1292°F)</u>
II-4 (4Cr, 2Mo)	545 Mpa (79 Ksi)	365 Mpa (53 Ksi)	200 Mpa (29 Ksi)
Fe <sub>3</sub> Al Baseline	214 Mpa (31 Ksi)	----	----
(Fe-35Al-4Cr 2Mo) <sup>(3)</sup>	510 Mpa (74 Ksi)	338 Mpa (48 Ksi)	262 Mpa (38 Ksi)

(1) Elastic limit in four-point bend tests

(2) Alloys II-8 (2Ta), II-13 (2Nb, 1Cr), II-15 (2Nb, 1V) not tested because of quench cracks.

(3) AFWAL alloy prepared as 150 gram (0.3 lb.) arc melted button isothermally forged 75% at 950°C (1742°F)

As shown in Table XV, Cr and Mo additions to Fe-35 a/o Al can also result in strength improvements compared to baseline  $\text{Fe}_3\text{Al}$ . It also appears that the Fe-35 a/o Al base can also offer some improvement in  $700^\circ\text{C}$  ( $1292^\circ\text{F}$ ) yield strength compared to Cr and Mo modified  $\text{Fe}_3\text{Al}$ . This general situation is further enhanced by the fact that the Fe-35 Al base would offer additional attractive features in terms of reduced density compared to the  $\text{Fe}_3\text{Al}$  baseline.

#### 4.2.4 Series II Summary

The Series II alloy studies included fifteen alloys divided into three groups as shown in Table XII. These included ternary or quaternary alloys with Cr, Ta, or Nb as the common alloying addition. The compositions were produced by isothermal forging of vacuum induction melted ingots. Plans called for specific compositions to be evaluated by elevated temperature four-point bend tests.

During preparation of material for testing, it was observed that the Cr series exhibited a single phase microstructure characterized by a large as-cast grain size. Isothermal forging parameters were defined followed by recrystallization anneals which produced a uniform equiaxed grain size of approximately 375 microns in diameter. Alloy II-4 (4 a/o Cr, 2 a/o Mo) was tested in four-point bending with the result that the  $600^\circ\text{C}$  ( $1112^\circ\text{F}$ ) yield strength improved by a factor of 2.5 compared to the baseline  $\text{Fe}_3\text{Al}$  alloy. These results confirmed the potent solid solution strengthening capability of Cr and Mo additions to  $\text{Fe}_3\text{Al}$  identified during the Series I testing.

Also during preparation of material for testing, it was observed that the Ta and Nb series exhibited a two phase microstructure characterized by the presence of precipitate particles the amounts of which were related to the refractory metal content in the alloy. Solution heat treatments were identified by AFWAL/SRL in parallel studies which were successful in completely solutioning the second phase particles in small metallographic specimens. A section size sensitivity was observed, however, in that severe quench cracking was encountered during the quenching of the full-size forged



pancakes intended for the screening evaluations. It was not possible to machine specimens from these quenched pancakes. This indicated that the vacuum induction melting/isothermal forging processing approach developed for these particular alloys would not be able to exploit the strengthening potential suggested by the precipitation behavior in small section sizes.

### 4.3 Alloy Characterization

For this effort, a single alloy composition was produced by the hot extrusion of vacuum induction melted ingots. The alloy was a quaternary composition designed on the basis of the results of the Series I and II alloys. Alloy characterization consisted of mechanical property tests including tensile, creep rupture and fatigue tests at elevated temperature. Oxidation resistance of the alloy was also characterized.

#### 4.3.1 Alloy Selection

The alloy selected for evaluation in this final portion of the program was Fe-35Al-4Cr-2Mo (in atomic percent). This selection was made in order to take advantage of the potent solid solution strengthening demonstrated by Cr and Mo additions during the Series I and II evaluations. In addition, it was desired to enhance the specific strength by utilizing a base alloy (Fe-35 a/o Al) exhibiting a lower density than the Fe<sub>3</sub>Al baseline. While it was recognized that two phase alloys based upon Ta and Nb additions do offer potential for precipitation strengthening, the quench crack sensitivity demonstrated in the Series II isothermally forged pancakes represented a possible limit to the applicability of these alloy development concepts within the scope of this program.

#### 4.3.2 Material Procurement/Processing

##### 4.3.2.1 Ingot Casting/Homogenization

In order to evaluate the Fe-35Al-4Cr-2Mo composition, new test stock was produced. To achieve a more refined grain size than was developed in the

isothermally forged cast ingots used for the Series II evaluations, a process routing including the hot extrusion of vacuum induction melted ingots was selected. The ingot casting procedures used to prepare the final alloy were identical to those described previously in Section 4.2.2.1 for the Series II alloys. For this effort, 11.3 kg (25 lb) ingots were prepared which exhibited the same large as-cast grain size as shown previously in Figure 50 for the II-1 (1 a/o Cr, 1 a/o Mo) alloy. Subsequent to casting, the ingots were treated with the same 1000°C (1832°F)/1 week homogenization treatment employed for the Series II ingots.

#### 4.3.2.2 Hot Extrusion

Hot extrusion of the vacuum induction melted ingots was employed in order to refine the large as-cast grain size of the Fe-35Al-4Cr-2Mo alloy. The canning procedures for these ingots were identical to those used for the Series I loose powder alloys and described previously in Section 4.1.2.2, including the extrusion can configuration shown schematically in Figure 3.

As part of this investigation, an extrusion matrix consisting of six extrusions was evaluated. A listing of the extrusion conditions including temperature and reduction ratio is presented in Table XVI, which also lists the grain sizes resulting from the various extrusion parameters.

The extrusion trials conducted at 843°C (1550°F) and modest reductions (reduction ratios less than 6:1) indicated poor results in that the 5.4:1 reduction caused the billet to stall in the extrusion press. Extrusion at the 3.5:1 reduction was successfully completed, but examination of the as-extruded microstructure indicated two problems, as shown in Figure 63a. The first included the fact that the microstructure was characterized by a non-uniform duplex grain size. Areas of the structure were characterized by a relatively small grain size, with an average grain diameter of 50 microns. Comparison of this grain size with that achieved for the Series I Fe<sub>3</sub>Al powder baseline alloy, shown in Figure 9, indicated a comparable grain diameter. There were, however, isolated grains larger than 250 microns in diameter throughout the

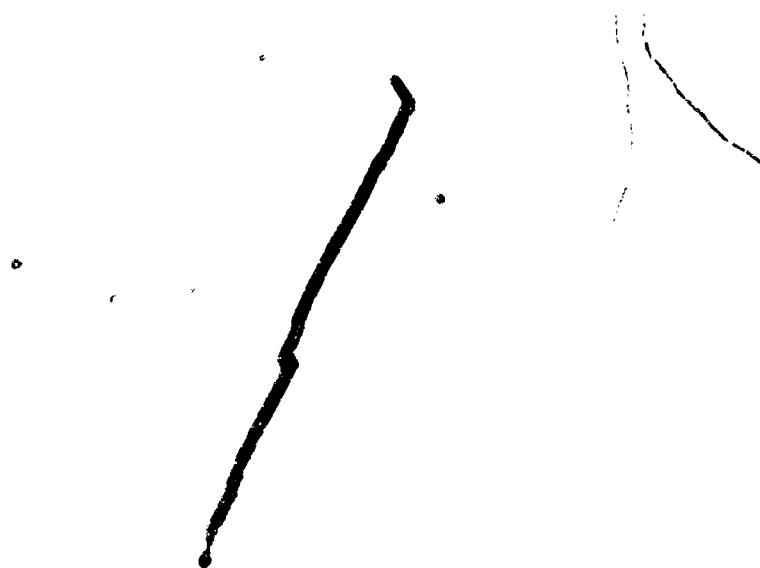
TABLE XVI

EXTRUSION RESULTS FOR Fe-35Al-4Cr-2Mo ALLOY

<u>EXTRUSION NO.</u>	<u>TEMPERATURE</u>	<u>REDUCTION RATIO</u>	<u>GRAIN SIZE</u>	<u>COMMENTS</u>
85009	843°C (1550°F)	5.4:1	-----	Extrusion stalled in press
85010	843°C (1550°F)	3.5:1	Duplex, average 50 microns Isolated grains >250 microns	Isolated internal cracking
85007	899°C (1650°F)	16:1	Duplex, average 90 microns Isolated grains >250 microns	Isolated internal cracking
85008	899°C (1650°F)	9:1	Duplex, average 70 microns Isolated grains >250 microns	Isolated internal cracking
85017	927°C (1700°F)	36:1	Duplex, average 15 microns Numerous grains >250 microns	Extensive internal cracking
85018	954°C (1750°F)	16:1	Uniform, average 125 microns	-----



(a) 100X



(b) 500X

Figure 63 Light photos of air-extruded Fe-50Al-4Cr-2Mn Vacuum induction melted ingot extruded at 1100°C and a 3.5:1 reduction ratio.

structure. The second problem included the presence of isolated instances of cracking throughout the microstructure. This cracking, shown in Figure 63b at 500X magnification, appeared to initiate at grain boundaries and propagate in a transgranular mode. Neither of these conditions suggested that the 843°C (1550°F), 3.5:1 reduction ratio extrusion should be used for mechanical property testing.

Increasing the extrusion temperature to 899°C (1650°F) and increasing the reduction ratios did not eliminate the problems observed in the lower temperature extrusion. The duplex grain size condition, as well as the isolated instances of internal cracking persisted. It was also observed that the average grain diameter of the areas of relatively small grains increased somewhat compared to the 843°C (1550°F) extrusion. A typical microstructure observed in these 899°C (1650°F) extrusions is shown in Figure 64a for material extruded at the 9:1 reduction ratio. The areas of relatively small grain size were characterized by grains with an overall average grain diameter of approximately 70 microns.

The final two extrusions were conducted at higher temperatures. The extrusion conducted at 927°C (1700°F) and 36:1 reduction ratio did not appear promising in that the duplex grain structure persisted and the degree of cracking appeared more severe. A typical microstructure for material extruded under these conditions is shown in Figure 64b. Groups of very small (average grain diameter of approximately 15 microns) grains were observed associated with more numerous large grains in excess of 250 microns. The severity of cracking is also evident in this microstructure.

The most optimum microstructure was observed in material extruded at 954°C (1750°F) with a 16:1 reduction ratio. Typical microstructure observed in this extruded material is shown in Figure 65. This was characterized by a uniform equiaxed grain size approximately 125 microns in average grain diameter, without the presence of cracking. While it was recognized that this grain size was significantly larger than the 50 micron grain size exhibited by extruded powder Fe<sub>3</sub>Al baseline alloy (Figure 9), it was smaller than the 375 micron grain size of the typical Series II Cr containing alloys (Figure 50).




(a)

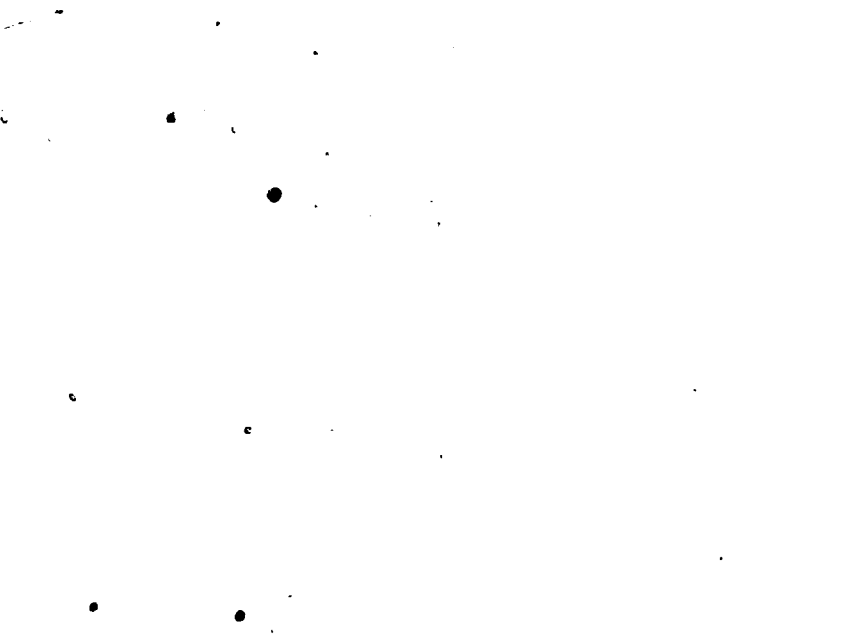


(b)

Figure 64 Light photos of as-extruded Fe-35Al-4Cr-2Mo vacuum induction melted ingot extruded at (a) 2990°C (1650°F) and a 9:1 reduction ratio and (b) 927°C (1700°F) and a 36:1 reduction ratio. 100X Magnification.



(a) 100X



(b) 500X

Figure 65 Light photos of as-extruded Fe-35Al-4Cr-2Mo vacuum induction melted ingot extruded at 954°C (1750°F) and a 16:1 reduction ratio.

As a consequence of these considerations, the material extruded at 954°C (1750°F) with a 16:1 reduction ratio was selected for mechanical properties testing.

#### 4.3.3 Properties Characterization

Properties characterization conducted on the Fe-35Al-4Cr-2Mo included elevated temperature tensile, creep rupture and low cycle fatigue tests, room temperature high cycle fatigue tests, and oxidation tests. The actual chemistry of the extrusion selected for evaluation was Fe-34.5Al-3.9Cr-2.1Mo in atomic percent. The test specimen configuration was identical to that shown schematically in Figure 33 for the Series I testing. The results of these properties characterizations are presented in the following sections.

##### 4.3.3.1 Tensile Test Results

The program objective included the development of compositions which offer improved room temperature ductility and high temperature strength compared to baseline Fe<sub>3</sub>Al. Tensile tests were conducted on the Fe-35Al-4Cr-2Mo alloy at room temperature and 600°C (1112°F) and the results are presented in Table XVII. On the average, this material exhibited an ultimate tensile strength of approximately 413 Mpa (60 Ksi), a yield strength of 361 Mpa (52 Ksi), elongation of 2.6 percent and reduction of area of 3.3 percent at room temperature. Comparison with the results listed in Table VIII for Fe<sub>3</sub>Al indicated that the quaternary alloy was inferior in performance on all accounts. It was significant to note that the ductility of the quaternary alloy was approximately 50% lower than that of the Fe<sub>3</sub>Al. Examination of the failed test specimens revealed that there was little deformation of the grains and, unlike the Fe<sub>3</sub>Al, the fracture mode was principally transgranular. An example of this structure is shown in Figure 66a. The fracture mode for Fe<sub>3</sub>Al at room temperature was principally intergranular, as shown in Figure 35.

Tensile testing at 600°C (1112°F) indicated an average ultimate tensile strength of 467 Mpa (68 Ksi), a yield strength of 344 Mpa (50 Ksi), elongation of 50 percent and reduction of area of 56 percent. Comparison with the





(a)



(b)

Figure 66 Light photos of Fe-35Al-40Cr-2Mo alloy (a) fracture and (b) 600°C (1112°F) tensile test specimen showing features of the fracture surfaces. 100X Magnification.

results listed in Table IX for  $\text{Fe}_3\text{Al}$  indicated that the quaternary alloy exhibited increased strength, but somewhat lower ductility. The yield strength of the quaternary was approximately 1.6 times that of the  $\text{Fe}_3\text{Al}$  alloy, with approximately 72 percent of the elongation. Comparison of the data presented in Table XV for the Series II testing, however, indicated that the quaternary alloy prepared by the extrusion of vacuum induction melted ingot did not exhibit the  $600^\circ\text{C}$  ( $1112^\circ\text{F}$ ) yield strength of either alloy II-4 (4 a/o Cr, 2 a/o Mo) or the Fe-35Al-4Cr-2Mo alloy processed at AFWAL, which exhibited yield strengths in the range 510-545 Mpa (74-79 Ksi). Examination of the failed test specimens indicated extensive deformation of grains near the fracture surface as well as separation along grain boundaries. An example of this structure is shown in Figure 66b for regions near the fracture surface. This general behavior was also observed for the  $\text{Fe}_3\text{Al}$  alloy, as shown in Figure 36. More extensive grain boundary separation was observed, however, in the  $\text{Fe}_3\text{Al}$  than in the quaternary alloy.

In summary, the results of the tensile tests conducted on the quaternary alloy confirmed the potent solid solution strengthening effects of Cr and Mo additions with regards to elevated temperature yield strength. The Fe-35Al-4Cr-2Mo alloy exhibited 1.6 times the yield strength capability of  $\text{Fe}_3\text{Al}$  at  $600^\circ\text{C}$  ( $1112^\circ\text{F}$ ). This strength increase, however, was achieved at the expense of a loss of approximately 50 percent of the room temperature tensile ductility (percent elongation) of the  $\text{Fe}_3\text{Al}$ .

#### 4.3.3.2 Creep Rupture Test Results

Creep rupture tests were conducted on the Fe-35Al-4Cr-2Mo quaternary alloy in the temperature range  $570^\circ\text{C}$  ( $1058^\circ\text{F}$ ) -  $649^\circ\text{C}$  ( $1200^\circ\text{F}$ ) and the results are listed in Table XVII. The tests conducted at  $649^\circ\text{C}$  ( $1200^\circ\text{F}$ )/241 Mpa (35 Ksi) exhibited extremely short rupture lives and time to 0.1% creep. Reducing the test conditions to  $570^\circ\text{C}$  ( $1058^\circ\text{F}$ )/207 Mpa (30 Ksi) resulted in an average rupture life of approximately 300 hours and an average time to 0.1% creep of approximately 34 hours. Comparison of these results can be made to commercial 410 martensitic stainless steel, which exhibits yield strength equivalent to that of the Fe-35Al-4Cr-2Mo at  $600^\circ\text{C}$  ( $1112^\circ\text{F}$ ), approximately 345 Mpa (50 ksi).

Under the same 570°C (1058°F)/207 Mpa (30 Ksi) rupture conditions, 410 martensitic stainless steel would exhibit a rupture life of approximately 20 hours, with a time to 0.1% creep of less than one hour.

Examination of the failed rupture bars indicated a similar fracture mode at both test conditions in that cracking was predominantly intergranular in nature. Examples of the structures observed in the failed rupture bars are shown in Figure 67. These structures are in marked contrast to that exhibited by the 600°C (1112°F) tensile test specimen shown previously in Figure 66a. Under the tensile test loading at 600°C (1112°F) considerable deformation was observed in the grains in addition to the intergranular type fracture. Under the creep loading at approximately 70% the yield strength, little grain deformation occurred with crack initiation and propagation occurring along the grain boundaries.

#### 4.3.3.3 High Cycle Fatigue Test Results

Room temperature high cycle fatigue tests were conducted on the Fe-35Al-4Cr-2Mo alloy and the results are presented in Table XVIII. The tests were conducted at a frequency of 10 Hz, in a tension-tension mode on smooth test specimens. The initial test specimen was to be loaded to a maximum of 413 Mpa (60 Ksi), which was the approximate ultimate tensile strength of the alloy as determined by the room temperature tensile tests, Table XVII. The specimen failed upon loading, however, at a maximum load of 410 Mpa (59.5 Ksi). Stress levels were then bracketed between 310 Mpa (45 Ksi) and 345 Mpa (50 Ksi) with the result that the specimens did not fail at or over one million cycles. These results suggest that the endurance limit (as defined by a failure life in excess of one million cycles) for this material lies between 345 Mpa (50 Ksi) and 410 Mpa (59.5 Ksi). These data also indicate that the conventional high cycle fatigue S-N curve for this material would be characterized by an extremely shallow slope and that the material could be loaded to a high percentage (83%) of the ultimate tensile strength without failure within one million cycles. The comparison of these results with data being generated at AFWAL on FeAl and FeAl + TiB<sub>2</sub> indicate inferior performance of the Fe-35Al-4Cr-2Mo alloy. At room temperature, the FeAl exhibited an endurance



(a)



(b)

Figure 67 Light photos of Fe-35Al-4Cr-2Mo failed (a) 30 Ksi (207 Mpa) tensile test specimen and (b) 649°C (1200°F) 241 Mpa (34.5 Ksi) rupture test specimen showing structures at the fracture surface. Magnification, 100 X.

TABLE XVII

TENSILE AND CREEP-RUPTURE DATA FOR Fe-35Al-4Cr-2Mo ALLOY

Tensile Data

<u>Temperature</u>	<u>Ultimate Strength</u>	<u>0.2% Yield Strength</u>	<u>% Elong.</u>	<u>% RA</u>
Room	404.7 MPa (58.7 Ksi)	363.3 MPa (52.7 Ksi)	2.6	2.9
Room	422 MPa (61.2 Ksi)	358.5 MPa (52.0 Ksi)	2.6	3.7
600°C (1112°F)	463.3 MPa (67.2 Ksi)	339.9 MPa (49.3 Ksi)	49.8	55.0
600°C (1112°F)	470.8 MPa (68.3 Ksi)	347.5 MPa (50.4 Ksi)	50.1	56.6

Creep Rupture Data

<u>Temperature</u>	<u>Stress Level</u>	<u>Rupture Life</u>	<u>Time to 0.1% Creep</u>	<u>% Elong. at Failure</u>
570°C (1058°F)	206.8 MPa (30 Ksi)	265.2 Hr	9.1 Hr	8.5
570°C (1058°F)	206.8 MPa (30 Ksi)	334.2 Hr	58.4 Hr	8.0
649°C (1200°F)	241.3 MPa (35 Ksi)	4.3 Hr	<0.1 Hr.	4.5
649°C (1200°F)	241.3 MPa (35 Ksi)	4.0 Hr	<0.1 Hr	4.0

limit of approximately 621 Mpa (90 Ksi) while the FeAl + TiB<sub>2</sub> exhibited an endurance limit of approximately 862 Mpa (125 Ksi).

Metallographic examination of the test specimens indicated that cracking had been initiated in spite of the fact that the specimens did not fail within one million cycles. An example of this type of cracking is shown in Figure 68 for the specimen exposed to 345 Mpa (50 Ksi) for over two million cycles. Transgranular cracking can be observed in this specimen, initiating at both the specimen surface and at a grain boundary, Figure 68a. This type of transgranular cracking was also observed in the room temperature tensile test specimens, as shown in Figure 66a.

#### 4.3.3.4 Low Cycle Fatigue Test Results

Low cycle fatigue testing was performed on the Fe-35Al-4Cr-2Mo alloy and included strain controlled, fully reversed cycling at 600°C (1112°F) and a frequency of 0.33 Hz. The results of these tests are listed in Table XVIII. The initial test was conducted at a total strain range of 0.010, with the result that failure occurred in a brittle manner after 8 cycles. The second test was conducted at a total strain range of 0.0050, and after 1013 cycles the strain range was increased to 0.0070, after which the specimen failed in a brittle manner after 4 cycles.

Examination of the failed test specimens indicated behavior in marked contrast to that observed for the tensile and creep rupture tests conducted at similar temperatures. As shown previously in Figure 66b, tensile test specimens exhibited considerable deformation in the grains as well as a predominantly intergranular fracture mode. As shown previously in Figure 67, creep rupture specimens exhibited an intergranular fracture mode. As shown in Figure 69a, however, low cycle fatigue Specimen No. 2 exhibited little deformation in the grains, but considerable evidence of transgranular cracking near the fracture surface. Examination of this specimen in the grip area also indicated the presence of transgranular cracks in this region. An example of this is shown in Figure 69b. These types of cracks are similar to those shown in Figures 63 and 64 for Fe-35Al-4Cr-2Mo alloy extruded at conditions other



(a) 100X



(b) 500X

Figure 68 Light photos of Fe-35Al-4Cr-2Mo room temperature high cycle fatigue test specimen loaded at 345 Mpa (50 Ksi) showing crack initiation sites.

TABLE XVIII

## FATIGUE DATA FOR Fe-35Al-4Cr-2Mo ALLOY

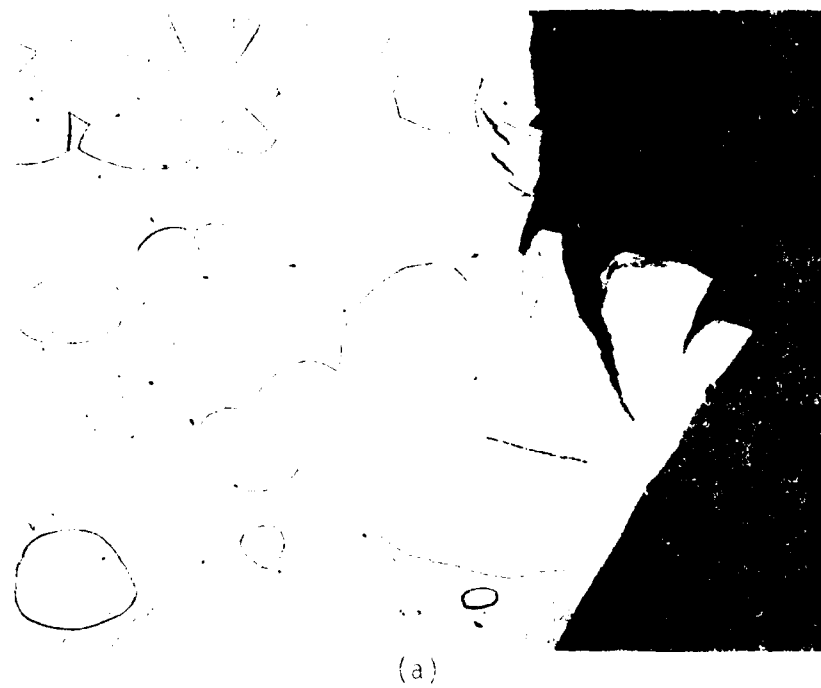
## Room Temperature High Cycle Fatigue Data

Specimen No.	Minimum Stress	Maximum Stress	Cycles To Failure
1306	---	410 MPa (59.5 Ksi)	Specimen Failed while loading
1307	31 MPa (4.5 Ksi)	310 MPa (45 Ksi)	1,000,000 Test discontinued
1308	35 MPa (5.0 Ksi)	345 MPa (50 Ksi)	349,000 Machine malfunction
1309	35 MPa (5.0 Ksi)	345 MPa (50 Ksi)	2,300,000 Test discontinued

## 600°C (1112°F) Low Cycle Fatigue Data

Specimen No.	Total Strain Range	Plastic Strain Range	Elastic Strain Range	Maximum Stress	Minimum Stress	Cycles to Failure
1	.010	.00346	.00654	400 MPa (58 Ksi)	-428 MPa (62 Ksi)	8 (Outside gage Length)
2	.0050	.00034	.00466	276 MPa (40 Ksi)	-310 MPa (45 Ksi)	1018 (strain range increased)
2	.0070	.00172	.00528	303 MPa (44 Ksi)	-359 MPa (52 Ksi)	4





(a)



(b)

Figure 69 Light photos of Fe-35Al-40Cr-2Mo alloy: (a) low cycle fatigue test specimen No. 2 showing fracture surface and (b) in the grain area.

than the 954°C (1750°F)/16:1 reduction ratio condition selected for the properties characterization. This suggested that the cracking observed near the fracture surface of the low cycle fatigue test specimen, Figure 69a, was not, in fact, the result of the fatigue cycling but was already present in the material prior to test. It was significant to note that this cracking was not observed in the sections examined to characterize the as-extruded material, nor was it observed in the grip areas of the tensile, creep-rupture, or high cycle fatigue specimens discussed previously. This suggested that the cracking was highly localized in the extrusion sections used to characterize the low cycle fatigue properties.

#### 4.3.3.5 Oxidation Results

Oxidation testing was performed on the Fe-35Al-4Cr-2Mo alloy and included exposure at 816°C (1500°F) in laboratory air for 240 hours. These were the same conditions used to evaluate the Series I alloys, the results of which were presented in Table X in terms of specific weight change. For the Fe-35Al-4Cr-2Mo alloy, the specimen was 1.3 cm (0.5 inch) in diameter and 1.3 cm (0.5 inch) in length. The results indicated no change in the 10.7442 gm (0.023 lb) weight of the test coupon. A photograph of this test coupon is shown in Figure 70. As shown in Table X, the Fe<sub>3</sub>Al baseline alloy exhibited a slight specific weight loss. The fact that the Fe-35Al-4Cr-2Mo alloy exhibited no specific weight change was not surprising in view of the higher Al and Cr content compared to the Fe<sub>3</sub>Al alloy.

#### 4.3.4 Alloy Characterization Summary

Properties characterization conducted on the Fe-35Al-4Cr-2Mo alloy included elevated temperature tensile, creep rupture and low cycle fatigue tests, room temperature high cycle fatigue tests, and oxidation tests. These tests were conducted on vacuum induction melted ingots extruded at 954°C (1750°F) and a reduction ratio of 16:1. This material exhibited a homogeneous grain size distribution of approximately 125 microns in average grain diameter.

Figure 70    Photograph of Fe-35Al-4Cr-2Mo oxidation test coupon after exposure to 816°C (1500°F) laboratory air for 240 hours.

The tensile results confirmed the potent solid solution strengthening effects of Cr and Mo additions with regards to elevated temperature yield strength. The quaternary alloy exhibited 1.6 times the yield strength capability of  $\text{Fe}_3\text{Al}$  at  $600^\circ\text{C}$  ( $1112^\circ\text{F}$ ). This strength increase, however, was achieved at the expense of a loss of approximately 50 percent of the room temperature tensile ductility (percent elongation) of the  $\text{Fe}_3\text{Al}$ .

The creep rupture results were compared to commercial 410 martensitic stainless steel, which exhibits yield strength equivalent to that of the quaternary alloy at  $600^\circ\text{C}$  ( $1112^\circ\text{F}$ ), approximately 345 Mpa (50 Ksi). Under the same  $570^\circ\text{C}$  ( $1058^\circ\text{F}$ )/207 Mpa (30 Ksi) rupture conditions, 410 stainless steel would exhibit a rupture life of approximately 20 hours (compared to an average life of 300 hours for the quaternary alloy) and a time to 0.1% creep of less than one hour (compared to an average life of 34 hours for the quaternary alloy).

The room temperature high cycle fatigue results indicated that the endurance limit (as defined by a failure life in excess of one million cycles) of the quaternary alloy lies between 345 Mpa (50 Ksi) and 410 Mpa (59.5 Ksi). Further, the data indicated that the conventional high cycle fatigue S-N curve would be characterized by an extremely shallow slope and the material could be loaded to a high percentage (83%) of the ultimate tensile strength without failure within one million cycles.

The quaternary alloy exhibited poor low cycle fatigue characteristics at  $600^\circ\text{C}$  ( $1112^\circ\text{F}$ ). Brittle type failure was observed with low failure lives (less than 10 cycles) at relatively low total strain ranges (0.0010-0.007). Examination of the failed bars indicated the presence of transgranular cracks which appeared to exist in the material prior to testing. That these cracks were isolated in the extrusion was suggested by the fact that they were not observed in the as-extruded specimens used to characterize the extrusions nor were they observed in the tensile, creep rupture and high cycle fatigue specimens.

Oxidation testing included exposure for 240 hours in laboratory air at 816°C (1500°F). There was no specific weight change as the result of this exposure, which was not surprising in view of the high Al content and the presence of Cr.

## 5.0 SUMMARY AND CONCLUSIONS

A program was conducted in order to develop improved iron-aluminide alloys for potential Air Force applications. More specifically, efforts were focused on the  $\text{Fe}_3\text{Al}$  system which exhibits the  $\text{DO}_3$  ordered crystal lattice with particular emphasis being addressed towards improving the high temperature strength and room temperature ductility of this system. To accomplish this the experimental approach involved the screening evaluation of two experimental series of alloys which then formed the basis for the selection of a single alloy composition for more complete properties testing. The alloy design philosophy was based on the concept of improving strength and ductility through an investigation of the effects of ternary and quaternary element additions on the resultant microstructures and changes in the  $\text{DO}_3$  - B2 transformation temperature. Powder metallurgy as well as isothermal forging processing routes were explored for these experimental alloys.

The first alloy series included twenty compositions in addition to the baseline material,  $\text{Fe}_3\text{Al}$ . These alloys were processed through powder metallurgy routings and included ternary additions of ten elements at two levels each, as shown in Table VI. It can be seen that four of the alloys were actually quaternary compositions due to the inadvertent mixing of the powders prior to the hot extrusion consolidation operation. The alloys investigated in this study were characterized by either a single phase (solid solution strengthening) or a two-phase (precipitation strengthening) type microstructure. Screening evaluations including oxidation, workability, and tensile property tests were conducted on these alloys.

Oxidation tests involved exposures in laboratory air at  $816^\circ\text{C}$  ( $1500^\circ\text{F}$ ). Visual and weight gain results indicated that only two alloys (5 a/o Ti and 10 a/o V) exhibited significant degradation compared to the baseline alloy. Workability testing involved upset isothermal forging at  $954^\circ\text{C}$  ( $1750^\circ\text{F}$ ) and indicated that none of the alloying additions adversely affected the workability as exhibited by the baseline alloy.

The results of room temperature and 600°C (1112°F) tensile tests are shown in Tables VIII and IX. The single phase alloys exhibited varying degrees of solid solution strengthening at elevated temperature. Si additions, at the 3 and 5 atomic percent levels, for example, resulted in approximately 2.5-3.0 times the 600°C (1112°F) yield strength of Fe<sub>3</sub>Al, but with only approximately 10 percent of the room temperature elongation. More modest increases in elevated temperature strength were exhibited by alloys containing Cr and Mo, with accompanying higher levels of ductility. The most optimum of the solid solution strengthened alloys contained 3.5 Cr + 0.5 Mo (atomic percent) and exhibited 1.3 times the 600°C (1112°F) yield strength of Fe<sub>3</sub>Al, with equivalent room temperature ductility (4.8 percent elongation).

The two phase alloys (Nb and Ta) also showed improved elevated temperature strength while maintaining some of the baseline ductility. This strengthening was apparently due primarily to solid solution effects since the properties could not be related to the volume fraction of precipitates. This indicated that potential exists for further strengthening via refinement of the precipitate size. Researchers at SRL determined that the 2 a/o Nb alloy could indeed be further strengthened by solution and aging heat treatments. This alloy exhibited approximately 4 times the 600°C (1112°F) yield strength of Fe<sub>3</sub>Al with about 60% the room temperature elongation. SRL efforts also established that alloy additions did affect the DO<sub>3</sub> - B2 transition temperature in all of the Series I alloys, but there was little correlation, however, between 600°C (1112°F) strength and change in T<sub>c</sub> values. This suggested that factors other than the stabilization of the DO<sub>3</sub> phase to a higher temperature control high temperature strength in these alloys.

The second alloy series included fifteen alloys divided into three groups as shown in Table XII. These included ternary or quaternary alloys with Cr, Ta, or Nb as the common alloying addition. The compositions were produced by isothermal forging of vacuum induction melted ingots. The Cr series exhibited a single phase microstructure characterized by uniform, equiaxed grains approximately 375 microns in average grain diameter in the isothermally forged and annealed condition. Alloy 11-4 (4 a/o Cr, 2 a/o Mo) was tested in four-point bending with the result that the 600°C (1112°F) yield strength

improved by a factor of 2.5 compared to the baseline  $\text{Fe}_3\text{Al}$  alloy. These results confirmed the potent solid solution strengthening capability of Cr and Mo additions to  $\text{Fe}_3\text{Al}$  identified during the Series I testing. During the preparation of material for testing, the two phase Ta and Nb series of alloys exhibited quench cracking sensitivity during quenching from the solution temperature. It was not possible to machine specimens for testing. This indicated that the vacuum induction melting/isothermal forging processing approach developed for these particular alloys would not be able to exploit the strengthening potential demonstrated in the Series I evaluations.

The alloy selected for final evaluation in this program was Fe-35Al-4Cr-2Mo (in atomic percent). This selection was made in order to take advantage of the potent solid solution strengthening demonstrated by Cr and Mo additions during the Series I and II evaluations. It was also desired to enhance the specific strength by utilizing a base alloy exhibiting a lower density than the  $\text{Fe}_3\text{Al}$  baseline. While it was recognized that two phase alloys based upon Ta and Nb additions do offer potential for precipitation strengthening, the quench crack sensitivity demonstrated in the Series II alloys represented a possible limit to the applicability of these alloy development concepts within the scope of this program. Alloy characterization consisted of mechanical property tests including tensile, creep rupture, fatigue and oxidation tests conducted on material produced by the hot extrusion of vacuum induction melted ingots.

The tensile results confirmed the potent solid solution strengthening effects of Cr and Mo additions. The quaternary alloy exhibited 1.6 times the yield strength of  $\text{Fe}_3\text{Al}$  at  $600^\circ\text{C}$  ( $1112^\circ\text{F}$ ), with a loss, however, of approximately 50 percent of the room temperature ductility (percent elongation). The creep rupture results were compared to commercial 410 martensitic stainless steel, which exhibits  $600^\circ\text{C}$  ( $1112^\circ\text{F}$ ) yield strength equivalent to that of the quaternary alloy, approximately 345 Mpa (50 Ksi). Under the same  $570^\circ\text{C}$  ( $1058^\circ\text{F}$ )/207 Mpa (30 Ksi) rupture conditions, 410 stainless steel would exhibit a rupture life of approximately 20 hours (compared to an average life of 300 hours for the quaternary alloy) and a time to 0.1% creep of less than one hour (compared to an average life of 34 hours



for the quaternary alloy). The room temperature high cycle fatigue results indicated that the endurance limit (as defined by a failure life in excess of one million cycles) of the quaternary alloy lies between 345 Mpa (50 Ksi) and 410 Mpa (59.5 Ksi). The quaternary alloy exhibited poor low cycle fatigue characteristics at 600°C (1112°F). Brittle type failure was observed with low failure lives (less than 10 cycles) at relatively low total strain ranges (0.010-0.007). Examination of the failed bars indicated the presence of transgranular cracks which appeared to exist in the material prior to testing. That these cracks were isolated in the extrusion was suggested by the fact that they were not observed in the as-extruded specimens used to characterize the extrusions nor were they observed in the tensile, creep rupture and high cycle fatigue specimens. Oxidation testing at 816°C (1500°F) for 240 hours indicated no specific weight change, which was not surprising in view of the high Al content and the presence of Cr.

In summary, this effort indicated that the most significant potential for combined high temperature strength and room temperature ductility was demonstrated for two-phase alloys based upon Nb. Further alloy optimization is required to define the maximum strengthening potential. These subsequent studies would also have to address processing sensitivity, however, especially with regards quench cracking during the heat treatments necessary to develop full strengthening.

APPENDIX I - SRL ACTIVITIES

by

MADAN G. MENDIRATTA

CHIEF, MATERIALS RESEARCH

RESEARCH APPLICATIONS DIVISION

SYSTEMS RESEARCH LABORATORIES, INC.

## APPENDIX I

### 1.0 INTRODUCTION

TRW was teamed with Systems Research Laboratories, Inc. (SRL) on this program with SRL responsible for in-depth microscopic characterization of the alloys under study. The SRL efforts included homogenization studies, a screening of the  $\text{DO}_3$  - B2 transition temperatures ( $T_c$ ) for the various alloys as well as a characterization of the precipitation behavior of the Nb containing alloys. The findings are presented in the following sections.

### 2.0 HOMOGENIZATION STUDIES

Heat treatment studies of selected blended alloys (5 a/o Ti, 3 a/o Ni), and the prealloyed 3 a/o Mo alloy, which was also found to contain Cr, were conducted in order to define treatments to homogenize the alloy content. The results of these studies are presented in the following sections.

#### 2.1 Alloy I-2 (5 a/o Ti)

Examination of the as-extruded microstructure revealed that Ti was not homogeneously distributed in this blended alloy. However, it was found that a  $1100^\circ\text{C}$  ( $2012^\circ\text{F}$ ) hold for 168 hours (one week) homogenized the material without producing excessive grain growth. A SEM micrograph which displays the homogenized structure is shown in Figure A1. The grain size is approximately 60 microns. SEM energy-dispersive X-Ray analysis (EDAX) showed uniform Ti content from grain to grain. Two types of grains were observed: a) those showing no pull-outs (i.e., no impurity ceramic particles); these grains were thought to nucleate in powder particles originally rich in Ti, the Ti appearing to scavenge interstitial impurities; and b) those showing significant pull-outs, these grains were thought to nucleate in  $\text{Fe}_3\text{Al}$  powder particles originally containing no Ti. It was considered difficult to identify the ceramic particles owing to their extremely small size (0.1-0.3 microns).

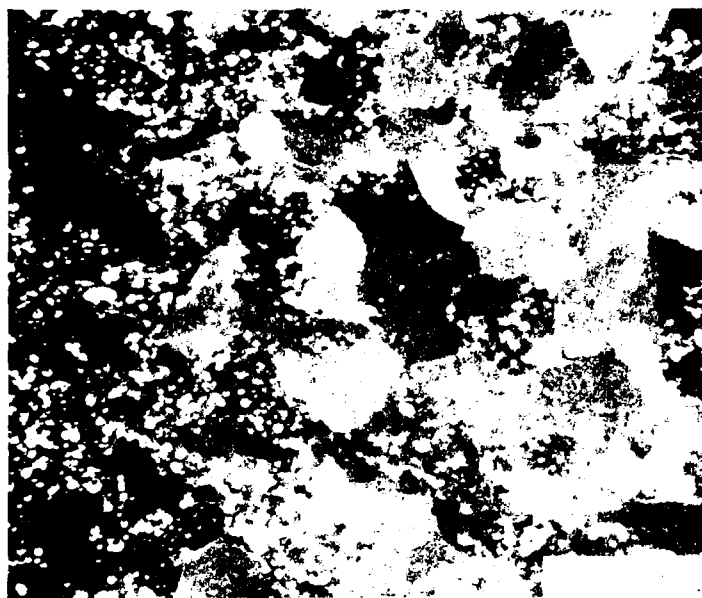


Figure A1. Microstructure of Fe<sub>70</sub>Ti<sub>5</sub>Al<sub>25</sub> in the As-Extruded-Plus-1100°C/1 week Heat-Treated Condition.

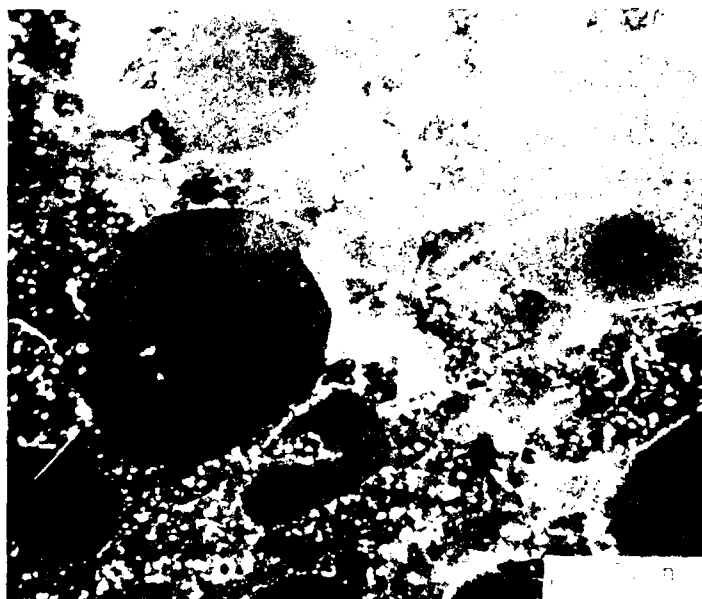


Figure A2. Microstructure of Fe<sub>72</sub>Ni<sub>3</sub>Al<sub>25</sub> in the As-Extruded-Plus-1100°C/1 week Heat-Treated Condition.

## 2.2 Alloy I-9 (3 a/o Ni)

This alloy was a blend of the  $\text{Fe}_3\text{Al}$  and the I-10 (10 a/o Ni) alloy and, in the as-extruded condition, was not uniform with regard to Ni distribution. After a homogenization treatment of  $1100^\circ\text{C}$  ( $2012^\circ\text{F}$ ) for 168 hours (one week), the alloy was found to be homogeneous. The microstructure, shown in Figure A2, was almost identical to that in homogenized I-2 (5 a/o Ti) alloy. The pull-outs were observed only in regions which were originally  $\text{Fe}_3\text{Al}$ . The regions which were originally Ni-rich did not show pull-outs but evidenced a larger average grain size than regions which were originally Ni-free.

## 2.3 Alloy I-13 (3 a/o Mo)

This was a blended alloy in which, by error, Cr and Mo were mixed. In the as-extruded condition, Cr-rich and Mo-rich segregated islands were observed in the microstructure; therefore, the decision was made to perform a  $1100^\circ\text{C}$  ( $2012^\circ\text{F}$ )/168 hour (one week) homogenization treatment. SEM EDAX analysis revealed the alloy to be homogeneous and contain a single phase. The average grain size was determined to be approximately 100 microns.

## 3.0 SCREENING OF $\text{DO}_3$ - B2 TRANSITION TEMPERATURES

The  $\text{DO}_3$   $\text{Fe}_3\text{Al}$  phase transforms to the B2  $\text{FeAl}$  phase at  $540^\circ\text{C}$  ( $1000^\circ\text{F}$ ). Since the ternary additions in  $\text{Fe}_3\text{Al}$  were expected to change the transition temperature  $T_c$ , and this change may have an effect upon the mechanical properties, a decision was made to characterize this effect upon  $T_c$ . The approach included determining whether  $T_c$  was higher or lower than  $600^\circ\text{C}$  ( $1112^\circ\text{F}$ ) and, in cases where  $T_c$  was higher, to determine the approximate temperature range in which  $T_c$  might fall.

### 3.1 Experimental Procedures

Small specimens of extruded (prealloyed) and extruded-plus-homogenized (blended) alloys were held at  $600^\circ\text{C}$  ( $1112^\circ\text{F}$ ) for one hour in vacuum and then

water quenched. Thin foils were prepared from these specimens for TEM examination of the  $DO_3$  and B2 domains. If the observed  $DO_3$  domains were extremely small (say less than 200 Angstroms), then it would indicate that only quenched-in domains were present and, therefore,  $600^{\circ}\text{C}$  ( $1112^{\circ}\text{F}$ ) was above the  $DO_3$  - B2 phase boundary. However, if  $DO_3$  domains were to have a significant size (say 5000 Angstroms), then it would indicate that  $600^{\circ}\text{C}$  ( $1112^{\circ}\text{F}$ ) was in the  $DO_3$  phase field. Some alloys indicated the latter; in those cases specimens were held at  $650^{\circ}\text{C}$  ( $1200^{\circ}\text{F}$ ) for one hour and water quenched, and thin foils were prepared for TEM examination. These steps were repeated with the temperature being raised in  $50^{\circ}\text{C}$  ( $90^{\circ}\text{F}$ ) intervals until TEM examination revealed that the  $DO_3$  - B2 boundary had been crossed.

For TEM examination the grains were tilted to produce (110)-zone diffraction patterns. Phase-angle calculations indicated that the superlattice reflections of the type  $\{111\}$  reveal contrast from both the  $DO_3$  and the B2 anti-phase domain boundaries, while  $\{002\}$ -type reflections reveal contrast from only the B2 anti-phase domain boundaries.

### 3.2 Results

Since the number of alloys investigated was large, only representative examples of TEM micrographs are presented in this Appendix. Figure A3 contains dark-field electron micrographs taken with  $g = (\bar{1}11)$  for specimens quenched from  $600^{\circ}\text{C}$  ( $1112^{\circ}\text{F}$ ),  $650^{\circ}\text{C}$  ( $1200^{\circ}\text{F}$ ) and  $700^{\circ}\text{C}$  ( $1292^{\circ}\text{F}$ ) for the I-14 alloy (6 a/o Mo); also included is the  $[110]$ -zone-axis diffraction pattern for a specimen quenched from  $600^{\circ}\text{C}$  ( $1112^{\circ}\text{F}$ ). Similar diffraction patterns were observed for the other two quenching temperatures, with no significant differences being found in the intensities of the superlattice reflections  $(\bar{1}11)$  and  $(002)$ . The  $DO_3$  domains are visible in these micrographs, and it can be seen that they are slightly larger for  $650^{\circ}\text{C}$  ( $1200^{\circ}\text{F}$ ) than for  $600^{\circ}\text{C}$  ( $1112^{\circ}\text{F}$ ); however, the domain size is very small in the  $700^{\circ}\text{C}$  ( $1292^{\circ}\text{F}$ ) quenched specimen. It may be concluded, therefore, that up to  $650^{\circ}\text{C}$  ( $1200^{\circ}\text{F}$ ), the alloy is in the  $DO_3$  phase field and that at  $700^{\circ}\text{C}$  ( $1292^{\circ}\text{F}$ ) the  $DO_3$  phase boundary is exceeded. Thus,  $T_c$  must fall somewhere between  $650^{\circ}\text{C}$  ( $1200^{\circ}\text{F}$ ) and  $700^{\circ}\text{C}$  ( $1292^{\circ}\text{F}$ ).

600°C/1 HR → W.Q.  $\bar{g} = (\bar{1}11)$



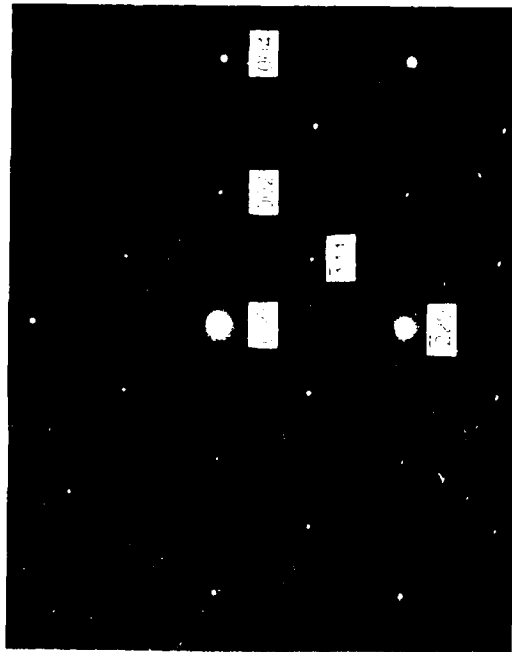
650°C/1 HR → W.Q.  $\bar{g} = (\bar{1}11)$



700°C/1 HR → W.Q.  $\bar{g} = (\bar{1}11)$

Figure A3 Dark-Field Electron Micrographs Showing Variation of  $DQ_3$  Domain Size with Temperature in  $Fe_{60}Al_{25}Mo_6$ .

[ $\bar{1}\bar{1}0$ ] ZONE AXIS



Figures A4a and A4b contain (111) and (002) dark-field electron micrographs, respectively, for the I-16 alloy (5 a/o Ta) quenched from 600°C (1112°F). Figure A4a shows extremely fine quenched-in DO<sub>3</sub> domains, while Figure A4b shows large B2 domains. Thus, for this alloy, T<sub>c</sub> was below 600°C (1112°F). Figures A5a and A5b are (111) dark-field electron micrographs for the I-1 alloy (1 a/o Ti) and the I-2 alloy (5 a/o Ti), respectively. Both alloys were quenched from 600°C (1112°F); the former shows quenched-in DO<sub>3</sub> domains indicating that T<sub>c</sub> is below 600°C (1112°F), while the latter shows large DO<sub>3</sub> domains with anti-phase domain boundaries parallel to certain crystallographic planes. Therefore, addition of 5 a/o Ti in Fe<sub>3</sub>Al not only increases T<sub>c</sub> but makes the anti-phase boundary energy highly anisotropic. (In Fe<sub>3</sub>Al the DO<sub>3</sub> domain boundaries have no preference with respect to crystallographic planes and exhibit random domain structure). For the 5 a/o Ti alloy, the planes on which these boundaries lie were not determined.

The type of data included in the above examples was generated for the remainder of the ternary alloys. A summary of the temperature range in which T<sub>c</sub> falls is given in Table AI. Also included in this table is the yield strength of the ternary alloys determined at 600°C (1112°F). It is apparent from this table that a number of ternary additions increase T<sub>c</sub> above 600°C (1112°F); these are (in atomic percent additions): 5Ti, 5Cr, 6Mn, 12Mn, 10Ni, 3Mo, 6Mo, 3Si, and 5Si. The greatest increase in T<sub>c</sub> corresponds to a 5 a/o Si addition. The strength at 600°C (1112°F) showed little correlation with changes in T<sub>c</sub> values, e.g., 1 a/o Cr alloy (Alloy I-5) with T<sub>c</sub> below 600°C (1112°F) exhibited higher strength, 354 Mpa (51.3 Ksi), than the 5 a/o Cr alloy (Alloy I-6), 273 Mpa (51.3 Ksi), with T<sub>c</sub> falling between 600°C (1112°F) and 650°C (1200°F). This suggests that factors other than the stabilization of the DO<sub>3</sub> phase to a higher temperature control the high temperature yield strength.

#### 4.0 Precipitation Strengthening Potential in Fe<sub>3</sub>Al + Nb Alloys

In the as-extruded condition alloy I-11 (2 a/o Nb) and alloy I-12 (5 a/o Nb) exhibited a two-phase microstructure, as shown by the SEM micrographs in Figure A6. The second phase is in the form of reasonably well distributed



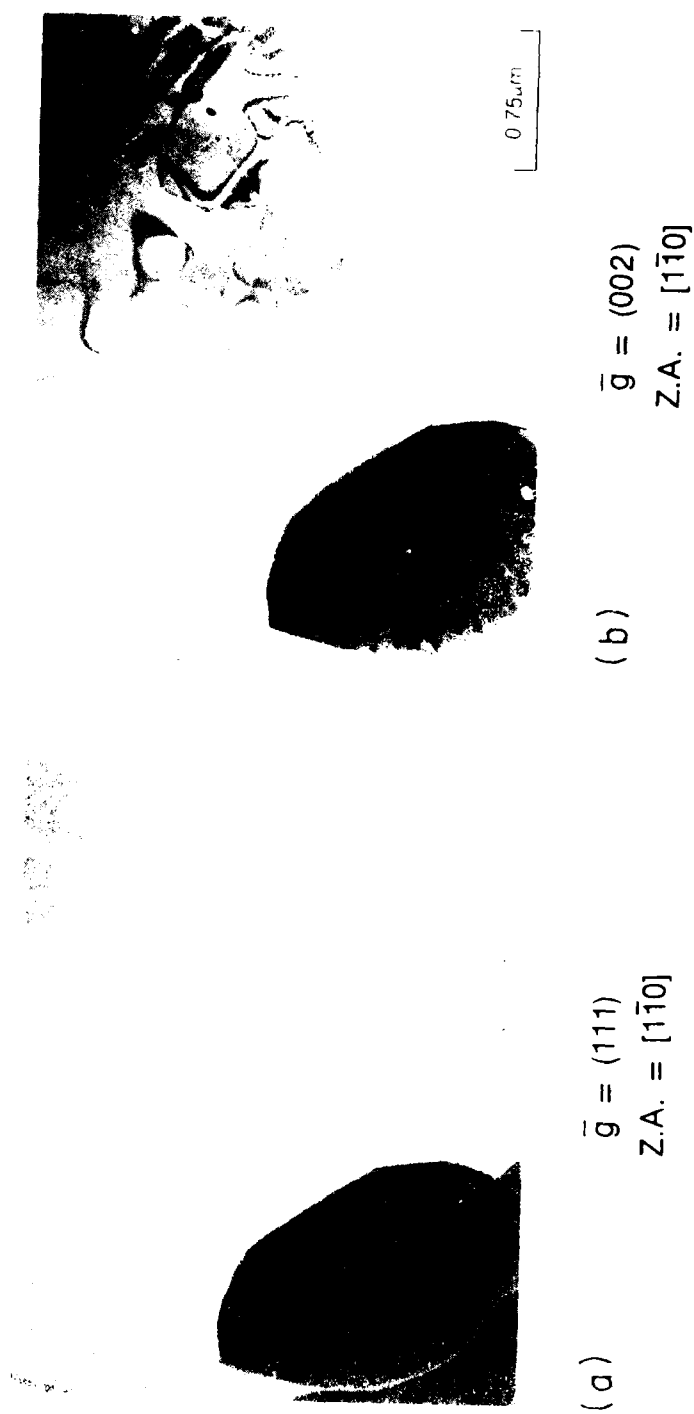
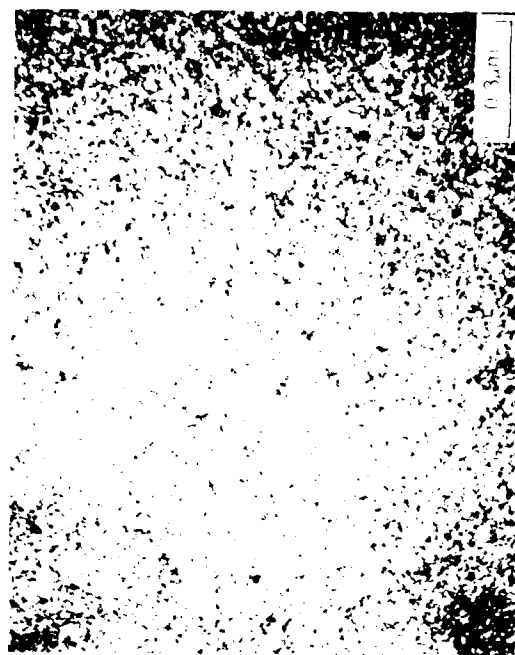
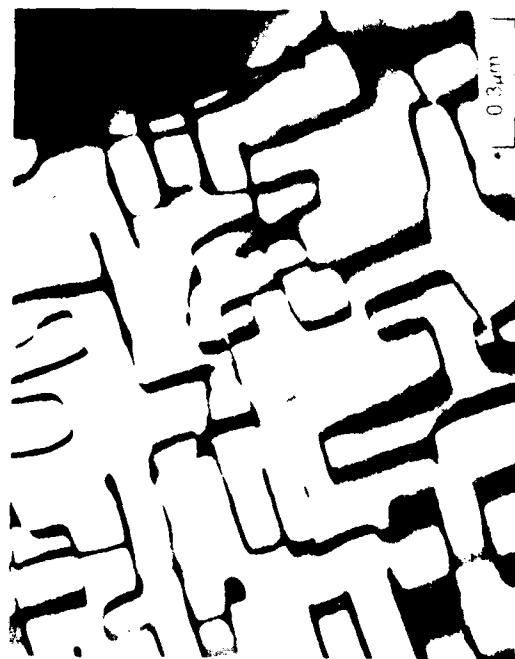


Figure A4. Dark-Field Electron Micrographs Showing (a) Quenched-In  $\text{DO}_3$  Domains and (b) Large B2 Domains in  $\text{Fe}_{70}\text{Al}_{25}\text{Ta}_5$  Alloy Quenched from  $600^\circ\text{C}$ .



(a)  $\text{Fe}_{74}\text{Al}_{25}\text{Ti}_1$



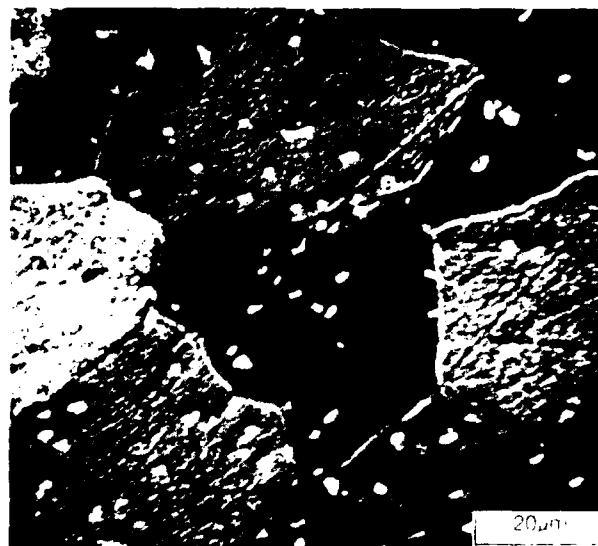
(b)  $\text{Fe}_{70}\text{Al}_{25}\text{Ti}_5$

Figure A5. (111) Dark-Field Electron Micrographs Showing (a) Quenched-In  $\text{D0}_3$  Domains in  $\text{Fe}_{74}\text{Al}_{25}\text{Ti}_1$  and (b) Large  $\text{D0}_3$  Domains in  $\text{Fe}_{70}\text{Al}_{25}\text{Ti}_5$ . Both alloys were quenched from 600°C. Notice crystallographic antiphase domain boundaries in  $\text{Fe}_{70}\text{Al}_{25}\text{Ti}_5$ .

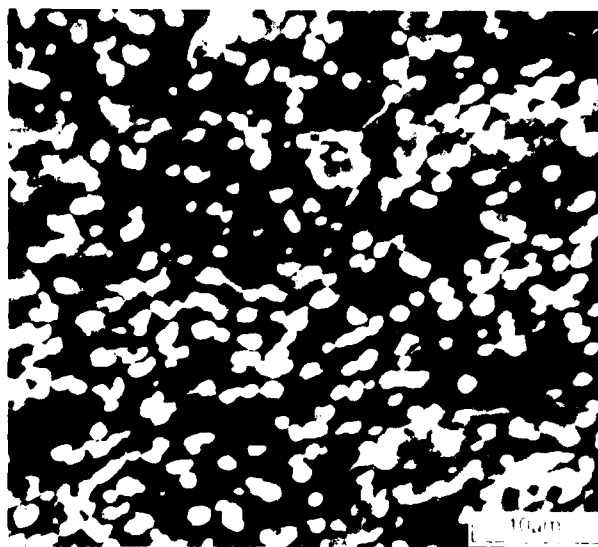
TABLE A I

# SUMMARY OF $T_c$ DATA ( $T_c$ for $Fe_3Al \approx 540^\circ C$ )

ALLOY	$T_c$ ( $^\circ C$ )	$\sigma_y$ at $600^\circ C$ (KSI)	REMARKS
$Fe_{74}Al_{25}Ti_1$	<600	43	HIGHLY CRYSTALLOGRAPHIC DOMAIN BOUNDARIES
$Ti_5$	>600	36	
$V_5$	—		
$V_{10}$	—		} OXIDATION PROBLEM
$Cr_1$	<600	51	
$Cr_5$	600-650	39	RELATIVELY SLUGGISH DOMAIN GROWTH
$Mn_6$	650-700	38	
$Mn_{12}$	600-650	29	
$Ni_3$	<600		
$Ni_{10}$	600-650	57	
$Nb_2$	<600	61	} ? TWO PHASES
$Nb_5$	<600	63	
$Mo_3$	600-650	49	TWO PHASES
$Mo_6$	650-700	53	
$Ta_1$	<600	54	} TWO PHASES
$Ta_5$	<600	66	
$Cu_5$	<600	25	} TWO PHASES
$Cu_{10}$	—	25	
$Si_3$	650-700	87	} PREVIOUS WORK
$Si_5$	700-725	77	



AS-EXTRUDED  $\text{Fe}_{73}\text{Al}_{25}\text{Nb}_2$



AS-EXTRUDED  $\text{Fe}_{70}\text{Al}_{25}\text{Nb}_5$

Figure A6. Two-Phase Microstructure in  $\text{Fe}_3\text{Al-Nb}$  Alloys.

particles and offers the possibility of precipitation strengthening. However, in order to exploit such a potential, it is important to characterize the second phase and the matrix solubility of Nb at different temperatures and to explore whether the second phase can be solutionized and reprecipitated in a controlled manner. This portion of the report presents results of a study of the precipitation behavior of these two alloys and also includes preliminary tensile-strength data from room temperature to 700°C (1292°F).

#### 4.1 Experimental Procedures

A number of heat treatments were carried out with the following objectives: 1) to change the solute content in the matrix as a function of temperature, 2) to dissolve the second phase, 3) to precipitate the second phase in a controlled manner, and 4) to determine the thermal stability of the precipitates. The details of the heat treatments are presented in the results section.

Quantitative electron probe microanalysis (EPMA) was performed to determine the chemistry of the second phase. X-ray and TEM were utilized to determine the crystal structure of the equilibrium second phase and to characterize the metastable intermediate phase (i.e., coherent precipitates). Finally, the alloy I-11 (2 at/o Nb), in which a uniform distribution of coherent precipitates was produced by an aging treatment, was tested in four-point bending to determine its tensile strength up to 700°C (1292°F).

#### 4.2 Results

##### 4.2.1 Characterization of the Precipitation Behavior

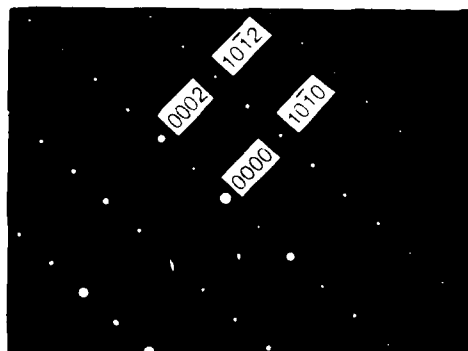
Quantitative EPMA performed on the second phase particles shown in Figure A6 revealed the second phase to be approximately  $\text{Fe}_{56}\text{Al}_{19}\text{Nb}_{25}$ . For alloy I-12 (5 at/o Nb), a number of heat treatments at temperatures ranging from 700°C (1292°F) to 1350°C (2462°F) were carried out to change the volume fraction of the particles as well as the Nb solute content in the matrix. The Nb solubility in  $\text{Fe}_3\text{Al}$  as a function of temperature, was determined by EPMA,

however, subsequent results revealed that the heat treatment temperatures were in error. The correct results indicated a sufficient curvature in Nb solubility with temperature to permit controlled precipitation.

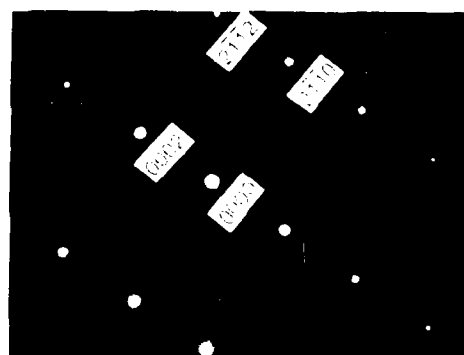
A large number of single-crystal TEM diffraction patterns generated from the second phase particles were analyzed to determine the crystal structure (Mr. Dennis Dimiduk of AFWAL/MLLM assisted in this portion of the research and analyzed the diffraction patterns). An example of a TEM bright-field image of a particle and associated diffraction patterns (two zone axes obtained by tilting the same particle) are shown in Figure A7. The diffraction patterns could be self-consistently indexed based upon a hexagonal lattice and exhibited a crystal lattice which is isostructural with a known compound,  $\text{Fe}_2\text{Nb}$ . X-ray diffraction peaks confirmed this analysis. Since the crystal structure of the particles is complex and appreciably different from the ordered BCC ( $\text{DO}_3$ ) structure of the matrix, a strong possibility exists that these particles, even when extremely small, are not coherent with the matrix.

Heat treatment studies were conducted on alloy I-11 (2 a/o Nb) to help in defining the precipitation behavior in this material. Solution studies were conducted over the temperature range  $700^\circ\text{C}$  ( $1292^\circ\text{F}$ ) -  $1350^\circ\text{C}$  ( $2462^\circ\text{F}$ ) and on the basis of these studies  $1350^\circ\text{C}$  ( $2462^\circ\text{F}$ ) was selected as the solution heat treat temperature. Alloy I-11 (2 a/o Nb) was held at  $1350^\circ\text{C}$  ( $2462^\circ\text{F}$ ) for two hours, water-quenched, and subjected to different aging treatments at temperatures ranging from  $650^\circ\text{C}$  ( $1200^\circ\text{F}$ ) to  $800^\circ\text{C}$  ( $1472^\circ\text{F}$ ) and for times from 1 to 192 hours. Figure A8 includes a bright-field transmission electron micrograph showing the microstructure in a specimen quenched from  $1350^\circ\text{C}$  ( $2462^\circ\text{F}$ ). No evidence of precipitation was found; the background contrast originates from the thermal B2 anti-phase boundaries. The diffraction patterns in the quenched condition corresponded to the  $\text{DO}_3$  phase; appropriate dark-field observations revealed the presence of extremely fine  $\text{DO}_3$  domains enclosed by larger B2 domain boundaries.

The transmission electron micrographs in Figure A9 reveal the microstructure in a specimen which was aged at  $700^\circ\text{C}$  ( $1292^\circ\text{F}$ ) for one hour after the quenching treatment. Coherent precipitates with modulated contrast can be



ZONE AXIS =  $[1\bar{2}10]$



ZONE AXIS =  $[01\bar{1}0]$

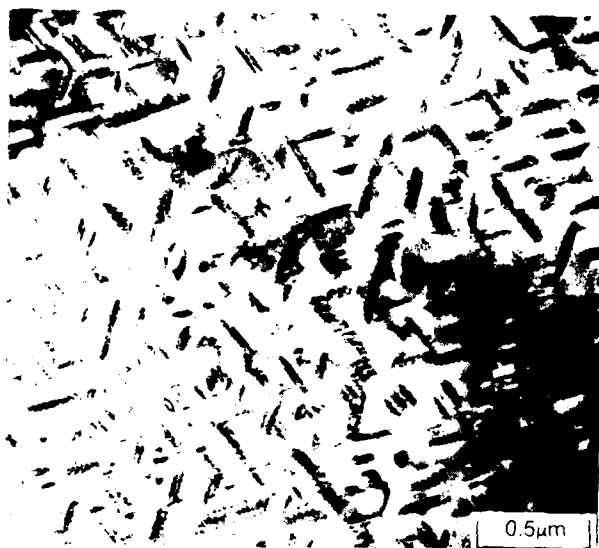
Figure A7. Diffraction Patterns from Equilibrium Annealed Specimen in  $\text{Fe}_{70}\text{Al}_{25}\text{Nb}_5$  (1350°C 2 hr. Water Quenched) Exhibiting  $\text{Fe}_{21}\text{Nb}$ -Type Hexagonal Crystal Structure.



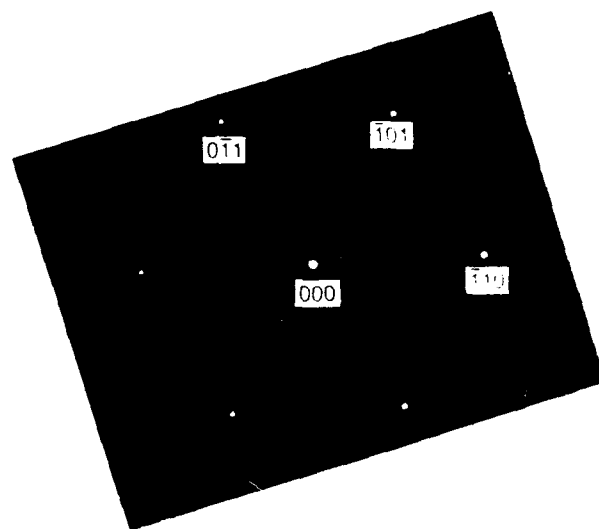
Z.A. = NEAR [110],  $\bar{g} = (2\bar{2}0)$

Figure A8. Microstructure in Fe<sub>73</sub>Al<sub>25</sub>Nb<sub>2</sub> Quenched from 1350°C/2 hr. No second-phase precipitates were observed.





(a) ZONE AXIS =  $[111]$



(b)



(c) DF,  $\bar{g} = (111)$ , Z.A.  $\approx [1\bar{1}0]$

Figure A9. Coherent Precipitates in  $\text{Fe}_{73}\text{Al}_{25}\text{Nb}_2$  Annealed at 700°C for 1 hr.  
(a) TEM Bright-Field Micrograph, (b) Associated  $[111]$ -Zone Diffraction Pattern, and (c)  $(111)$  Dark-Field Micrograph.

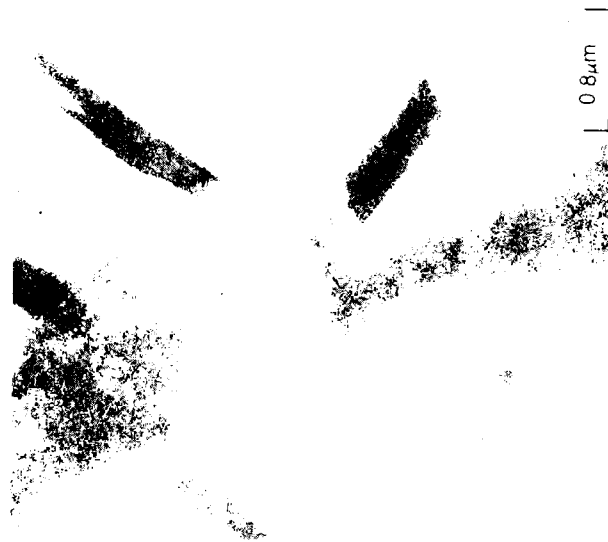
observed in Figure A9a; the corresponding (111)-zone diffraction pattern, Figure A9b, contains reflections corresponding only to the  $\text{DO}_3$  phase. In several other zones [e.g., (110), (100)], only  $\text{DO}_3$ -phase diffraction patterns were observed with no extra reflections which could be associated with the precipitates. Figure A9c is a (111) dark-field micrograph showing that the particles as well as the small  $\text{DO}_3$  domains in the matrix are illuminated. However, dark-field examination using primary reflections did not illuminate the particles. The absence of reflections other than those for the  $\text{DO}_3$  phase and the illumination of the precipitates by the  $\text{DO}_3$  superlattice reflection (111) indicate that the crystal structure of the precipitates is associated closely with the  $\text{DO}_3$  structure. Additional effort would be required to determine the exact crystal structure of the precipitates.

When specimens were aged for longer times and/or at higher temperatures, the coherent precipitates were no longer present; instead, large incoherent particles were observed, as shown in Figure A10, which corresponds to a specimen aged at  $750^\circ\text{C}$  ( $1382^\circ\text{F}$ ) for 24 hours. Trace analysis revealed no connection between the crystallographic growth directions of the coherent precipitates and the large incoherent precipitates. The diffraction patterns obtained from the large particles revealed a hexagonal,  $\text{Fe}_2\text{Nb}$ -type crystal structure. These data indicate that the small coherent precipitates belong to a metastable phase; however, this phase is not a crystallographic precursor of the large incoherent particles belonging to the equilibrium  $\text{Fe}_2\text{Nb}$ -type phase.

Table AII summarizes the results of different aging treatments conducted to alter the precipitation behavior in alloy I-11 (2 a/o Nb). The data include aging time and temperature, nature of the precipitate, and hardness values. It can be seen that the coherent particles are not stable at higher temperatures and longer times (e.g.,  $700^\circ\text{C}$  ( $1292^\circ\text{F}$ )/192 hours,  $750^\circ\text{C}$  ( $1382^\circ\text{F}$ )/24 hours,  $800^\circ\text{C}$  ( $1472^\circ\text{F}$ )/20 minutes). The hardness data indicate that the coherent precipitates provide only a small amount of hardening.



ZONE AXIS = [111]



ZONE AXIS = [111]

Figure A10. Incoherent  $\text{Fe}_2\text{Nb}$ -Type Precipitates in  $\text{Fe}_{73}\text{Al}_{25}\text{Nb}_2$  Alloy Aged at  $750^\circ\text{C}$  for 24 hr.

TABLE A II

# PRECIPITATION BEHAVIOR: Fe<sub>73</sub>Al<sub>25</sub>Nb<sub>2</sub>

HEAT TREATMENT	NATURE OF PPT	HARDNESS (ROCKWELL 1/16 IN. BALL, 60 KG)
1350°C/2 HR → WQ	NO PPT	22.5
+ 650°C/4HR	COHERENT	26
+ 650°C/24 HR	COHERENT	25.5
+ 700°C/1 HR	COHERENT	25
+ 700°C/8 HR	COHERENT	24.5
+ 700°C/192 HR	INCOHERENT LARGE	
+ 750°C/1 HR	COHERENT	
+ 750°C/8 HR	COHERENT	25
+ 750°C/24 HR	INCOHERENT LARGE	
+ 800°C/5 MIN	NO PPT	21
+ 800°C/20 MIN	INCOHERENT LARGE	21.5
+ 800°C/1 HR	INCOHERENT LARGE	

It was not possible to dissolve all second phase particles in alloy I-12 (5 a/o Nb), even at temperatures as high as 1400°C (2552°F). Holding this alloy at 1350°C (2462°F) for 2 hours, however, should produce an equilibrium volume fraction of large Fe<sub>2</sub>Nb-type particles and a matrix having some Nb in solution. A lower temperature aging after quenching from 1350°C (2462°F), therefore, should produce a microstructure consisting of large Fe<sub>2</sub>Nb-type particles and, in the matrix, fine coherent particles. Figure A11 (a and b) contains microstructures obtained by such heat treatments. In the quenched condition, Figure A11a, the darker grains (particles) are the Fe<sub>2</sub>Nb-type phase and the larger, lighter grains are the B2 phase; the grain boundaries are free of precipitation. In the aged condition, Figure A11b, additional precipitation of the stable phase occurred at the grain boundaries; however, no coherent precipitates were observed in the grains. This suggests that the aging temperature of 700°C (1292°F) is above the coherent solvus. The reason for such behavior may be associated with the significantly smaller grain size and consequent large grain boundary area in this alloy, as compared with that in alloy I-11 (2 a/o Nb). An aging temperature lower than 700°C (1292°F) may produce the coherent precipitates in the grains.

#### 4.2.2 Tensile Properties

The decision was made to obtain preliminary tensile-property data for alloy I-11 (2 a/o Nb) containing the coherent precipitates in order to assess the precipitation strengthening potential. Tensile data were generated by four-point bend testing. Figure A12 shows the proportional-limit strength as a function of test temperature (solid circles) for bend bars subjected to a heat treatment of 1350°C (2462°F)/2 hours water quench + 700°C (1292°F)/2 hours air cool. The strength at room temperature is approximately 1379 Mpa (200 Ksi), at 600°C (1112°F) is approximately 827 Mpa (120 Ksi), and at 700°C (1292°F) is approximately 483 Mpa (70 Ksi). The total (elastic + plastic) elongation at room temperature was determined to be 2.8%. The strength of the as-extruded alloy (containing very large particles, Figure A6) is also shown in Figure A12 as well as that of unalloyed Fe<sub>3</sub>Al. These data indicate that this alloy exhibits significant precipitation strengthening.



(a) 1350°C/2 hr - W.Q.



(b) 1350°C/2 hr - W.Q. + 700°C/4 hr - A.C.

Figure A11. Etched and Tinted Micrographs of 6061-T6

# Fe<sub>73</sub>Al<sub>25</sub>Nb<sub>2</sub>

R.T. DUCTILITY

PPT. HARDENED = 2.8%

AS EXTRUDED = 2.3%

Fe<sub>3</sub>Al = 5%

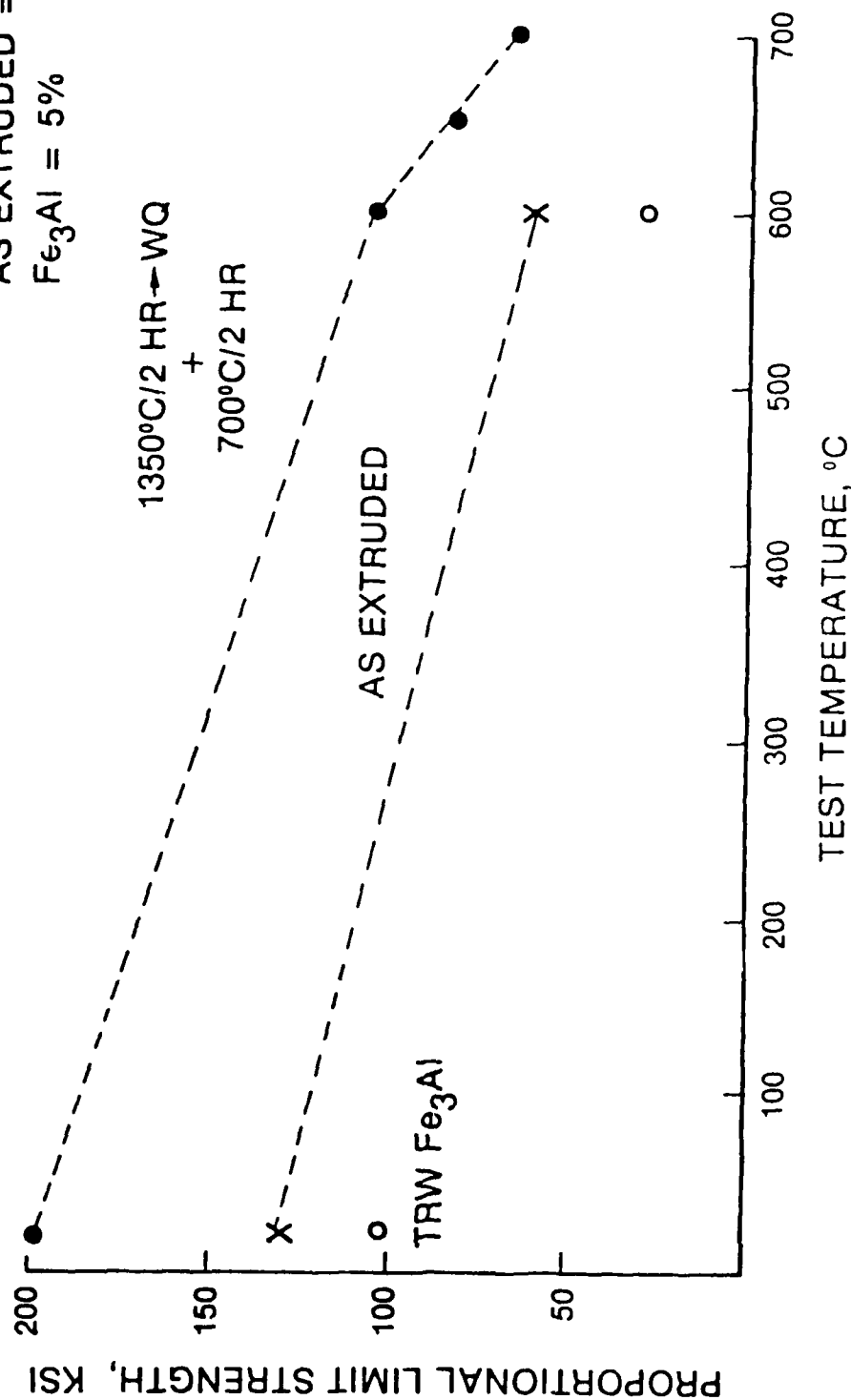


Figure A12 Variation of Proportion-Limit Strength with Test Temperature in Aged (and Extruded) Fe<sub>73</sub>Al<sub>25</sub>Nb<sub>2</sub> Alloy.

END

DTIC

7-86